Summer 8-13-2013

Physics of Resonating Valence Bond Spin Liquids

Julia Saskia Wildeboer
Washington University in St. Louis

WASHINGTON UNIVERSITY IN ST. LOUIS

Department of Physics

Dissertation Examination Committee:

Alexander Seidel, Chair

Zohar Nussinov

Michael C. Ogilvie

Jung-Tsung Shen

Xiang Tang

Li Yang

Physics of Resonating Valence Bond Spin Liquids

by

Julia Saskia Wildeboer

A dissertation presented to the
Graduate School of Arts and Sciences
of Washington University in
partial fulfillment of the
requirements for the degree
of Doctor of Philosophy

August 2013

St. Louis, Missouri

TABLE OF CONTENTS

Page

LIST OF FIGURES v

ACKNOWLEDGMENTS ix

DEDICATION ix

ABSTRACT xi

1 **Introduction** 1

1.1 Landau's principle of symmetry breaking and topological order 2

1.2 From quantum dimer models to spin models 5

1.2.1 The Rokhsar-Kivelson (RK) point 12

1.3 QDM phase diagrams 14

1.4 Z_2 quantum spin liquid and other topological phases 15

1.4.1 Z_2 RVB liquid 16

1.4.2 U(1) critical RVB liquid 17

1.4.3 Crystalline phases 18

1.5 Fractionalization 21

1.6 Experimental search for quantum spin liquids 22

Page

1.7 Outline of the thesis 24

2 **Existence of a Z_2 quantum spin liquid** 27

2.1 A local, SU(2) invariant spin-1/2 Hamiltonian and its ground state . 28

2.2 Pfaffian Monte Carlo 35

2.3 Results 42

2.4 Discussion 49

3 **Linear independence of nearest neighbor valence bond states** . . . 51

3.1 Applications and usefullness of linear independent valence bond states 52

3.2 Proof for linear independence and results 58

3.2.1 Derivation of the linear independence condition 58

3.2.2 Twelve different 2D lattices 66

3.2.3 Fullerene-type lattices 70

3.2.4 The square lattice 73

3.3 Summary and discussion 78

3.4 Extensions of the proof: Linear independence of Resonating Valence Loops (RVL) on the honeycomb and star lattices 80

4 **Destruction of valence-bond order in a S=1/2 sawtooth chain with a Dzyaloshinskii-Moriya term** 87

4.1 Introduction 88

Page

4.2 Spinon dispersions 94

4.2.1 $D = 0$ 94

4.2.2 $D \neq 0$ 96

4.3 Exact diagonalization 98

4.4 Spin correlations in the ground state 101

4.5 Discussion 102

Bibliography 109

LIST OF FIGURES

Figure Page

1.1 a) and b) show two different dimer coverings on the square lattice. c) shows the transition graph (the overlap $\langle a|b\rangle$) of the two coverings when both coverings $|a\rangle$ and $|b\rangle$ are laid on top of each other. 8

1.2 a) - d) show all possible loop coverings up to rotations for the kagome lattice. a) and b) contain three and six dimers, respectively. c) shows the possibilities how four dimers can cover the loop and d) shows the case of five dimers occupying the loop. 10

1.3 The topological degeneracy of topologically ordered states depends on the topology of the space, such as the genus g of two dimensional closed surfaces. Shown are three examples: the sphere has $g = 0$, the torus has $g = 1$, and a generalized torus with holes in it has $g = 2$ (n holes generalize to $g = n$). 11

1.4 The benzene molecule C_6H_6. The central hexagon, also called aromatic ring in chemistry, has three "double bonds". Since there are two configurations that the additional bonds can assume in the hexagon and since both configurations are equally energetically favored, it is understood that the system fluctuates (resonates) back and forth between the two configurations. 12

1.5 (a) Visons live on the dual lattice. (b) Taking a monomer around a vison causes the number of dimers intersecting the dashed line, and hence, the wave function, to change sign. Figure taken from Ref. [36]. 17

1.6 Shown are three examples of valence bond solids: a) the columnar state. (b) the staggered state. (c) the plaquette state. 19

1.7 (a) Shown is the structure of $ZnCu_3(OH)_6Cl_2$ with only Cu^{2+} (large brown spheres) and Zn^{2+} (small red spheres) displayed. The Cu-Cu bonds (thick black solid lines) are all equivalent as are the Cu-Zn bonds (thin green dotted lines). (b) A single-crystal sample of $ZnCu_3(OH)_6Cl_2$. Figure taken from Ref. [49]. 23

2.1 Shown is an orientation of links on the kagome lattice used to fix the sign of valence bond states. All links are oriented counterclockwise around the hexagon they belong to. Figure is taken from Ref. [51]. 31

Figure Page

2.2 Shown is the 12-site "star" that serves as the minimal unit of the lattice that the Hamiltonian acts on. Also shown is the chosen link orientation for this cell. All links are oriented counterclockwise around the central hexagon. Figure is taken from Ref. [51]. 32

2.3 Eight different types of dimer loops around a central hexagon. [52] Loops may be formed by three (a), six (b), four (c), or five (d) dimers. Each loop can be realized by two different dimer configurations related by a resonance move. Dashed lines indicate dimer configurations after a resonance move. The loops should be regarded as the transition graphs between the original and the resonated configuration, i.e. the set of all links carrying either a dimer or a dashed line. Using rotational symmetry, there are 32 different loops corresponding to 64 dimer configurations. 33

2.4 A Kasteleyn orientation for the kagome lattice taken from Ref. [56]. . . 39

2.5 a) Shape of the kagome lattice used in the calculations. The lattice consists of m unit cells in the $\mathbf{a}$ direction and n unit cells in the $\mathbf{b}$ direction, for a total of $3mn$ sites. Periodic boundary conditions may or may not be introduced with periods $m\mathbf{a}$ and $n\mathbf{b}$. b) The orientation used in the sign convention for the triangular lattice. 42

2.6 The dimer-dimer correlation function shown for kagome lattices with PBCs and OBCs. Insensitivity to system size and short correlation length are evident. The PBC case has been calculated within a fixed topological sector. The inset shows a logarithmic plot including a linear fit, yielding a correlation length of 1.12(3). 43

2.7 The dimer-dimer and spin-spin correlation functions for a 400 sites triangular lattice with OBCs. The inset shows logarithmic plot with fits, giving a correlation length of 1.15(2) for the dimer-dimer decay. The spin-spin correlations display stronger even/odd effects at short distance. Fitting only odd distances in the spin-spin case gives a correlation length of 1.61(2). 44

2.8 The spin-spin correlation functions $\langle \vec{S}_i \vec{S}_{i+\kappa} \rangle$ and $\langle S_i^z S_{i+\kappa}^z \rangle$ for different kagome lattices (PBC and OBC). Again, the topological sector was fixed in the PBC case. The inset shows a logarithmic plot with linear fit yielding a correlation length of 2.08(2). 45

2.9 The expectation value of the dimer operator for links of the three possible directions and various lattice sizes. The average for one system size is shown as horizontal bar. A topological sector has been fixed. The discrepancy between nonequivalent links rapidly decreases with system size, restoring the lattice symmetry. 46

Figure Page

3.1 A square lattice a with dimer covering. Dimers are indicated by ovals. . 53

3.2 (Color online.) The kagome lattice. a) shows the structure of the kagome lattice, while b) shows the minimal (smallest) cell for which the local independence property defined in the text was proven. [51] Different dots are used to label the sites which are defined as inner and outer sites, respectively. 60

3.3 (Color online.) The star lattice (a), and its minimal cell (c) for which the local independence property could be established. (b) shows the martini-A lattice, with the same minimal cell (c). Different shades (colors) of dots identify internal and boundary sites. (d) shows a possible dimer covering: the internal sites must be touched by a dimer, boundary sites may or may not form a dimer (valence bond) with an internal site. In a local valence bond state, boundary sites not participating in valence bonds may be in an arbitrary spin configuration. 65

3.4 (Color online.) Honeycomb and related structures. (a) The honeycomb lattice. (b) its minimal cell with internal and boundary sites identified. (c) The minimal cell of the buckyball lattice (Fig. (3.9)). (d) A similar heptagonal cell that also satisfied the local independence property. . . . 67

3.5 (Color online.) The square-octagon lattice (a) and the squagome lattice (b). (c) and (d) show the respective minimal cells. 68

3.6 (Color online.) Two types of pentagonal lattices. (a) shows the pentagonal lattice and (b) shows the "Cairo" pentagonal lattice structure, (c) and (d) the respective minimal cells. 69

3.7 (Color online.) Two more types of martini lattices. (a) and (b) show the lattice structures of the martini-B lattice and the martini-C lattice, respectively, (c) and (d) the respective minimal cells. 70

3.8 (Color online.) Two types of archimedean lattices. (a) shows the archimedean-A lattice and (b) shows the archimedean-B lattice structures, (c) and (d) the respective minimal cells. Note that the minimal cell in (d) is the same as that of the honeycomb lattice, Fig. (3.4b). 71

3.9 The lattice of the C_{60} molecule, or "buckyball". The lattice can be covered by the minimal cell of the honeycomb lattice, Fig. (3.4b). The actual minimal cell of this lattice is the pentagonal cell shown in Fig. (3.4c). . 72

Figure Page

3.10 (Color online.) The square lattice. The general lattice structure is shown in Fig. (3.1). (a) The minimal cell for which the refined local independence property of Section 3.2.4 holds. (b) A local valence bond state with the central site forming a bond with its upper neighbor, corresponding to $\sigma =\uparrow$ as defined in the text. 74

3.11 (a) shows the minimal cell of the star lattice for which the linear independence of both the RVB and the RVL states could be established. Red dots indicate inner sites that have all their 3 nearest neighbors also present in the cell, while blue dots label outer sites that do not all neighbor sites contained in the cell. (b) shows the minimal cell for the honeycomb lattice. 82

3.12 a) all inner sites participate in the loop while the three outer sites are in an arbitrary eigenstate of S^z = -1, 0, +1. b) all inner sites and two outer sites form the loop, apart from the configuration shown, there exists two rotated versions, thus, the total number for this kind of covering is three. 83

3.13 a) - e) show all possible loop coverings up to rotations for the honeycomb lattice. 84

4.1 (a) The Kagome lattice. (b) and (c) In-plane and out-of-plane components of the DM vector $\mathbf{D}_{ij}$ shown for directed links $(i \to j)$ on the lattice. . . 89

4.2 (a) The sawtooth chain. (b) and (c) Its valence-bond ground states. (d) Spin-1/2 excitations: kink (left) and antikink (right). (e) Orientation of the DM vectors $\mathbf{D}_{ij}$. (f) The ground state of the classical model has a commensurate magnetic order with the wave number $q/2\pi = -1/3$. . . . 93

4.3 Low-energy spectra of the sawtooth chain with a uniform DM term in the $S_z = 0$ sector. Energy levels, measured relative to the ground state, are shown as a function of total momentum. Circles are the results of exact diagonalization for a periodic chain of length $L = 15$. Solid curves show the bottoms of the two-spinon continua computed analytically. Dashed straight lines show a linear dispersion with the speed $v = 0.36J$. 105

4.4 Low-energy spectra in the $S_z = +1$ sector. Notations are the same as in Fig. 4.3. 106

4.5 The splitting of the ground state doublet as a function of the system length L for (a) $D < D_c = 0.115J$ and (b) for $D > D_c$. (c) The dependence of the inverse tunneling length $1/\xi$ and the wavenumber k in the scaling form (4.13) on the DM coupling strength D. 107

4.6 The amplitude of transverse spin correlations (4.15) as a function of the chord distance (4.16) on a log-log plot (left) and a simple log plot (right). 108

ACKNOWLEDGMENTS

I like to thank all people who have contributed in any form to the success of this thesis. The first person to be mentioned, of course, is my advisor, Prof Alexander Seidel. Without him this work would not have been possible. I thank him for sharing his ideas with me, for his patience, advice, and support. The second person who I greatly enjoyed working with is Prof Zohar Nussinov. His willingness to collaborate and his interest in many, many different areas of physics make him a very valuable and irreplaceable partner of discussion. Also, I thank Prof Oleg Tschernyshyov from the John Hopkins University and Prof Stuart Solin (Washington University) and their group members for the possibility to do a collaboration with them. Finally, I thank all the group members of the condensed matter theory group at WashU for their company and support. I thank the people of my defense committee, the above mentioned Prof Alexander Seidel and Prof Zohar Nussinov, Prof Mike Ogilvie, Prof Li Yang, Prof J.T. Sheng, and Prof Xiang Tang.

Dedicated to all unflipped dimers and spins - and unbraided anyons.

ABSTRACT

Physics of Resonating Valence Bond Spin Liquids

by

Julia Saskia Wildeboer

Doctor of Philosophy in Physics

Washington University in St. Louis, 2013.

Professor Alexander Seidel, Chairperson

This thesis will investigate various aspects of the physics of resonating valence bond spin liquids. After giving an introduction to the world that lies beyond Landau's priciple of symmetry breaking, e.g. giving an overview of exotic magnetic phases and how they can be described and (possibly) found, we will study a spin-rotationally invariant model system with a known parent Hamiltonian, and argue its ground state to lie within a highly sought after exotic phase, namely the Z_2 quantum spin liquid phase. A newly developed numerical procedure –Pfaffian Monte Carlo– will be introduced to amass evidence that our model Hamiltonian indeed exhibits a Z_2 quantum spin liquid phase. Subsequently, we will prove a useful mathematical property of the resonating valence bond states: these states are shown to be linearly independent. Various lattices are investigated concerning this property, and its applications and usefullness are discussed. Eventually, we present a simplified

model system describing the interplay of the well known Heisenberg interaction and the Dzyaloshinskii-Moriya (DM) interaction term acting on a sawtooth chain. The effect of the interplay between the two interaction couplings on the phase diagram is investigated. To do so, we employ modern techniques such as the density matrix renormalization group (DMRG) scheme. We find that for weak DM interaction the system exhibits valence bond order. However, a strong enough DM coupling destroys this order.

1. Introduction

We begin with an introduction divided into several sections. All of the single sections present important facts necessary for an understanding of the physics of resonating valence bond (RVB) states [1] and resonating valence bond spin liquids. Such a valence bond state is pictorially described as a state that has all (valence) electrons forming singlet bonds with each other. This grouping of the electrons into pairs of two forming the singlets is not unique and under certain conditions the system switches back and forth (resonates) between different singlet configurations. If this is the case, we speak of a resonating valence bond state.

Before discussing these states in more detail, we will recall the history of a new kind of order –topological order– that is found in the resonating valence bond states and point out the thereby resulting failure –or rather the limitations– of Landau's principle of symmetry breaking.

We will then discuss a simplified approach, namely the so-called quantum dimer model (QDM), that has shed light on issues concerning whether a resonating valence bond liquid state exists and in which model system it can be expected. Eventually, we close the introductory chapter by describing several attractive features and properties that have been found or are expected to be found in exotic quantum states such as the resonating valence bond spin liquids. Additionally, to make connection with the

experimental side, we recall and discuss some new exciting experimental discoveries and comment on the state of the art concerning the challenging experimental search for a quantum spin liquid in an experimental compound.

1.1 Landau's principle of symmetry breaking and topological order

One of the most important concepts in condensed matter theory is the concept of order. Different orders in a material lead to different properties exhibited by the material. The particles that order can be protons, neutrons, or electrons. Landau's symmetry breaking [2, 3] provides an understanding and a way to classify and distinguish different states (phases) of matter. The fundamental principle of Landau's theory is that different orders correspond to different symmetries that are respected by the particles that order. A phase transition is a change in the system which sees a change in the way that the particles are arranged; thus, the symmetry of the system changes. In the case of temperature T = 0, this is called a *quantum* phase transition. A feature of Landau's principle guarantees that one can always find a so-called order parameter which distinguishes different phases from each other; a local parameter being zero in one phase and having a finite value in the other one. A standard example for this is the two dimensional Ising model on the square lattice:

$$H = -\sum_{\langle ij \rangle} J_{ij}\sigma_i\sigma_j \,. \tag{1.1}$$

Here, σ_i, $\sigma j \in \{-1; +1\} \forall\, i\,(j) = 1, \ldots, L_x\,(L_y)$ with $L_{x(y)}$ is the dimension of the lattice in x(y)-dimension. The system can exist in two different phases depending

on the temperature T . At low enough temperatures, the system is permanently magnetized. At sufficiently high temperatures, the magnetization of the system is zero. There is a critical value of the temperature T_c called the Curie temperature at which a phase transition between the ferromagnetic (permanently magnetized) and paramagnetic phases occurs. For this system, a proper order parameter would be the magnetization m with m being finite in the ferromagnetic phase and $m = 0$ in the disordered phase. For a long time, it was generally accepted that Landau's theory of symmetry breaking would capture all possible kinds of order and all possible (continuous) phase transitions that can occur in a material/system.

The first cracks in the theory surfaced in the late eighties after the discovery of high T_c superconductors [4]. Various quantum spin liquids were introduced in an attempt to gain an understanding of the mechanism that governs the T_c superconductors [5–10]. Landau's theory neither explains nor allows for the existence of spin liquids since they can not be distinguished by a local order parameter. We note that one type of spin liquid used in an attempt to get a better understanding of the high T_c superconductors was a so-called chiral spin liquid [11, 12]. The chiral spin liquid state breaks time reversal and parity symmetries, but not spin rotation symmetry [12]. However, it was quickly realized that there are indeed many kinds of chiral spin liquids with the same symmetry. Thus, they are indistinguishable within the framework of Landau's symmetry breaking theory [13]. Their new kind of order was called topological order [14]. The motivation behind this choice of name is the low

energy effective theory for the chiral spin states, which is a topological quantum field theory.

In order to identify and classify topologically ordered phases, it is unavoidable to go beyond local order parameters and long range correlations. In the case of the chiral spin liquids, one introduces a range of new quantum numbers such as for example ground state degenerancy [13] and edge excitations [15]. A fairly new way of characterizing topological order is characterization through topological entanglement entropy [16, 17].

However, experimental progress soon found evidence that high T_c superconductors to not break time reversal and parity symmetry. This brought the idea that the chiral spin liquid states are suitable candidates to describe the superconductors to an abrupt end. But the idea that there are states beyond Landau's symmetry breaking principle survived Consequently, Laughlin proposed a set of wave functions for the fractional quantum Hall effect [18]. Just like the chiral liquids, the FQH states all have the same symmetry and therefore are beyond Landau's theory of symmetry breaking. They have a ground state degeneracy [19] that depends on the topology of the space [14,18]. This property is stable under any local perturbation. Subsequently, it was noted that different orders in the fractional quantum Hall states can be described by topological orders. This was a significant milestone in the (still young) history of topological order since it had just become a theory with experimental realizations. Apart from the FQH states which exhibit topological order, another important "class" of states to be topologically ordered are different types of quantum spin liquids such as the

already mentioned chiral spin liquid states. In the late eighties, researchers started to introduce several symmetric spin liquids [6–10, 20–23], some having excitations with a finite energy gap, others gapless. However, all liquid states do not break any symmetry and are thus beyond the description of Landau's symmetry breaking. The concept of topological order is only applicable to the case of gapped spin liquids which are described by a topological quantum field theory at low energy. An example for this is the Z_2 quantum spin liquid. It is described by the Z_2 gauge theory and it –or the search for it– will be our main concern in this thesis. Indeed, the Z_2 quantum spin liquid first appeared in the literature in 1991 [21, 22]. Here it was the short-ranged flavor of Anderson's resonating valence bond (RVB) type state. Interesting properties arise from such a state, such as spin-charge separation [22], fractional statistics [22], and topologically protected ground state degeneracy [8, 21].

The next two sections will provide more information concerning the spin liquid phase, and we will comment on the challenging search for spin liquid states on the theoretical side and on the experimental one.

1.2 From quantum dimer models to spin models

Pioneering work to answer the question if quantum spin liquids do exist in nature has been done on the experimental and the theoretical side. On both sides, the researchers faced great challenge. We will first turn our attention to the theoretical progress. In 1988, the so-called Rokhsar-Kivelson quantum dimer model (QDM) was introduced [8]. The original motivation behind the quantum dimer model was the

high T_c superconductivity problem mentioned in the preceding section. The task was to find a suitable non-magnetic state for the undoped Mott insulator phase. Upon doping, the system is expected to change into a superconductor. This was achieved by allowing all spins to form singlets that minimize the antiferromagnetic exchange energy. Systems that are dominated by valence bonds are of interest because they are a simple stating point for describing phases of magnets dominated by local singlet formation. This thesis will focus on singlets formed by spins on nearest neighbor sites, so-called short-range valence bonds. Longer bonds between sites that are not nearest neighbors will *not* be discussed in the following. To summarize the obstacles and the accomplishments/achievements on the theoretical side, we go back to the year 1988. In 1988, Rokhsar and Kivelson published a seminal paper [8] in which they presented the above mentioned quantum dimer model. Here, a dimer represents the SU(2) singlet between the two spins at its endpoints. The frustration is captured by the hardcore constraint, e.g. every site is touched by one and only one dimer. Quantum dimer models can be used as a simplified starting point to describe how exotic phases such as a quantum spin liquid phase can arise from the competition of the dimers at various potential energy.

Before discussing the general structure of the phase diagram of the QDMs and describing its tremendous success at finding a quantum liquid phase, we will first discuss the basic features and properties of a dimer model and point out it simplifications compared to a spin model. A more detailed review of the properties of dimer models can be found for example in Ref. [24].

The quantum dimer models were introduced to model the physics of the resonating valence bonds and a simplified way, that is, the original spin Hilbert space gets heavily truncated and the only degrees of freedom kept of the original spin systems are the valence bonds (singlets), represented as dimers which live on the lattice bonds. Typically, the dimers must not overlap ("hardcore constraint"). Generally, any two sites can form a dimer, but in the simplest case –the short ranged-flavor version– only sites that are nearest neighbors to each other are allowed to form a dimer. The resulting dimer covering of the underlying lattice form a complete orthonormal set of basis states:

$$\langle D|D'\rangle = \begin{cases} 0 & \text{if } D \neq D' \\ 1 & D = D' \end{cases} \tag{1.2}$$

Herein lies an important difference between dimer coverings and the original *singlet* coverings of the lattice, namely the difference in their scalar products. In contrast to the dimer covering scalar product given above, the scalar product (overlap) of any two singlet product states is never zero. In an influential paper, Sutherland [25] pointed out that if *all* overlaps are either positive or negative, the system corresponds to a classical loop gas model. We will come to this point later in Section 2.2 when presenting a novel Monte Carlo scheme especially derived to calculate correlation functions on nonbipartite lattices.

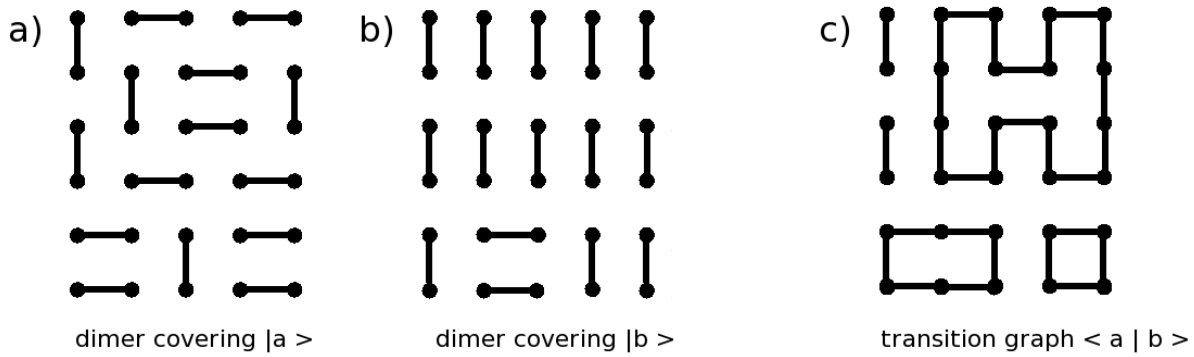

Figure 1.1. a) and b) show two different dimer coverings on the square lattice. c) shows the transition graph (the overlap $\langle a|b\rangle$) of the two coverings when both coverings $|a\rangle$ and $|b\rangle$ are laid on top of each other.

To explain the (simplest) Hamiltonian that describes the energetics of the dimers, we first resort to the QDM on the square lattice and then point out how the following carries over to other lattices.

The original QDM of Rokhsar and Kivelson was defined on the square lattice as follows:

$$H_{\text{QDM}} = \sum -t(|\,\rangle\langle\,| + \text{h.c.}) + v(|\,\rangle\langle\,| + |\,\rangle\langle\,|) \tag{1.3}$$

The first and second term with the tunable parameters t and v respectively flip and count the dimers if the plaqette has parallel dimers, otherwise the state gets annihilated, the sum goes over all 4-site plaquettes. The flipping of the dimers on a single plaquette is the simplest way to endow the system with dynamics.

The first term in equation (1.3), the kinetic one, describes the resonance between two different dimerizations of the 4-site plaquette of the square lattice.

In other lattices of general interest, the flippable plaquettes may correspond to minimal resonance loops, resonance loops being closed lines of links of even length that are alternatingly occupied/unoccupied by dimers. In the triangular lattice, the elementary flippable units are still of length four, since the triangular lattice is topologically equivalent to the square lattice with an additional diagonal. (The horizontal, vertical, and diagonal bonds are defined to have the same length, hence, the triangular lattice has coordination number $z = 6$.) In the case of the kagome lattice which we will mainly focus on in this thesis, the flippable plaquettes are no longer of length four, but at least of length six and at most of length twelve. All closed loops along which the dimers can resonate are embedded on the 12-site star (see Fig. (1.2)). Requiring that all sites that form the internal hexagon are touch by one and only dimer, the shortest loop goes around the hexagon and shifts its three dimers along the hexagon by one link. The longest loop is the loop formed by all links that form the outer boundary/border with six dimers living on it (see Fig. (1.2)b)). All possible loop configurations (up to rotations) are shown in Fig. (1.2). From Fig. (1.2) it is clear that there are a total of 32 different loop coverings, each goes over into a new configuration by shifting the dimers along the green paths by one lattice link. Thus, we eventually have 64 possibilities for a loop covering. In the case that we assume a system with periodic boundary conditions, we have the so-called topological degeneracy. Topological (ground state) degeneracy is a phenomenon of quantum many-body

systems; the ground state of a gapped system becomes degenerate in the large system size limit. Such a topological degeneracy cannot be lifted by any local perturbations as long as the system size is large. [13, 18, 26, 27] The topological degeneracy for a given system is different for different topologies of the space. [19] For example, for the Z_2 topologically ordered state in two dimensions [12], the topological degeneracy

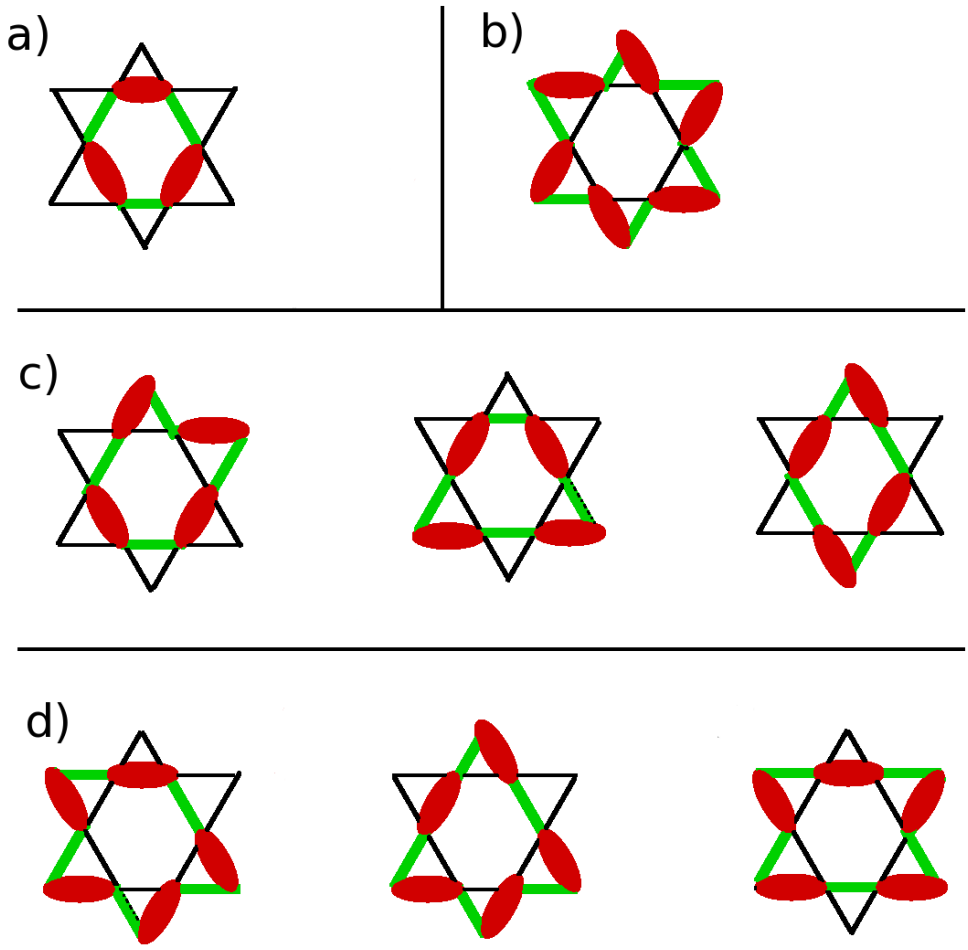

Figure 1.2. a) - d) show all possible loop coverings up to rotations for the kagome lattice. a) and b) contain three and six dimers, respectively. c) shows the possibilities how four dimers can cover the loop and d) shows the case of five dimers occupying the loop.

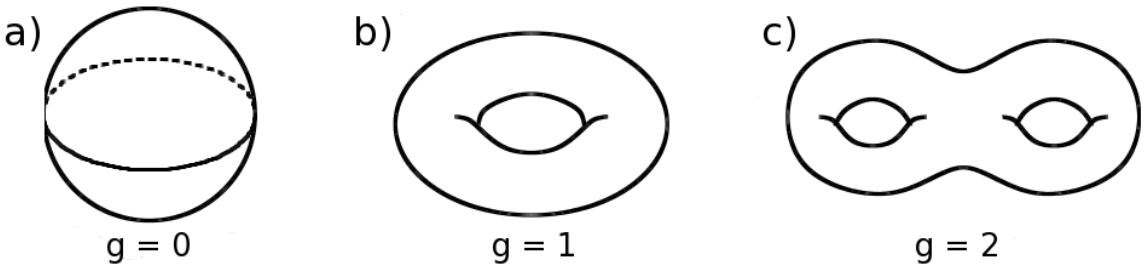

Figure 1.3. The topological degeneracy of topologically ordered states depends on the topology of the space, such as the genus g of two dimensional closed surfaces. Shown are three examples: the sphere has $g = 0$, the torus has $g = 1$, and a generalized torus with holes in it has $g = 2$ (n holes generalize to $g = n$).

is $D_g = 4g$ on a Riemann surface of genus g (see Fig. (1.3)). Topological degeneracy, being robust against any local perturbations, is not due to a symmetry of the system. Thus, the very existence of topological degeneracy is a surprising and amazing phenomenon.

Going back to the Hamiltonian (1.3) and its analogue on the respective lattice, a natural question is its ground state phase diagram depending on the choice of the two couplings strengths t and v. We will see that another important factor when it comes to the phase diagram is the above mentioned lattice topology. However, before specifying a particular lattice, we will now discuss an attractive feature of the RK Hamiltonian (1.3). At this point, for reasons of completeness, we recall the origin of the name "resonating valence bond" (RVB). The term "resonating valence bond" (RVB) stems from the analogy of the resonance between the two dimerizations of the

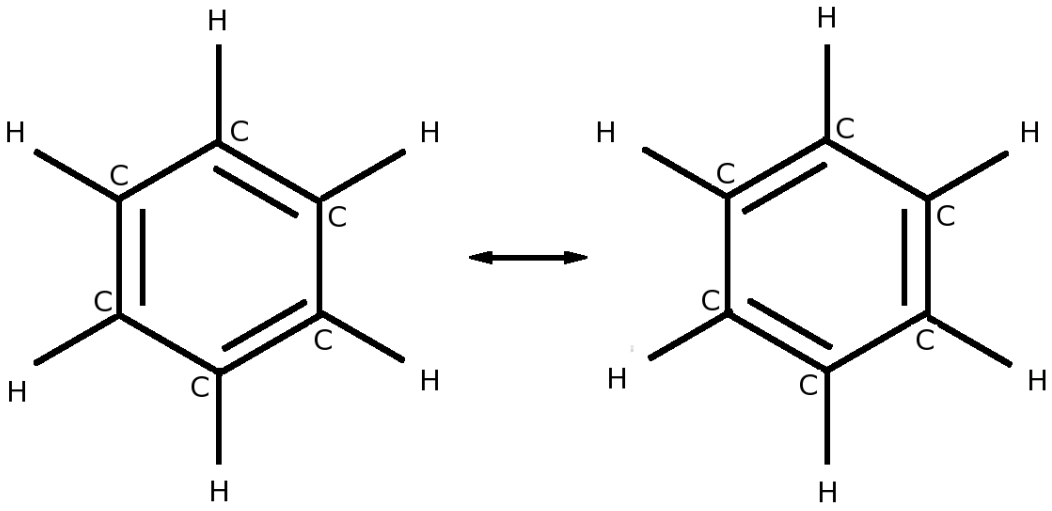

Figure 1.4. The benzene molecule C_6H_6. The central hexagon, also called aromatic ring in chemistry, has three "double bonds". Since there are two configurations that the additional bonds can assume in the hexagon and since both configurations are equally energetically favored, it is understood that the system fluctuates (resonates) back and forth between the two configurations.

benzene ring C_6H_6 (see Fig. (1.4)). Again, we point out that the QDM/RVB approach is not only an important approach to the high T_c problem as already described, the QDM/RVB approach has found applications and interest in other corners of condensed matter physics, e.g. it has been shown that the QDM can be used to shed light on issues such as topological order, and unusual (resonons and visons) and fractionalized (spinons and holons) excitations.

1.2.1 The Rokhsar-Kivelson (RK) point

Before specifying a particular lattice, we will now discuss an attractive feature of the QDM Hamiltonian Eq. (1.3). Assuming the Rokhsar-Kivelson (RK) point

$t/v = 1$, we note that in this case the (unique) ground state wave function is the *equal* amplitude superposition of all dimer coverings:

$$|\psi_{GS}\rangle = \sum_D |D\rangle \,. \tag{1.4}$$

To see that this is indeed the unique ground state, we point out that for every flippable plaquette, the second term in 1.3 gives a penalty v while the first term gives at most a benefit of t. Nonflippable plaquettes have zero energy. This gives the lower bound for the ground state energy to be

$$E_{GS} \geq min\{0, N_{plaq}(v-t)\} \,, \tag{1.5}$$

where N_{plaq} is the number of plaquettes in the lattice. The equal amplitude state ψ_{GS} has energy $n_{flip} \times (v-t)$, where n_{flip} is the average number of flippable plaquettes in the state. Choosing $t = v$ saturates the lower bound and, since the equal amplitude state is an eigenstate of the QDM (at $v = t$), we may conclude that it is a ground state when v = t. In the case of periodic boundary conditions, there is the previously mentioned ground state degeneracy according to the number of topological sectors.[1] In this case, the sum in (2.9) may be restricted to one specific topological sector. Dimer coverings contained in one sector will always lead to an equal amplitude wave function without any local order. Nonetheless, a nonlocal measurement will be able to tell the different sectors apart, e.g. will determine to which sector the wave function belongs. The RK point was investigated for numerous lattices in two dimensions. On

[1]A topological sector is defined as a set of all dimer coverings that can be connected through local dimer resonance moves. Starting from one state (dimer covering), one can get into any other state with a sequence of local resonance moves as long as the two states belong to the same topological sector.

the square lattice (as well as other bipartite lattices such as the honeycomb lattice), the RK point corresponds to a liquid ground state, however this turned out to be a critical point separating "valence bond solid" phases with broken translational symmetry. [28–31] In the bipartite case, the liquid is of type U(1). In 2001, Moessner and Sondhi showed that the QDM on the triangular lattice at the RK point lies in a stable quantum liquid phase. [32] Subsequently, similar findings were also made for the kagome lattice in 2002. [33] In these two cases, the quantum liquid was argued to be in the Z_2 universality class. For numerous bipartite lattices in three dimensions such as the cubic lattice, the RK point is part of a Coulomb phase. The Coulomb phase is also a liquid phase but with a different type of quantum order. The present understanding in the condensed matter community is that this type of behavior is generic. We will now devote a subsection to the description of the different phases mentioned above.Z_2 and U(1).

1.3 QDM phase diagrams

The detailed structure of the quantum phase diagram depends on several parameters: the ratio of the two parameters v/t, the dimensionality of the lattice, and the lattice geometry. We have just previously highlighted the existence of the RK point $v = t$. Here, the ground state of the model is the equal amplitude superposition of all dimer coverings. Depending on the lattice type, the RK point is part of different topological phases.

For the triangular lattice, Moessner and Sondhi showed in a seminal paper that the RK point of the QDM on the triangular lattice has ground states describing a Z_2 topological quantum liquid [32]. Subsequently, Misguich *et al.* [33] generalized these findings to the kagome lattice, which was found to have an additional feature: a crucial difference between the triangular and the kagome lattice is the fact that the kagome RK-point lies in the interior of the Z_2 liquid phase for the kagome. This is in contrast to the triangular case: here, the RK point of the QDM lies at a (apparently first order) phase boundary.

We now will discuss the properties of different exotic phases in the next sections.

1.4 Z_2 quantum spin liquid and other topological phases

This section shall provide an overview of the richness of the QDM phase diagrams. The simplest QDM Hamiltonians provide one parameter v/t. Of course, the choice of this parameter ratio has a fundamental effect on the phase that the Hamiltonian lies in. But apart from the v/t ratio[2] the phase diagram is also strongly dependent on the lattice geometry and on the dimensionality d of the lattice. The general structure of the phase diagram is expected to be further enriched with novel phases upon including additional (more complicated) interactions which make the Hamiltonian more complicated. However, we point out that there are a number of features common

[2]In contrast to the square lattice, the v term is trivial in the case of the kagome lattice, since all configurations are flippable.

to most models and describe a few phases which frequently are discussed in the literature.

1.4.1 Z_2 RVB liquid

The Z_2 quantum liquid spin phase belongs to the Z_2 universality class and, consequently, has Z_2 topological order [32]. In the case of a triangular and a kagome lattice with periodic boundary conditions, the ground state space consists of four degenerate gapped states. The ground states do not break any symmetry of the system and all correlations decay exponentially. The first time a phase of this type was proven to be the ground state was on the triangular lattice in 2001 [32] with numerical evidence supporting that the phase survives in the parameter range from $0.8 < v/t < 1$ [34]. Here, the RK point of the QDM lies at a (apparently first order) phase boundary. Shortly afterwards, it was also found on the kagome lattice. The QDM on the kagome lattice differs from the triangular counterpart insofar that the RK point lies in the interior of the Z_2 liquid phase. The general opinion on this matter is that this phase is a generic feature of nonbipartite QDMs in two and higher dimensions. Concerning nontrivial excitations of this model, it is known that monomer excitations are deconfined throughout the complete phase. A second type of excitation are the so-called Ising vortices or visons [35]. At the RK point, a variational wave function describing the vison state in a periodic system in sector a is given by

$$|\psi_{vison}\rangle = \sum_{D \in \, sector \, a} (-1)^{n_D} |D\rangle \, . \tag{1.6}$$

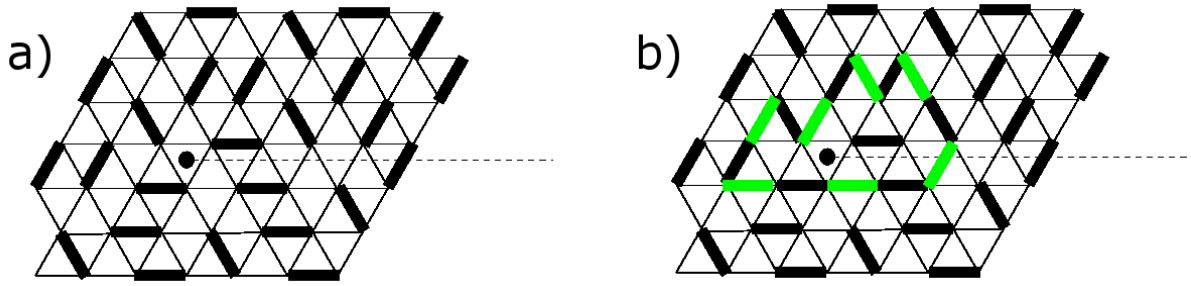

Figure 1.5. (a) Visons live on the dual lattice. (b) Taking a monomer around a vison causes the number of dimers intersecting the dashed line, and hence, the wave function, to change sign. Figure taken from Ref. [36].

n_D is the number of dimers crossing the dashed line (Fig. (1.5)a)). The excited state $|\psi_{vison}\rangle$ is orthogonal[3] to the ground state $|\psi_{GS}\rangle$. Current numerical data give evidence that the lowest lying excitation above the triangular lattice ground state is indeed vison-like [37].

1.4.2 U(1) critical RVB liquid

The U(1) RVB liquid phase cannot be characterized by a local order parameter just as its Z_2 counterpart cannot. However, the two phases differ by multiple properties. The Z_2 RVB liquid is a gapped phase with exponential correlations having a ground state degeneracy that depends on the lattice topology, this degeneracy is present throughout the entire phase. In contrast, the U(1) liquid is a gapless phase with correlations obeying a power law. The topological ground state degeneracy does exist

[3]This is only true if all configurations are flippable like it is in the case of the kagome lattice.

at the RK point, but is lifted upon entering the phase. Similar to the Z_2 flavor, the U(1) liquid also has deconfined monomers. However, the monomers do not interact via a force that is limited by a few lattice spacings as it is in the case of the Z_2 variant, but the monomers interact via a long-ranged inverse square force [38]. The gapped excitation in U(1) liquid that serves as the counterpart to the vison in the Z_2 case, is the monopole. Monopoles interact with each other through an inverse square force. [4]

1.4.3 Crystalline phases

Another important class of phases of the QDM are crystalline phase, so-called valence bond crystals. Here, in this kind of order, the dimer order in a specific manner. In this phase, still as in the liquid phase, all correlations decay exponentially. However, the important difference in contrast to the liquid is that translational symmetry is broken now. A model system which is believed to have such a ground state is the antiferromagnetic spin-1/2 Heisenberg model on the three dimensional highly frustrated hyperkagome lattice [39].

Going back to the QDM on the square lattice, it is noteworthy to discuss the plaquette phase.

This phase is shown together with the columnar and the staggered phase in Fig. 1.6. The choice of names becomes clear when looking at picture Fig. 1.6. The thick bonds indicate that the probability to find a dimer on this link is comparatively

[4] Another name for the U(1) liquid phase is Coulomb phase. The name stems from the matter of fact that the U(1) phase has a continuum description that resembles the Maxwell action of the free electromagnetic field.

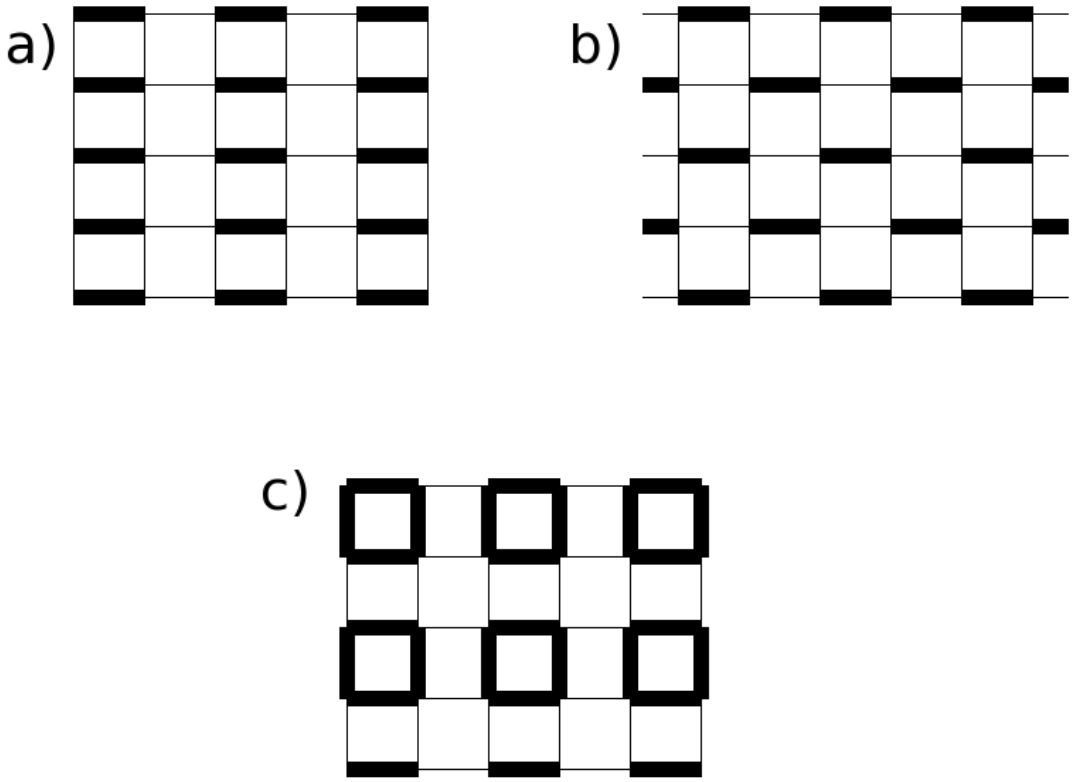

Figure 1.6. Shown are three examples of valence bond solids: a) the columnar state. (b) the staggered state. (c) the plaquette state.

high to the probability to find a dimer on a "thin" link. The square lattice plaquette state is symmetric under rotation and translation by two lattice spacings in x- and y-direction. The plaquette state is expected to be found (in a generalized form) on other two dimensional lattices and higher lattices. Today known is that the square [28, 29, 40] and honeycomb [30] lattice exhibit this phase with numerical evidence backing the picture that it starts immediately to the left of the RK point.

Apart from the here discussed columnar, staggered and plaquette state, there are more (complicated) ways to "freeze" the dimers on certain links in order to create a pattern. Theoretically there is no limit to the size of the unit cell. As an example we refer to the triangular lattice QDM where a crystalline state with a unit cell of 12 sites has been found. This phase is named "$\sqrt{12} \times \sqrt{12}$" phase and is thought to be the only phase between the columnar phase and the Z_2 liquid phase [34].

After the successful demonstration that exotic phases such as spin liquids and valence bond crystal do arise in QDM models, the next logical step is to ask about possible consequences for the corresponding spin models. Recalling the mismatch of the respective scalar products of the dimer coverings and the valence bond product states, it remains a non-trivial question if well established phases in the dimer model "carry over" to a corresponding spin model. Is it possible to find or construct a local SU(2)-invariant spin-1/2 Hamiltonian that has a Z_2 quantum spin liquid phase after Moessner and Sondhi [32] and Misguich *et al.* [33] proved the existence of a Z_2 quantum lattice liquid on the triangular and the kagome lattice roughly a decade ago ? The purpose of this thesis is to give a positive answer to this question. We note that in 2009, a local, SU(2)-invariant spin 1/2 Hamiltonian on the *kagome* lattice was constructed in Ref. [51]. To the best of our knowledge, this is the only Hamiltonian of its kind in the literature. However, it is still necessary to further investigate this Hamiltonian [51] and its properties. Before we do so, we will provide for reasons of completeness the contributions of other researchers to this question. A well known work that decorates the links of the lattice with additional degrees of freedom and

thereby make the lattice more complicated, lead to the construction of a SU(2)-invariant parent Hamiltonian [41]. More significant work in order to find parent Hamiltonians that have exotic ground states was also done in Ref. [42] and in Ref. [43]. However, Refs. [42] and [43] do not consider the case of a parent Hamiltonian on the *kagome* lattice.

1.5 Fractionalization

One striking feature of topological order is the concept of fractionalization. The fractional quantum Hall effect [18], the first experimental system from which evidence of topological order was retrieved, exhibits fascinating behavior: an electron gas can organize itself in such a way that its elementary excitations carry a fraction of the electron charge e and obey fractional statistics [44]. Another way of interpreting this is saying that the electron behaves as if had split into more basic constituents. We will provide a simple picture for the sake of understanding this phenomenon. An interesting modification of the system is provided by inserting monomers in the system. In the simplest case, we remove a dimer from the system and are then left with two unoccupied sites. They monomers can move through the system by shifting dimers neighboring the monomers in such a way that the shifted dimer occupies the sites of the monomers. For the dimer model, it is known that this type of excitations are deconfined, [5] since the monomers can be separated to large distance at a finite

[5]The word confine is chosen/borrowed from the field of quantum chromodynamics: however, here the situation is reverse, e.g. it is *not* possible to separate a pair of isolated quarks at a finite cost of energy. The quarks are confined.

cost of energy. Therefore, the removal of one dimer has given rise to two independent quasiparticles [6] [45]. Going back to the spin model, the dimers get replaced by a singlet. In the spin case, an elementary magnetic excitation refers to replacing a singlet with a triplet state. Upon breaking a triplet -fractionalizing a triplet- two spin-1/2 excitations called spinons can move independently through the system. The elementary excitations of conventional symmetry-broken (anti)-ferromagnets are spin waves (magnons) that always carry spin 1. Another scenario evolves from removing a single electron. Since this electron was just part of a singlet bond, we are left with a an unpaired electron. If these two defects –the lone electron and the hole from the removed electron– can move apart at a finite cost of energy, the electron has fractionalized into the spinon carrying a spin 1/2 and charged (+e), spinless holon. This variation of fractionalization is commonly called spin-charge separation [5].

1.6 Experimental search for quantum spin liquids

The experimental situation when it comes to the challenging search for the quantum spin liquid phase is similar to the theoretical situation: although proposed 40 years ago [1], experimental evidence emerged only in the last few years. Maybe the most prominent candidate compound for a spin liquid is the herbertsmithite, a naturally occurring mineral, [7] whose chemical formula is $ZnCu_3(OH)_6Cl_2$. The spin

[6] All the constituent particles of the system, e.g. all dimers, are associated with charge 2, then these elementary monomer excitations carry a charge of -1, thus, they are "fractionalized".

[7] It is named after the mineralogist Herbert Smith and was first found in 1972 in Chile. The compound is a polymorph of kapellasite and closely related to paratacamite; herbertsmithite is generally found in and around Anarak, Iran, hence its other name, anarakite.

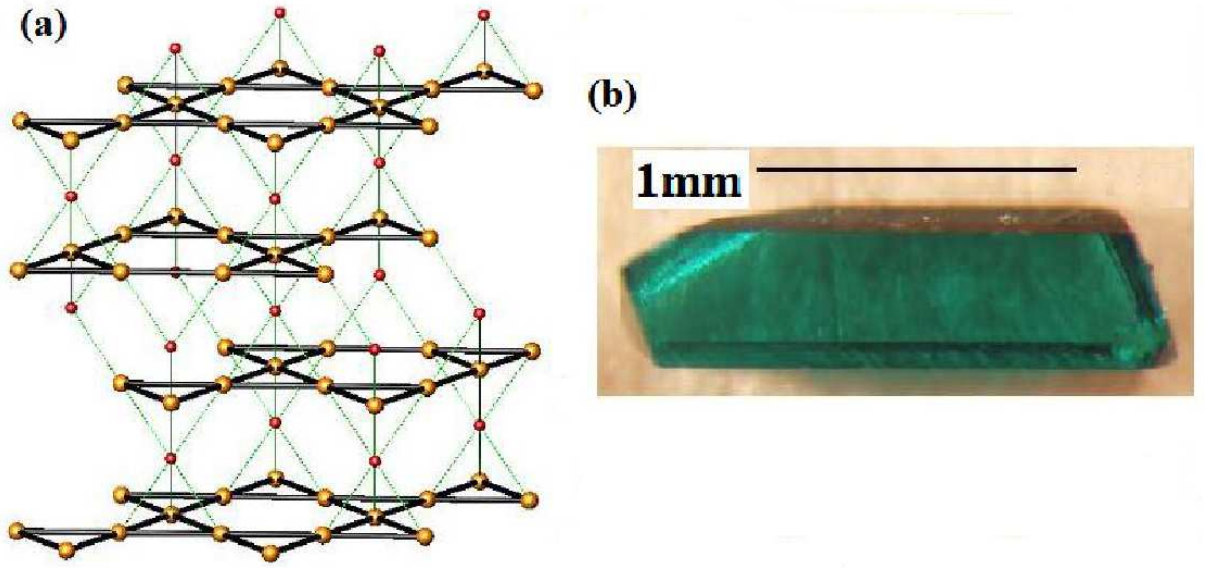

Figure 1.7. (a) Shown is the structure of $ZnCu_3(OH)_6Cl_2$ with only Cu^{2+} (large brown spheres) and Zn^{2+} (small red spheres) displayed. The Cu-Cu bonds (thick black solid lines) are all equivalent as are the Cu-Zn bonds (thin green dotted lines). (b) A single-crystal sample of $ZnCu_3(OH)_6Cl_2$. Figure taken from Ref. [49].

1/2 compound has a kagome lattice of corner-sharing triangles. Until now, there is no data showing any kind of order in this material down to very low temperatures. [46–48] Furthermore, just recently, MIT researchers employed the method of neutron scattering and found strong evidence of fractional excitation which is a signature of the exotic spin liquid state. [49] Nonetheless, researchers keep on adding other compounds to the pool of candidates. Very recently in 2011, chemists synthesized a new kagome antiferromagnet [50], designated DQVOF, which is different from herbertsmithite and other similar compounds in that its magnetic properties stem from ions of spin 1/2 vanadium, rather than copper. To get a better understanding of the mate-

rial, samples of this compound were studied with muon spin relaxation experiments. The data show an absence of spin freezing down to 40 mK, which is considered a clear spin liquid signature. However, in order to make a more rigorous statement on a possible spin liquid ground state, it is necessary to further investigate the magnetic excitation spectrum. [50]

1.7 Outline of the thesis

The thesis is organized as follows. After the presented brief summary and overview of the matter of topological phases, Chapter 2 will review a Hamiltonian that was constructed/claimed to realize a special topological phase, namely the Z_2 quantum spin liquid. Then, we will investigate the properties of the ground state of this Hamiltonian, thereby focusing on the behavior of local correlation functions. In order to be able to do so, we employed a newly developed (classical) Monte Carlo scheme, which we call Pfaffian Monte Carlo. We explore and discuss further issues of the uniqueness of the ground state of this Hamiltonian and the existence of a gap.

In chapter 3, we will solve a long standing problem of the physics of resonating valence bond physics: a proof that the nearest neighbor valence bond states on several 2D lattices are indeed linearly independent is shown and the possible application/usefulness of the linear independence (LI) property are discussed.

Chapter 4 introduces another Hamiltonian which is made of two types of interactions, the Heisenberg interaction and the Dzyaloshinskii-Moriya (DM) interaction, living on the sawtooth chain. We discuss this model in the context of being an approx-

imation to the same Hamiltonian on the kagome lattice. The effect of the interplay between the two interaction couplings on the phase diagram is investigated. To do so, we employ modern techniques such as the density matrix renormalization group (DMRG) scheme. We find that for weak DM interaction the system exhibits valence bond order. However, a strong enough DM coupling destroys this order.

2. Existence of a Z_2 quantum spin liquid

This chapter is devoted to present the necessary steps in order to provide (sufficient) evidence that indeed the Z_2 quantum spin liquid does exist in a spin system. Here, we focus on the case of spin 1/2 and we require the system -in other words our Hamiltonian- to be local and SU(2) invariant. We will mainly focus on the case that has the Hamiltonian living on the kagome lattice. Nonetheless, we will also show some results on the second nonbipartite lattice that frequently appears in the literature: the triangular lattice. The above mentioned Hamiltonian was already published [51] in 2009. Nonetheless, an investigation of its properties, more precisely the properties of its ground state wave function, was still missing. The ground state wave function is the *equal* amplitude superposition of all valence bond coverings. A valence bond state being a product state of nearest neighbor singlets:

$$|\psi_{GS}\rangle = \sum_D |D\rangle \,. \tag{2.1}$$

Here, D stands for a valence bond covering. Especially the question if the ground state wave function Eq. (2.11) indeed lies in the Z_2 quantum spin liquid ground state as claimed and conjectured in Ref. [51] is of interest. In order to investigate the properties of the ground state wave function of the Hamiltonian, it was necessary to derive a new Monte Carlo scheme since another previously in the literature appearing MC scheme -valence bond Monte Carlo- suffers from a sign problem on nonbipartite

lattice and is therefore inapplicable to our kagome lattice system. If the lattice is bipartite, valence bond Monte Carlo is applicable [54, 55]. The results of this chapter have been published in

Julia Wildeboer and Alexander Seidel, Phys. Rev. Lett. 109, 147208 (2012) .

2.1 A local, SU(2) invariant spin-1/2 Hamiltonian and its ground state

This section is devoted to the presentation of a local, SU(2) invariant spin-1/2 Hamiltonian. This Hamiltonian is constructed in such a way that its ground state is a Z_2 quantum spin liquid. To be more precise, Eq. (2.11) is per construction the ground state of the Hamiltonian. What is left to do at this point is provide evidence that Eq. (2.11) is indeed capable of describing a Z_2 spin liquid state. In order to motivate our choice of wave function, we recall the quantum dimer model on the kagome lattice. A well known work by Misguich *et al.* [33] showed that the RK point of the QDM lies in the interior of a Z_2 quantum spin liquid phase on the kagome lattice. The Hamiltonian of the QDM on the kagome lattice is a sum of operators acting on 12-site cells as depicted in Fig. 2.2). Any possible dimer covering of this cell defines a loop [52] around the central hexagon, given by the (shortest) line connecting all points touched by a dimer, see Fig. (2.3). Each loop is associated with with two possible dimer coverings of the 12-site cell. The two coverings are related to each other by a shift by one lattice link along the respective green line. Such a shift is called "resonance move". Every dimer covering D of the lattice imposes a

covering $D_{\mathcal{C}}$ of every 12-site cell C, and a corresponding loop. The Hamiltonian of the QDM of this lattice is a sum of operators acting on any 12-site cell of the lattice, where each operator performs a resonance move on the loop of dimers present on the cell it acts on [33]. The ground states of this Hamiltonian is the equal amplitude superpositions of all dimer states within a topological sector. In this case, there exists four degenerate ground states. The system being in one specific topological sector, stays in the same sector if the dynamics are governed by the above described "resonance moves". These four ground states, the equal amplitude superposition of all dimer coverings in a respective topological sector, were shown [33, 53] to be Z_2 quantum liquids.

In order to make connection with the spin model, we need to replace the dimers by singets. In order to properly define a singlet on a link, the link must be endowed with an orientation. This is so, since the singlet is of antisymmetric nature. In other words, to make a one-to-one correspondence between dimer covering and singlet covering, the overall phases of the valence bond states now matter and must be addressed. A convention for the overall phase of a valence bond state can be given by choosing an orientation for each link of the lattice. Thus, the sign of each valence bond singlet ($[ij] = -[ji]$) on the link (i, j), and thus of the full valence bond product state, which is fixed. A suitable way to orient links is to do so counterclockwise around each hexagon, Fig. (2.1). A resonance move can now be interpreted as a cyclic permutation of the spins long a loop of dimers. With the chosen orientation of links, the sign associated with the state is preserved by such moves. This is so since for any given 12-site cell

of the lattice, flipping the orientation of the links touching boundary sites does not change the sign of any valence bond state. The reason for this lies in the matter of fact that any possible dimer coverings of the 12-site cell shown in Fig. (2.3) covers an even number of such links. With this new orientation shown in Fig. (2.2), all links of the 12-site cell are oriented counterclockwise around the central hexagon. Thus, clearly a cyclic permutation of spins around a dimer loop preserves the overall sign belonging to the state. Consequently, if the basis of valence bond states is defined using the sign convention derived from this link orientation, resonance moves on dimer states will translate into cyclic permutations of spins in the associated valence bond states. Armed with this knowledge, we now recall the construction of the local, SU(2)-invariant spin-1/2 Hamiltonian that has the equal amplitude superposition of all singlet coverings as its ground state from Ref. [51]. The Hamiltonian will be written in form of projection operators. These projection operators act on certain states living on the 12-site star. The nature of these states and subsequently the nature of the projection operators will be explained in the following. The following Hamiltonian is considered in Ref. [51]

$$H_{RVB} = -\sum_{\mathcal{C}} R_{\mathcal{C}} \ . \tag{2.2}$$

Here, the sum goes over all 12-site "star-shaped" cells (as defined above, Fig.2.2a)) of the lattice, and the $R_{\mathcal{C}}$ are specific Hermitian projection operators that enforce a "resonance" condition. We assume that we work with periodic boundary conditions. All we need to do now is to specify how the projection operators $\mathcal{R}_{\mathcal{C}}$ are defined. To make progress, we note that the projection operators have two eigenvalues —1

and 0—, thus they either let a state that they act on survive or they kill the state. Consequently, we will now introduce that states that the $\mathcal{R}_{\mathcal{C}}$ act on. We note that every dimer pattern D on $\mathcal{C}$ corresponds to one of two realizations of a certain loop around the central hexagon, Fig. (2.3). D^* denotes the other realization, related to D by a resonance move. We can now define a set of "resonant states" $\mathcal{R}(\mathcal{C})$ via:

$$\mathcal{R}(\mathcal{C}) = \{ \left(|D\rangle + |D^*\rangle\right) \otimes |\psi_{D,j}\rangle \ : D \in \mathcal{D}(\mathcal{C}), j = 1 \ldots n_D \}. \tag{2.3}$$

Form the elements of $\mathcal{R}(\mathcal{C})$, we can linearly generate any state consisting of a resonant dimer loop, with the free sites not touched by the loop in an arbitrary state. Note that $\mathrm{free}(D) = \mathrm{free}(D^*)$, and we may without loss of generality assume that $\psi_{D,j} = \psi_{D^*,j}$.

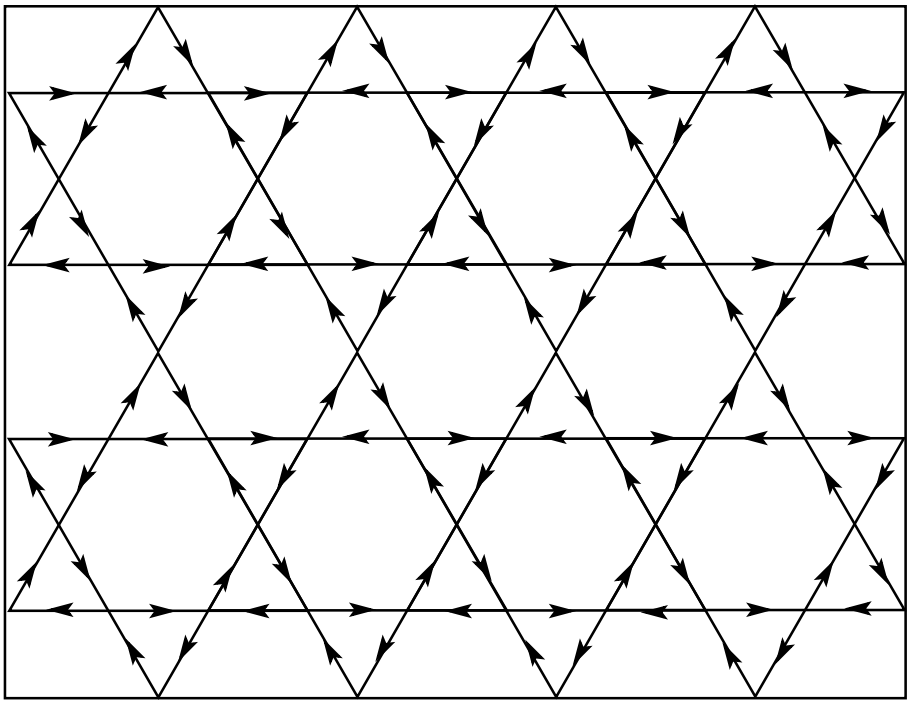

Figure 2.1. Shown is an orientation of links on the kagome lattice used to fix the sign of valence bond states. All links are oriented counterclockwise around the hexagon they belong to. Figure is taken from Ref. [51].

Now we are in the position to define the space $RL(\mathcal{C})$ of "resonance loop" states on $\mathcal{C}$, via

$$RL(\mathcal{C}) = \sum_{D \in \mathcal{D}(\mathcal{C})} \mathcal{H}(|D\rangle + |D^*\rangle) \ . \tag{2.4}$$

The set $\mathcal{R}(\mathcal{C})$ linearly generates the space $RL(\mathcal{C})$, and in fact turns out to be a basis of $RL(\mathcal{C})$.It is now only natural to define the operator $R_{\mathcal{C}}$ to be the *orthogonal* projection onto the subspace $RL(\mathcal{C})$. At this point it should be pointed out that the Hamiltonian Eq. (2.2) then has all the symmetries of the underlying lattice. In addition, it is invariant under SU(2) rotations, since the space $RL(\mathcal{C})$ is SU(2)-invariant for each $\mathcal{C}$.

Now we turn our attention to spin-1/2 realizations of wave functions of the following form

$$|\psi\rangle_\Omega = \sum_{D \in \Omega} |D\rangle \ , \tag{2.5}$$

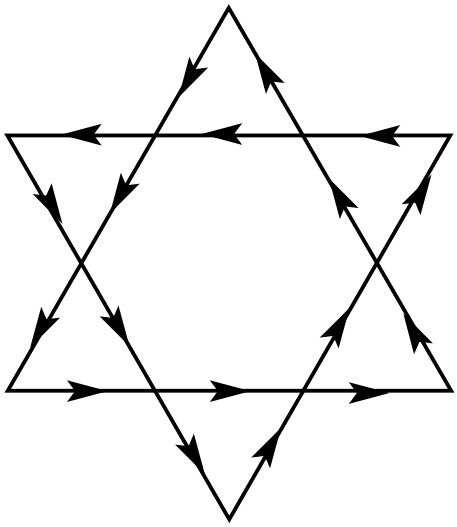

Figure 2.2. Shown is the 12-site "star" that serves as the minimal unit of the lattice that the Hamiltonian acts on. Also shown is the chosen link orientation for this cell. All links are oriented counterclockwise around the central hexagon. Figure is taken from Ref. [51].

where $\Omega \subset \mathcal{D}(\mathcal{C})$ contains all dimer coverings in a topological sector as described above.

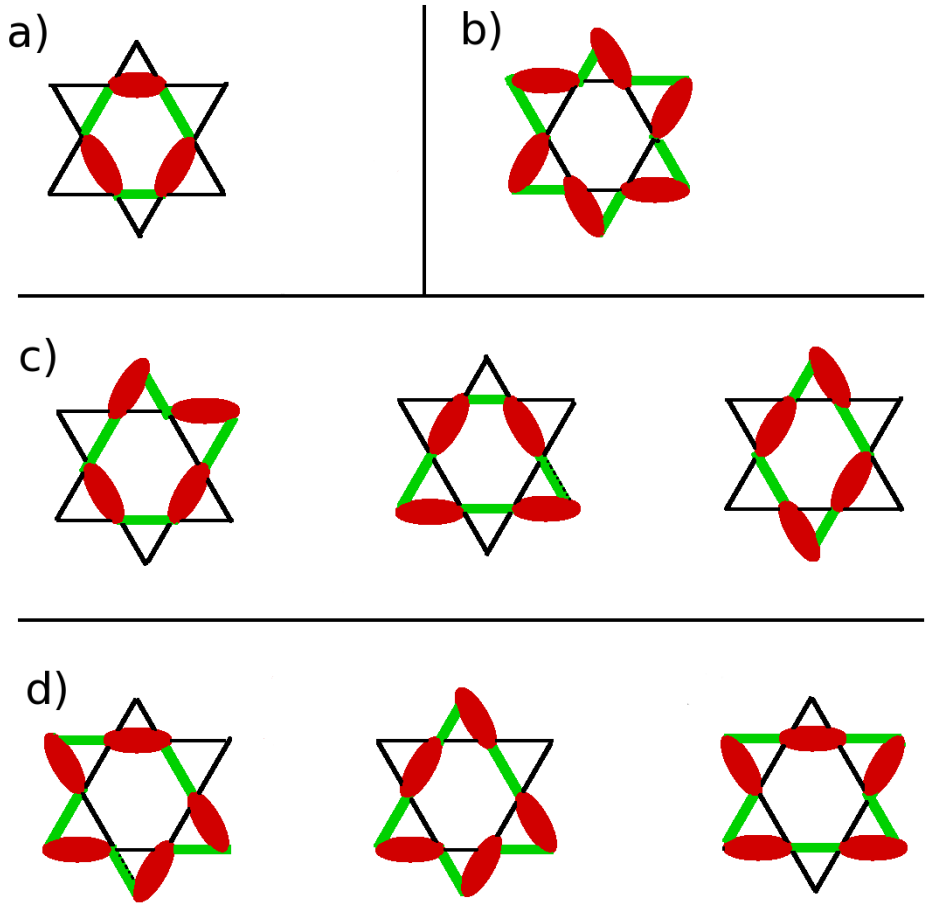

Figure 2.3. Eight different types of dimer loops around a central hexagon. [52] Loops may be formed by three (a), six (b), four (c), or five (d) dimers. Each loop can be realized by two different dimer configurations related by a resonance move. Dashed lines indicate dimer configurations after a resonance move. The loops should be regarded as the transition graphs between the original and the resonated configuration, i.e. the set of all links carrying either a dimer or a dashed line. Using rotational symmetry, there are 32 different loops corresponding to 64 dimer configurations.

Eq. (2.5) is a ground state of Eq. (2.2) and of every operator $-R_{\mathcal{C}}$. Every state of the form

$$(|D_{\mathcal{C}}\rangle + |D_{\mathcal{C}}^*\rangle) \otimes |S\rangle\,, \tag{2.6}$$

is invariant under the action of $R_{\mathcal{C}}$, where again $D_{\mathcal{C}}$ is a dimer covering of the cell $\mathcal{C}$, and $|S\rangle$ is any state on the "rest" of the lattice, e.g. all sites except for the ones on the 12-star forming the dimer covering that has two spin realizations as discussed above. Eq. (2.6) can be thought of as having a "resonance loop" on the cell $\mathcal{C}$. Since the eigenvalues of $R_{\mathcal{C}}$ are 0 and 1, Eq. (2.6) is thus a ground state of $-R_{\mathcal{C}}$. To clarify it even more, we write Eq. (2.5) as a double sum

$$|\psi\rangle_\Omega = \sum_{D_{\mathcal{C}}} \sum_{\overline{D_{\mathcal{C}}}} |D_{\mathcal{C}}\rangle \otimes |\overline{D_{\mathcal{C}}}\rangle \tag{2.7}$$

The outer sum goes over all dimer coverings of the cell $\mathcal{C}$, whereas the inner sum goes over all possible complements $\overline{D_{\mathcal{C}}}$ of $D_{\mathcal{C}}$ such that $D_{\mathcal{C}} \cup \overline{D_{\mathcal{C}}} =: D$ is a dimer covering of the full lattice in the topological sector Ω. Note that for $D_{\mathcal{C}}^*$ instead of $D_{\mathcal{C}}$, the possible choices for $\overline{D_{\mathcal{C}}}$ are exactly the same, since $D_{\mathcal{C}}^*$ and $D_{\mathcal{C}}$ live in the same sites and the dimer coverings $D_{\mathcal{C}} \cup \overline{D_{\mathcal{C}}}$ and $D_{\mathcal{C}}^* \cup \overline{D_{\mathcal{C}}}$ are in the same topological sector by definition, since they differ only by a local resonance move. Consequently, we can rewrite Eq. (2.7) as

$$|\psi\rangle_\Omega = \sum_{(D_{\mathcal{C}}, D_{\mathcal{C}}^*)} \sum_{\overline{D_{\mathcal{C}}}} (|D_{\mathcal{C}}\rangle + |D_{\mathcal{C}}^*\rangle) \otimes |\overline{D_{\mathcal{C}}}\rangle \tag{2.8}$$

where the first sum now goes over (unordered) pairs $(D_{\mathcal{C}}, D_{\mathcal{C}}^*)$. Since Eq. (2.8) is a sum over states of the form Eq. (2.6), it is invariant under the action of $R_{\mathcal{C}}$. This proves that $|\psi\rangle_\Omega$ is a ground state of $-R_{\mathcal{C}}$ for each $\mathcal{C}$. Hence $|\psi\rangle_\Omega$ is a ground state

of the Hamiltonian Eq. (2.2). The interested reader may turn to Ref. [51] for more details describing how this Hamiltonian is brought to life.

2.2 Pfaffian Monte Carlo

After the presentation of the Hamiltonian and its ground state wave function

$$|\psi_{GS}\rangle = \sum_{D} |D\rangle \,. \tag{2.9}$$

we now want to amass evidence that this wave function indeed is capable of describing a Z_2 quantum spin liquid state. To make progress on this task, it is necessary to investigate the behavior of local correlation functions. We note at this point that the analogos wave function from above has been studied on the square lattice. This was done by using valence bond Monte Carlo. [54,55] We will now see how the investigation of observables can be expressed is a simple statistical mechanics problem. A general correlator between two local operators $\mathcal{O}_1$ and $\mathcal{O}_2$ takes on the form:

$$\frac{\langle RVB|\mathcal{O}_1\mathcal{O}_2|RVB\rangle}{\langle RVB|RVB\rangle} = \frac{\sum_{D,D'}\langle D|\mathcal{O}_1\mathcal{O}_2|D'\rangle}{\sum_{D,D'}\langle D|D'\rangle} \tag{2.10}$$

Here the sum is over pairs of dimer coverings D, D'. Any such pair describes a close packed loop configuration on the lattice. For this reason, as observed long ago by Sutherland [25], the problem of evaluating the correlation function (2.10) maps onto that of evaluating a correlation function of a *classical* loop gas model, *provided that* all the overlaps $\langle D|D'\rangle$ in the denominator (which plays the role of a

partition function) are positive. At this it shall be pointed out that Marshall's sign rule guarantees the existence of a link orientation that satisfies the condition that all overlaps $\langle D|D'\rangle$ are positive for all bipartite lattices. This is the reason why valence bond Monte Carlo is a sign problem free algorithm for the square lattice from Refs. [54] and [55]. Unfortunately, the last condition is not satisfied for the sign convention chosen in Fig. (2.2), or for any sign convention for valence bond states on the kagome lattice. This means that the analogy with classical loop models is not perfect, and the evaluation of the correlator (2.10) using Monte Carlo methods would suffer from a sign problem. Subsequently, we note that valence bond Monte Carlo is not applicable to the kagome lattice.

The question now after understanding that the valence bond basis is not a suitable basis for a Monte Carlo scheme is: Is it possible to find a basis and recast the wave function in the new basis so that all overlap of valence bond configurations is positive ? The answer is yes. The idea now to overcome this sign problem is to write the correlator of (2.10) as a sum of an entirely different sort, not over dimer coverings but in fact over the Ising-basis of the full spin-1/2 Hilbert space. By "Ising-basis", we mean the basis $|\{\sigma\}\rangle$ of states where each spin on the lattice has a well defined z-projection given by $\frac{1}{2}\sigma_i$, $\sigma_i = \pm 1$. Certainly, we can expand the wave function (2.9) in this basis:

$$|RVB\rangle = \sum_{\{\sigma\}} a_{\{\sigma\}} |\{\sigma\}\rangle \ . \tag{2.11}$$

We will soon see that expressing the wave function in this way will solve the sign problem, since now there are only diagonal overlaps contributing to the partition func-

tion (the Ising basis is orthogonal), and hence there are no negative signs. However, the big issue is whether the coefficients $a_{\{\sigma\}}$ are easily available. We will now show that they can be expressed through a Pfaffian, and should thus be computable in polynomial time. This may make the problem similarly hard (or perhaps slightly less so due to its discrete nature) as calculating correlation functions in Pfaffian quantum Hall wave functions.

We proceed in two steps. We first show that the coefficients in (2.11) can be written in terms of a Haffnian. The Haffnian relates to the Pfaffian like the permanent related to the determinant, i.e. it has the same definition without the negative signs from characters of permutations. Unfortunately, the Haffnian, like the permanent, cannot be calculated in polynomial time. Only the determinant and the Pfaffian can. Luckily, however, it turns out that the same trick due to Kasteleyn [57] that allows the calculation of correlation functions in classical dimer models through Pfaffian methods also works in this case, and allows us to recast our Haffnian as a Pfaffian.

We begin by writing the coefficients $a_{\{\sigma\}}$ in (2.11) as the Haffnian of a matrix defined in terms of the Ising configuration $\{\sigma\}$. To this end, we first define a matrix Θ_{ij} that encodes the link orientation of the lattice

$$\Theta_{ij} = \begin{cases} 0, & i = j \text{ or } i,j \text{ not nearest neighbors} \\ -1, & i < j \\ +1, & i > j \end{cases} \tag{2.12}$$

Here, the statements $i < j$ and $i > j$ just refer to the orientation of the arrow on the link between the nearest neighbors i and j in the orientation of Fig. (2.2). We also define the wave function of a singlet pair on sites i and j:

$$\chi(\sigma_i, \sigma_j) = \delta_{\sigma_i,\uparrow}\delta_{\sigma_j,\downarrow} - \delta_{\sigma_i,\downarrow}\delta_{\sigma_j,\uparrow}\,. \tag{2.13}$$

With these definitions, we introduce a symmetric matrix $M_{ij}(\{\sigma\})$, where i, j are site indices, as

$$M_{ij}(\{\sigma\}) = \Theta_{ij}\chi(\sigma_i, \sigma_j)\,. \tag{2.14}$$

In terms of this matrix, it turns out that the coefficients $a_{\{\sigma\}}$ can be written as:

$$\begin{aligned} a_{\{\sigma\}} &= \text{Haff}(M_{ij}) \qquad (2.15)\\ &\equiv \frac{1}{2^{N/2}(\frac{N}{2}!)} \sum_{\lambda\in S_N} M_{\lambda_1\lambda_2}(\{\sigma\})M_{\lambda_3\lambda_4}(\{\sigma\}) \times \cdots \times M_{\lambda_{N-1}\lambda_N}(\{\sigma\}) \end{aligned}$$

Here, N is the dimension of M_{ij}, i.e. the number of spins or lattice sites. It is not difficult to see that the sum over permutations λ effectively runs over all possible dimer coverings, modulo re-arrangements of dimers and modulo exchanges of the two sites of any pair. Specifically, any λ that gives a non-zero contribution is such that the pairing induced by $(\lambda_{2n-1}, \lambda_{2n})$ corresponds to a dimerization of the lattice. All λ's corresponding to the same pairing enter with the same amplitude, and the overall factor $2^{N/2}(\frac{N}{2}!)$ which is divided out just is the multiplicity with which each dimer covering is represented by such permutations. It is thus clear that the expression

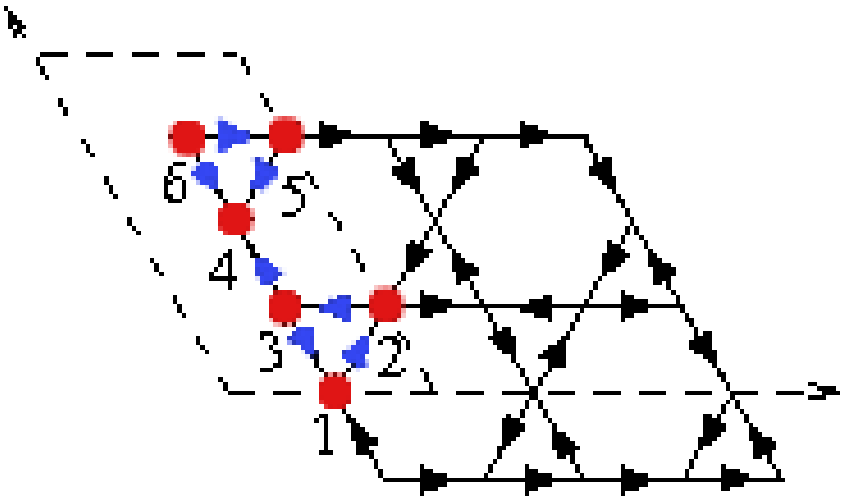

Figure 2.4. A Kasteleyn orientation for the kagome lattice taken from Ref. [56].

on the right hand side is just a wave function equal to the sum over all products of admissible singlet configurations, evaluated for the Ising configuration $\{\sigma\}$.

We have thus succeeded in writing the coefficients $a_{\{\sigma\}}$ as a Haffnian. This is not quite good enough yet for efficient evaluation, as discussed above. To make progress, we define a "Kasteleyn orientation" of the lattice, as shown in Fig. (2.4).

For this orientation, we also define a matrix Θ^K_{ij} exactly as in Eq. (2.12), but with respect to the different orientation shown in Fig. (2.4). With this we can now define a new anti-symmetric matrix $\tilde{M}_{ij}$:

$$\tilde{M}_{ij} = M_{ij}\Theta^K_{ij} \; . \tag{2.16}$$

It turns out that in terms of $\tilde{M}_{ij}$, the coefficients $a_{\{\sigma\}}$ can be expressed as a Pfaffian:

$$\begin{aligned} a_{|\sigma_1 \ldots \sigma_N\rangle} &= \text{Pfaff}(\tilde{M}_{ij}) \qquad (2.17) \\ &\equiv \frac{1}{2^{N/2}(\frac{N}{2}!)} \sum_{\lambda \in S_N} (-1)^{\lambda} \tilde{M}_{\lambda_1\lambda_2}(\{\sigma\})\tilde{M}_{\lambda_3\lambda_4}(\{\sigma\}) \times \cdots \times \tilde{M}_{\lambda_{N-1}\lambda_N}(\{\sigma\}). \end{aligned}$$

The reason why this works is that for all λ's corresponding to dimer coverings, the additional sign $(-1)^\lambda$ is precisely canceled by the additional signs coming from the Θ_{ij}^K factors (possibly up to a constant factor -1 which does not depend on $\{\sigma\}$ and is thus irrelevant). This was shown by Kasteleyn [57], who was facing almost the exact same technical problem. (If M_{ij} is replaced by its modulus, Haff(M_{ij})=Pfaff($\tilde{M}_{ij}$) is just the partition function of the classical hard core dimer gas).

We are now in a position to cast the problem of evaluating the correlation functions (2.10) as a classical statistical mechanics problem. To ease the notation, we will now write $I \equiv \{\sigma\}$ for Ising configurations. We then have:

$$\begin{aligned} \frac{\langle RVB|\mathcal{O}_i\mathcal{O}_j|RVB\rangle}{\langle RVB|RVB\rangle} &= \frac{\sum_I \sum_{I'} a_I a_{I'} \langle I'|\mathcal{O}_i\mathcal{O}_j|I\rangle}{\sum_I |a_I|^2} \\ &= \frac{\sum_I |a_I|^2 \sum_{I'} \frac{a_{I'}}{a_I} \langle I'|\mathcal{O}_i\mathcal{O}_j|I\rangle}{\sum_I |a_I|^2} \end{aligned} \tag{2.18}$$

This may now be interpreted as the classical expectation value $\langle f\rangle$ of a quantity f:

$$\langle f\rangle = \frac{\sum_I f_I e^{-E_I}}{\sum_I e^{-E_I}}\,. \tag{2.19}$$

Here,

$$e^{-E_I} = |a_I|^2\,, \tag{2.20}$$

and the value f_I of the quantity f in the Ising configuration I is given by

$$f_I = \sum_{I'} \langle I'|\mathcal{O}_i\mathcal{O}_j|I\rangle \frac{a_{I'}}{a_I} \tag{2.21}$$

It is important to note that for given local operators $\mathcal{O}_i$, $\mathcal{O}_j$, the sum over I' in (2.21) can be restricted to a very few terms which are a priori known. Specifically, if $\mathcal{O} = S_z$

is the z-component of a local spin, the product $\mathcal{O}_i\mathcal{O}_j$ is diagonal in the Ising basis, and only $I' = I$ contributes, so the sum has only one term.

We have now solved the sign problem in principle, by casting the correlator (2.18) as a classical expectation value, with "Boltzmann factors" that can be evaluated in polynomial time, the evaluation of correlation functions can be cast in terms of a partition function, whose weights are positive. For reasons of numerical efficiency, one should make use of the matter of fact that the structure of our Pfaffian allows a reduction to the determinant of an $N/2 \times N/2$ matrix. Returning to our earlier caveat, we moreover found that once we have an initial Ising configuration I with $a_I \neq 0$, performing updates by exchanging neighboring spins has a high chance of leading to a new configuration I' with $a_{I'} \neq 0$, The basic requirements for Monte Carlo evaluation are thus met. To close this chapter, we note that in the case of periodic boundary conditions, we have a fourfold ground state degeneracy. Our method allows to access each ground state wave function for itself, we can restrict us to a single sector. Another newly developed method applied to investigation short-ranged RVB wave functions is the "Projected Entangled Pair States" (PEPS) method. [58] However, using PEPS, it not possible to employ PBC and subsequently it is not possible to investigate the topological degeneracy.

2.3 Results

In order to execute our Pfaffian Monte Carlo scheme, [1] we start by choosing a sign convention for the links of the lattice for the kagome and the triangular lattice. For both lattice types, it is not possible to employ VB Monte Carlo because of a sign problem. However, the equal amplitude superposition of valence bond states has never been investigated before. Therefore, we now investigate this wave function with our new Pfaffian Monte Carlo method. For the kagome lattice, we orientate all links counterclockwise along the hexagons. Simulations are now performed for differnt lattices sizes. For the kagome lattice, we have chosen (m, n) as defined in Fig. (2.5)

[1] The code was partially based on the ALPS code. [65, 66]

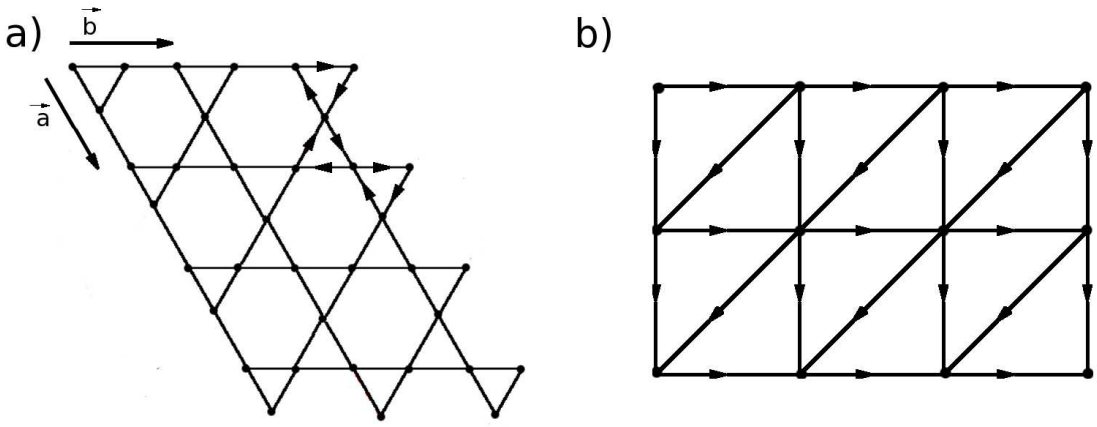

Figure 2.5. a) Shape of the kagome lattice used in the calculations. The lattice consists of m unit cells in the **a** direction and n unit cells in the **b** direction, for a total of $3mn$ sites. Periodic boundary conditions may or may not be introduced with periods $m\mathbf{a}$ and $n\mathbf{b}$. b) The orientation used in the sign convention for the triangular lattice.

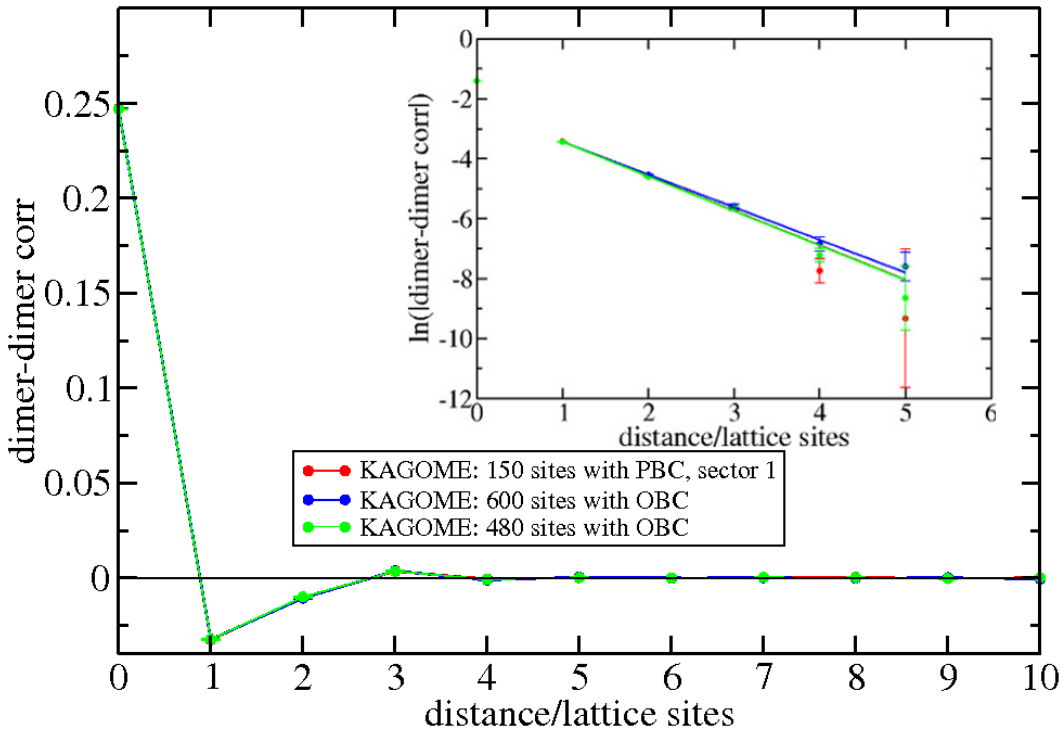

Figure 2.6. The dimer-dimer correlation function shown for kagome lattices with PBCs and OBCs. Insensitivity to system size and short correlation length are evident. The PBC case has been calculated within a fixed topological sector. The inset shows a logarithmic plot including a linear fit, yielding a correlation length of 1.12(3).

to be (10,5) for periodic boundary conditions (PBCs) and to be (20,8) and (20,10) for open boundary conditions (OBCs), resulting in a total number of $N = 150$, 480, and 600 sites, respectively, (and in lattices with roughly unit *perpendicular* aspect ratio).

For the triangular lattice, we show data belonging to a 20×20 "square" with diagonals (see Fig. (2.5)) giving a lattice of 400 sites. In one Monte Carlo sweep through the lattice, we attempt to do a number of N exchanges of two neighboring spins. All expectation values were calculated by making about 1,500,000 measurements on the configurations produced by the Monte Carlo process, allowing the system to equili-

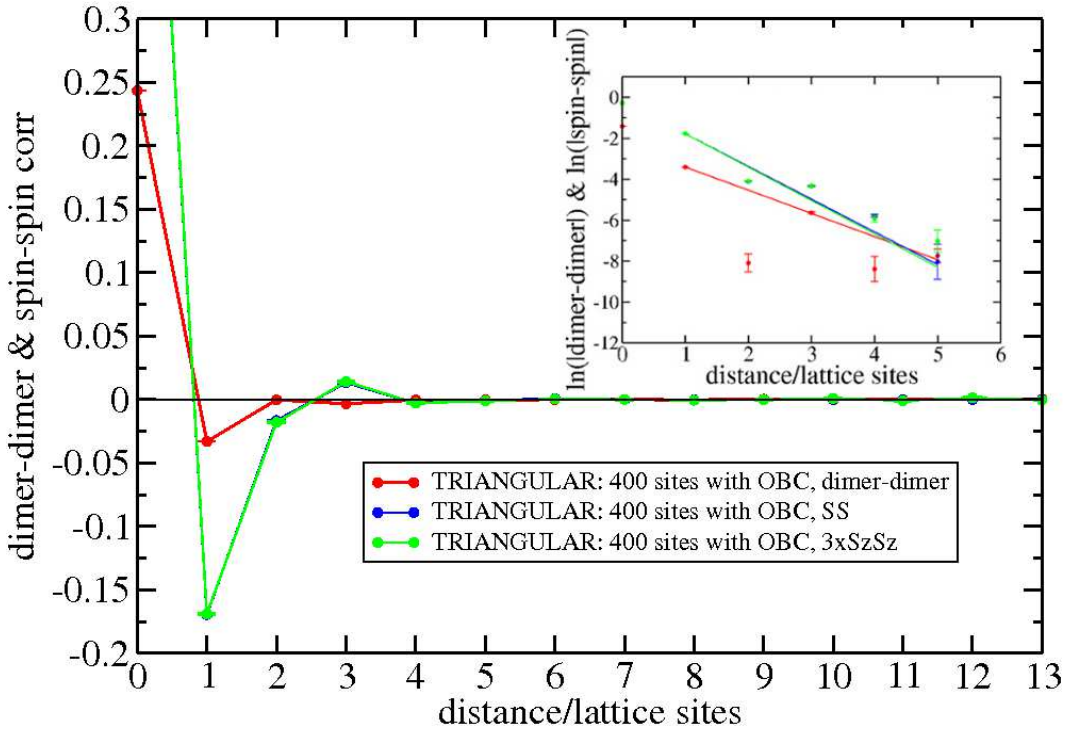

Figure 2.7. The dimer-dimer and spin-spin correlation functions for a 400 sites triangular lattice with OBCs. The inset shows logarithmic plot with fits, giving a correlation length of 1.15(2) for the dimer-dimer decay. The spin-spin correlations display stronger even/odd effects at short distance. Fitting only odd distances in the spin-spin case gives a correlation length of 1.61(2).

brate for 8000 sweeps. Autocorrelation times are generally quite low, on the order of 1.

Fig. (2.6) presents the connected correlation function of the "dimer" or valence bond operator $\vec{S}_i \cdot \vec{S}_{i+x}$, where i and $i+x$ are nearest neighbors, for different lattice sizes and boundary conditions. It is evident that there is a finite and very short correlation length. From the inset it is clear that the absolute values of the correlation functions follow a simple exponential law already at short distance, from which we obtain a correlation length of $\xi = 1.12(3)$. Moreover, the plot for 600 sites and OBCs

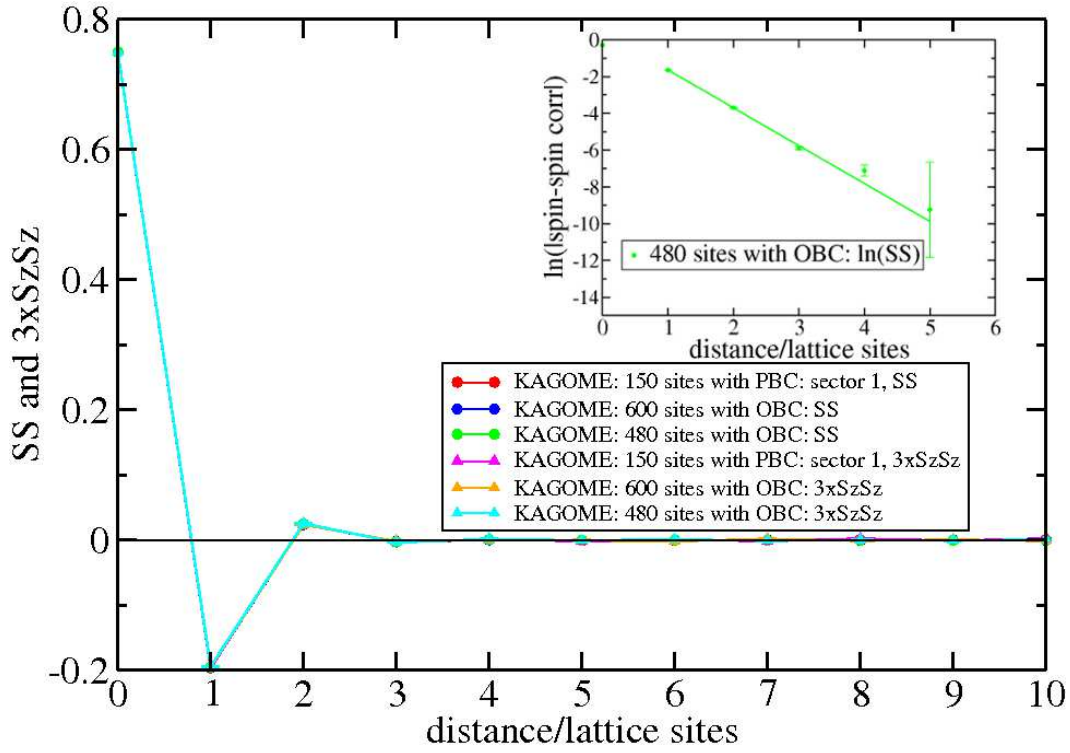

Figure 2.8. The spin-spin correlation functions $\langle \vec{S}_i \vec{S}_{i+\kappa} \rangle$ and $\langle S_i^z S_{i+\kappa}^z \rangle$ for different kagome lattices (PBC and OBC). Again, the topological sector was fixed in the PBC case. The inset shows a logarithmic plot with linear fit yielding a correlation length of 2.08(2).

coincides very well with that for 150 sites and PBCs. We note that for the case of PBCs, the method used to treat the classical dimer case [56] can again be adapted to the present situation, and yields an expression of the amplitude a_I as a superposition of four Pfaffians. Different such superpositions can be used to project onto different topological sectors of the toroidal system. While only one topological sector is shown, we have also convinced ourselves that results for different topological sectors agree within error bars. The fact that the dimer-dimer correlations are apparently insensitive to both lattice size *and* boundary conditions, already for a relatively small size of

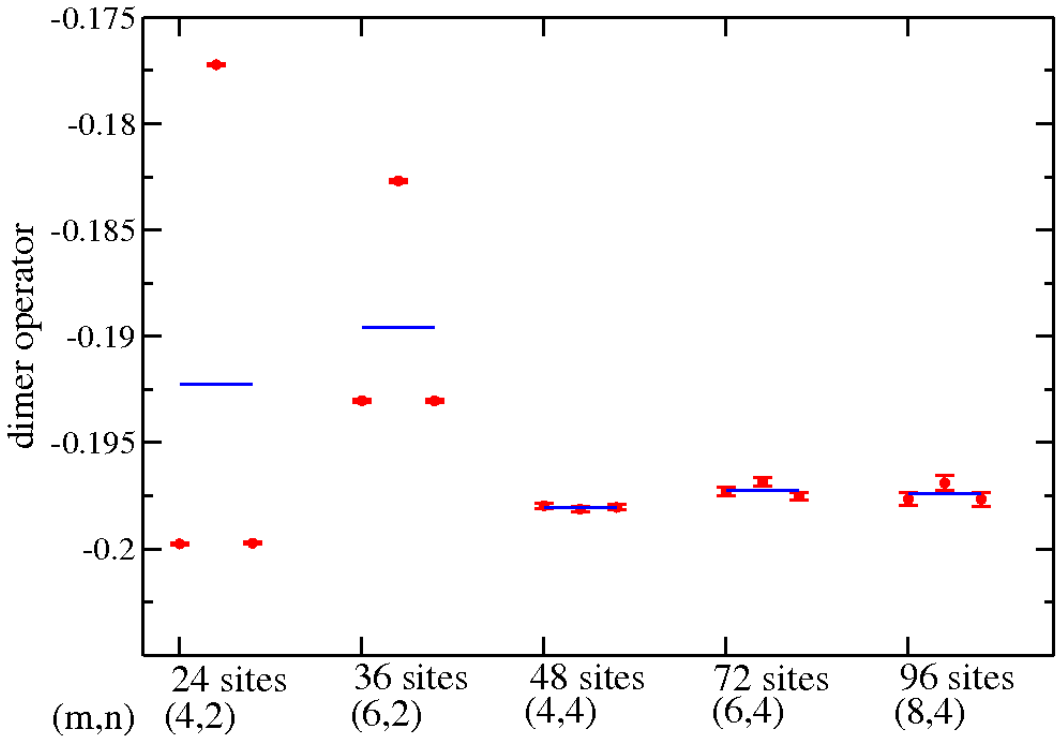

Figure 2.9. The expectation value of the dimer operator for links of the three possible directions and various lattice sizes. The average for one system size is shown as horizontal bar. A topological sector has been fixed. The discrepancy between nonequivalent links rapidly decreases with system size, restoring the lattice symmetry.

150 sites, is consistent with the hypothesis of a gapped state. We note moreover that the decay is very reminiscent of the quantum dimer model case, where dimer-dimer correlations have been shown to decay super-exponentially, with correlations being exactly zero beyond distance 2 [53]. While this is clearly not the case for the RVB state, a very short correlation length of order 1 still mimics this behavior fairly closely. The qualitative agreement between the quantum dimer model and the RVB state is thus quite striking.

Fig. (2.7) shows the dimer-dimer correlations for a 400 site triangular lattice, displaying similarly short ranged correlations. Subdominant corrections to the dominant exponential decay are clearly somewhat more important than for the kagome, as one would generically expect; however a correlation length close to 1.6 is still clearly visible in the inset. All linear fits are obtained from a weighted least square regression, where the weights have been chosen as the inverse squares of the error bars. Note that although the value at distance zero has not been included into any fit, even this shortest distance data point tends to follow the exponential trend very well.

We also computed spin-spin correlation functions $\langle \vec{S}_i \cdot \vec{S}_j \rangle$. Results are shown for the kagome in Fig. (2.8) and for the triangular lattice in Fig. (2.7). Spin-spin correlations decay exponentially even in the critical square-lattice case [61], and by theoretical prejudice should decay exponentially for all short ranged RVB states. Moreover, even on the kagome, DMRG work has predicted a spin liquid phase with gapped spin but gapless singlet excitations [62]. This might render the singlet sector more crucial in the present context. Nonetheless, direct demonstration of the exponential decay of spin-spin correlations is not straightforward, especially in the presence of the sign problem discussed initially. Again, the short-ranged nature of the correlations is apparent in both cases. As a consistency check, both $\langle \vec{S}_i \cdot \vec{S}_j \rangle$ and $3\langle S_i^z S_j^z \rangle$ are shown, which must agree by $SU(2)$ symmetry. This symmetry is, however, not manifest in the Ising-basis we are working with. [2]

[2]We note that $S^z S^z$ correlations for the kagome were also calculated very recently using a PEPS representation [58]. However, we find a direct comparison of our results not straightforward, due to the blocking procedure carried out in [58].

Up to now we have demonstrated that connected correlations for the RVB states on the kagome and triangular lattice are short-ranged. This does, however, by itself not guarantee the liquid property of these states. In particular, the four degenerate RVB ground states on the torus transform nontrivially under the space group of the lattice, and to demonstrate the liquid property and rule out the possibility of a valence bond solid [63], it is essential to show that the full lattice symmetry is restored in the thermodynamic limit, for each individual ground state (within each topological sector). We restrict ourselves to the kagome lattice here. In the following, we will refer to lattice links as "symmetry inequivalent" if they are not related by a symmetry of the *wave function* (even though they may be related by a symmetry of the lattice). For lattices of the shape shown in (Fig. (2.5)a), with m, n both even, any three links along different directions will always exhaust all possible classes of nonequivalent links. In Fig. (2.9), we plot the expectation values of the dimer operator for three such links, evaluated in one topological sector, for various "even/even" lattices. One observes that the discrepancy between nonequivalent links rapidly decreases, by a factor of *at least* 60 between 24 sites and 48 sites, taking into account error bars. (The consistency between symmetry equivalent links suggests that the error is much smaller than shown, and the factor is really on the order of 100). For larger lattice size, the calculation becomes increasingly demanding, since, presumably, increasingly smaller error bars are needed to resolve the discrepancy in expectation values, while even maintaining the size of the error bars is more costly (Fig. (2.9)). It is worth noting, though, that the average of the three expectation values for 72 and 96 sites appears to have

converged, and we are thus approaching the thermodynamic limit. In all, these findings are highly consistent with the general expectation that the RVB-states describe a topological spin liquid: not only correlations decay exponentially as expected, but also lattice symmetry remains unbroken in the thermodynamic limit for the kagome lattice. For the kagome, this greatly adds to the amassed evidence that local $SU(2)$ invariant Hamiltonians stabilizing a topological spin liquid state are possible [51, 58]. Further possible applications of our method include the investigation of short-ranged RVB wave functions on other nonbipartite lattices. In particular, certain next nearest neighbor links may be introduced in standard lattice geometries such as the square lattice [64], as long as the planarity of the lattice is maintained. This makes it natural to introduce different weights for different types of valence bonds. Furthermore, our method allows for the introduction of any number of mobile (delocalized) holes and thus the study of monomer correlations and the related confinement/deconfinement issue.

2.4 Discussion

In order to further strenghten the claim that our Hamiltonian Eq. (1.3) indeed is the parent Hamiltonian to a Z_2 quantum liquid phase, we still need to rule out other ground states; we want the equal amplitude superpositions of singlet coverings to be the only ground state(s). This uniqueness issue is work in progress [59]. After obtaining all numerical data, we noticed that the data –the exponential decay of the correlations– is not very system size sensitive. This, together with the observed

exponential decay, indicates that the system indeed should have a gap. Still, however, one might desire a strict proof to show the gap. This is left for future work.

3. Linear independence of nearest neighbor valence bond states

This chapter is devoted to the question whether the nearest neighbor valence bond (NNVB) states are linearly independent on various two dimensional lattices. To answer this question, we utilize and generalize a method that was recently introduced and applied to the kagome lattice [51]. The key point of the procedure derived in Ref. [51] lies in finding an appropriate (possibly small) cell for the respective lattice, for which a certain local linear independence (LI) property can be demonstrated. Whenever this is achieved, linear independence follows for arbitrarily large lattices that can be covered by such cells, for *both* open and periodic boundary conditions. We find that this method is applicable to the kagome, honeycomb, square, squagome, two types of pentagonal, square-octagon, the star lattice, two types of archimedean lattices, three types of "martini" lattices, and to fullerene-type lattices, e.g., the well known "Buckyball". Also, we present an example that proves that our method does not only apply to NNVB states that are constructed out of spin 1/2 electrons, but also to a group of states called "resonating valence loop" (RVL) states made out of spin 1 electrons.

The above briefly summarized results of this chapter have been published in

Julia Wildeboer and Alexander Seidel, Phys. Rev. B 83, 184430 (2011) .

3.1 Applications and usefullness of linear independent valence bond states

At this point, we will make an effort to justify why the linear independence property is such a crucial property. The linear independence issue of the short-ranged resonating valence bond (RVB) states on several two dimensional lattices was considered a hard problem; the only results previously obtained on this matter were published in 1989 by Chayes, Chayes, and Kivelson [67]. Unfortunately, Ref. [67] only gives the linear independence on three different types of two dimensional lattices, namely the square, the honeycomb, and the square-octagonal lattice. In all three cases, the result is only obtained for open boundary conditions. Thus, until Ref. [68] appeared in 2011, there was no information available on the linear independence property of valence bond states living on lattices with periodic boundary conditions.

We will now describe the usefulness of the linear independence property. Moreover, we will start with an a very important application of the LI property, namely the role it plays when it comes to finding exotic magnetic quantum states such as the quantum spin liquid state. As described in the introductory chapter 1, Rokhsar and Kivelson invented an ingenious scheme to explore the non-magnetic part of the phase diagram of quantum spin-1/2 systems through effective "quantum dimer" models (QDMs) [8]. They focused on the case where a gap in the system renders all correlations

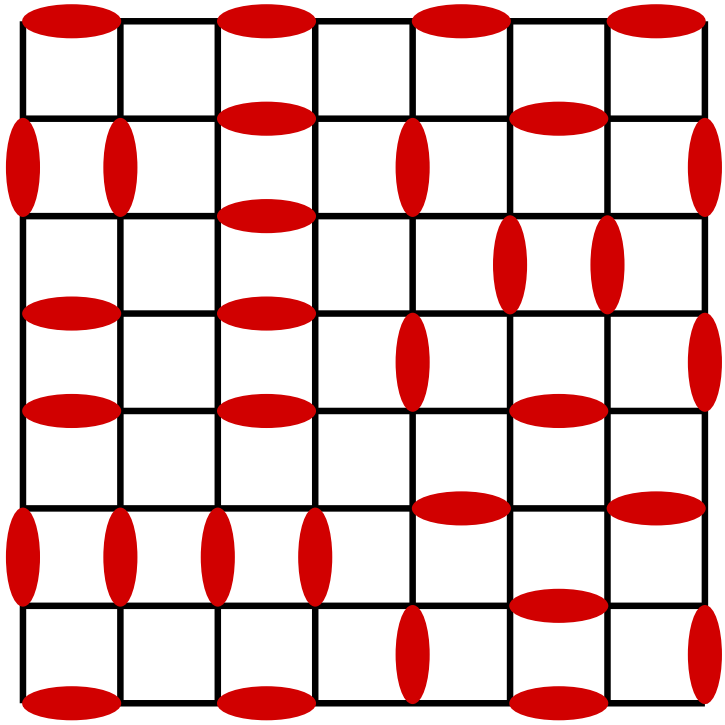

Figure 3.1. A square lattice a with dimer covering. Dimers are indicated by ovals.

short ranged. In this case, the RVB spin liquid ground state can be thought of as superposition of states where spins pair up into short range valence bonds. A quantum dimer model is obtained by first truncating the Hilbert space to include only states where each spin participates in a nearest neighbor valence bond (NNVB). The second simplification is to regard the NNVB states that generate the Hilbert space as an *orthogonal* basis. In reality, no two different NNVB states on a finite lattice are orthogonal. The overlap (scalar product) between two different RVB states is always finite. Thus, it is more appropriate to think of the degrees of freedom of these new effective theories not as valence bonds, but as hardcore bosons or "dimers" living on the links of the original lattice. As sets, however, both the hard core dimer states and

the NNVB states are in one-to-one correspondence with dimerizations of the lattice into nearest neighbor pairs, see Fig. 3.1.

The exploration of QDMs has given rise to profound insights into possible realizations of short range RVB spin liquid physics, in particular on nonbipartite lattices [33, 70]. It has remained challenging, however, to rigorously establish the status of simple QDMs as viable effective theories for quantum spin-1/2 systems within a certain parameter regime. The lack of orthogonality of the NNVB states that QDMs seek to describe makes it difficult to establish a direct mapping between QDMs and the low energy sector of quantum spin-1/2 models. This difficulty can be dealt with by treating the non-orthogonality as a "small parameter", and setting up a systematic expansion in this parameter. This notion already played a central role in the original literature, [8, 25, 69] and was recently explored in great detail in a series of insightful papers [71, 72]. Within this scheme, one can thus get the issue of the non-orthogonality of the NNVB states under control.

However, the validity of this perturbative scheme depends crucially on the fact that the NNVB states, while not orthogonal, are at least linearly independent, like their counterparts in QDMs. In technical terms, the overlap matrix obtained from the NNVB states must be invertible. The need for an invertible overlap matrix was noticed early on, [69] and from thereon linear independence of NNVB states was routinely quoted as an assumption in the literature, e.g. in estimates of the low temperature entropy of highly frustrated quantum magnets [73, 74]. Furthermore, exactly solvable, $SU(2)$-invariant spin-1/2 models with RVB and/or spin liquid ground

states on simple lattices have only been constructed quite recently, [42, 43, 51, 75] in addition to work on decorated lattices [41]. In Ref. [51], rigorous (albeit partial) statements on the uniqueness of the RVB-type ground states of the model constructed there were intimately tied to the linear independence of NNVB states on the kagome lattice. Subsequently, from a purist point of view, there is a need to demonstrate that superpositions of NNVB wave functions, which may be considered as variational [25,73,74,76,77] or exact [42,43,51] solutions to various problems, do not vanish identically, whenever the overlaps between the NNVB states forming these wave functions do not have a uniform sign. Also, the normalizability of such wave functions is an obvious byproduct of the linear independence of NNVB states (on the respective lattice). The explicit or implicit assumption of the linear independence of the NNVB states is thus a prevalent theme in the literature on short range RVB physics, and in some cases has been studied extensively on finite clusters. [78, 79]

As mentioned above, rigorous proofs of the LI property have been available since 1989, through a seminal work of Chayes, Chayes, and Kivelson [67]. The proof, however, has been limited to three different types of planar lattices, the square, honeycomb, and square-octagon lattice, and only for the case of open boundary conditions. Now with the publication of Ref. [68] a more general method is available, that can, in principle, be applied to any lattice, in the presence of both open and periodic boundary conditions. While we usually have Born–von Karman periodic boundary conditions in mind which give a rectangular (or parallelogram) lattice strip the topology of a torus, our method applies to other lattice topologies as well. To demonstrate

this, we also apply our method to the C_{60} lattice and other fulleren-type lattices, where the linear independence of NNVB (or "Kekulé") states has direct applications in chemistry [76]. Though, we will restrict our results in the following to two dimensional lattices and the C_{60} "Buckyball" lattice, we also point out that our approach should, in principle, also be applicable to dimensions higher than two, as there are some three dimensional lattices in the literature such as the hyperkagome or the three different cubic lattices that would be of interest when it comes to the question if their NNVB coverings are indeed linearly independent. Also, we first restrict ourselves to spin-1/2 systems, however, in the final Section 3.4 of this chapter, we show that our proof is so powerful that it can be generalized to the case of spin 1. The spin-1 state analogous to the spin-1/2 NNVB states are call resonating valence loop states; they will be introduced in Section 3.4 and their linear independence on the honeycomb and on the star lattice will be proven.

Although there is no guarantee that our proof strategy works for every lattice where the linear independence holds, we do demonstrate its applicability to many new two-dimensional (2D) lattices, for which the linear independence of NNVB states is first established in this work. At the same time, we generalize the aforementioned previous results on linear independence of NNVB states to the case of periodic boundary conditions. It is well known that the physics of short range RVB states becomes enriched in subtle ways when periodic boundary conditions are imposed. On a toroidal square lattice, e.g., NNVB states come in a large number of topological sectors characterized by two integer winding numbers (n_x, n_y). (For a review, see e.g. Ref. [80]).

When the same lattice is viewed as a rectangle with open boundary conditions, the remaining allowed NNVB state all belong to a *subset* of just the $(0,0)$ sectors. In the thermodynamic limit, the number of NNVB states for open boundary conditions thus becomes a vanishing fraction of the corresponding number for periodic boundary conditions. It is thus clear that the statement of linear independence becomes considerably stronger for periodic boundary conditions, and is often desirable in applications.

We proceed by applying and refining a method that has recently been developed for the kagome lattice, [51] making it amenable to more general lattice structures. In Section 3.2.1 we review this method. In Section 3.2.2, we report that this method can be applied without much alteration to the honeycomb lattice, the star lattice, the square-octagon lattice, the squagome lattice, two types of pentagonal lattices (studied in a magnetic context, e.g., in Refs. [81] and [41]), three types of "martini" lattices, [82] and two types of archimedean lattices. In Section 3.2.3, we apply the same method to fulleren-type lattices. We find that the case of the square lattice requires a generalization of this method, which is introduced and applied in Section 3.2.4. In Section 3.3 we summarize our results and discuss possible further applications. Eventually, a further modification/application of our proof is provided through the above mentioned RVL states, whose LI property is proven on the star and the honeycomb lattice.

3.2 Proof for linear independence and results

This section is subdivided into four parts. First, we will derive the general proof scheme without referring to any specific lattice, dimension of the lattice, or its topology. We do so in order to make it clear how applicable our proof is when it comes to multiple systems to be distinguished by the above mentioned properties. Then we will move on to the results. Here, we distinguish between several cases: first, we will prove the LI property of twelve planar lattices in Section 3.2.2 that frequently appear in the literature. Afterwards, we turn our attention to a different type of lattice topology; we discuss and show results concerning fullerene-type lattice stuctures, e.g. the most prominent example here is the famous C_{60} "Buckeyball" frequently appearing in the (chemistry) literature. The LI of the NNVB states of the square lattice harbors a speciality that requires a modification of our above mentioned proof scheme. This will be discussed in Section 3.2.4.

3.2.1 Derivation of the linear independence condition

In this section we review the method used in Ref. [51] to prove the linear independence of the nearest neighbor valence bond states on the kagome lattice. We find that this method can be extended straightforwardly to most other lattices to be considered here. A refinement necessary to study the case of the square lattice will be given further below.

The general starting point of this method is the identification of a suitable (ideally, smallest) cell for which a rather strong local linear independence property holds true. This local linear independence property can conveniently be verified numerically, although in many cases an analytic proof seems feasible as well. As shown in Ref. [51], this local property then implies the linear independence of nearest neighbor valence bond states on arbitrarily large lattices that can, in a certain sense, be covered by such cells.[1] We will present the proof in the following now. For the kagome lattice, the smallest possible cell that satisfies these requirements is the 19-site "double star" shown in Fig. (3.2).

For any given cell of a lattice, we define as interior or inner sites of the cell those sites for which all nearest neighbors are also contained within the cell. Here, the nearest neighbors of a site are all sites connected to it through a link of the lattice. Sites that are not interior are called the boundary sites of the cell. For the kagome cell depicted in Fig. (3.2), all sites belonging to one of the internal hexagons are interior, while the remaining ones are boundary sites, unless the cell happens to be at a boundary of the lattice itself. In this work we will, however, mostly consider lattices without boundary. Statements about lattices with boundary can then be obtained as simple corollaries. Therefore, the distinction between interior and boundary sites within a cell such as shown in Fig. (3.2) will not depend on the position of the cell within the lattice.

[1]While here we will usually consider the case where a single type of cell suffices, one may in some cases want to identify several types of cells that satisfy the local linear independence property, such that the lattice can be conveniently covered by this family of cells.

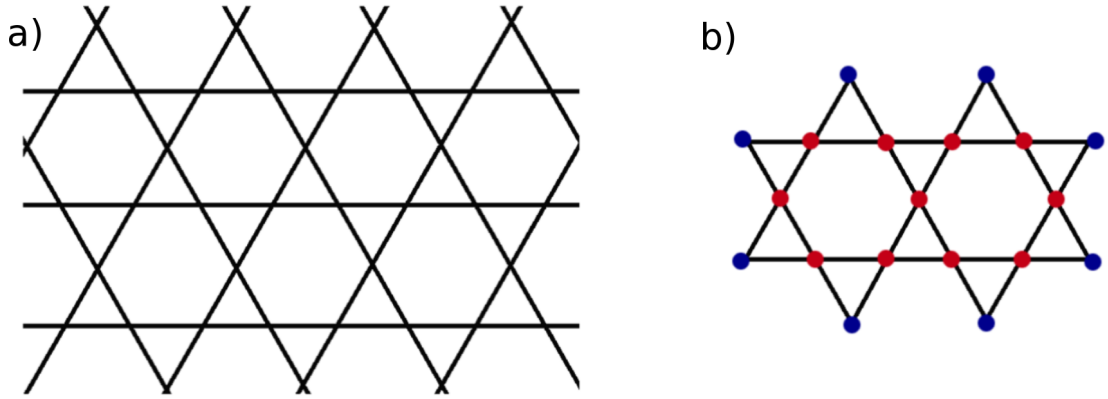

Figure 3.2. (Color online.) The kagome lattice. a) shows the structure of the kagome lattice, while b) shows the minimal (smallest) cell for which the local independence property defined in the text was proven. [51] Different dots are used to label the sites which are defined as inner and outer sites, respectively.

To proceed, we will now define a certain class of states living on the local cells. We will refer to these states as "local valence bond states". This does, however, not imply that these states completely dimerize the cell, i.e. that every site of the cell must participate in a valence bond within the cell. Rather, we think of these states as local "snapshots" of a lattice that is in a (globally defined) nearest neighbor valence bond state. In such a snapshot, every internal site of the cell must certainly form a valence bond with one of its nearest neighbors within the cell. A boundary site of the cell, however, may or may not participate in a valence bond with a site within the cell under consideration. In particular, it may participate in a valence bond with a site *outside* that cell. In the latter case, the local density matrix describing the state

of the cell contains no information about the state of the spin of such a boundary site. This motivates the following definition of local valence bond "snapshot" states on the cell $\mathcal{C}$. Let us consider states of the form

$$|D\rangle \times |\psi_f\rangle \ . \tag{3.1}$$

Here, D represents a dimer covering of the cell $\mathcal{C}$. By this we mean a pairing of the sites of the cell $\mathcal{C}$ into nearest neighbor pairs, where each internal site is a member of a pair, but not necessarily each boundary site. An example for such a pairing is given for the cell of the star lattice shown in Fig. (3.3d), and that of the square lattice shown in Fig. (3.10c). By $|D\rangle$ we denote a state where each pair of D forms a singlet, with an arbitrary phase convention. In Eq. (3.1), the state $|\psi_f\rangle$ then denotes any state of the "free" sites that are left untouched by the dimer covering D. This can again be seen in Figs. (3.3d), (3.10c). In (3.10c), every dimer covering D leaves behind at least one free site, because of the odd number of sites in this cell. For cells of even size, we leave it understood that the factor $|\psi_f\rangle$ in Eq. (3.1) is absent if D covers all sites of the cell.

We find it convenient to denote by $\mathcal{H}(D, \mathcal{C})$ the linear space formed by all local states of the form (3.1), for a *fixed* dimer covering D, and will also write $\mathcal{H}(D)$ instead of $\mathcal{H}(D, \mathcal{C})$ whenever it is clear what cell is being referred to. The space spanned by all states of this form, without fixing D, is called the local valence bond space of the cell $\mathcal{C}$, $VB(\mathcal{C})$:

$$VB(\mathcal{C}) = \sum_D \mathcal{H}(D, \mathcal{C}) \ . \tag{3.2}$$

Here, the sum denotes the linear span. For a given cell $\mathcal{C}$, we will now ask whether the sum in Eq. (3.2) is *direct*. This means that the expansion of any state in $VB(\mathcal{C})$ into members of the various spaces $\mathcal{H}(D)$ is possible in one and only one unique way. Whenever this property holds for some cell $\mathcal{C}$, we will say that the NNVB states are "locally independent" on the cell $\mathcal{C}$, or satisfy the "local independence property" on the cell $\mathcal{C}$.

The local independence property, whenever it can be established for some cell $\mathcal{C}$, extends to arbitrarily large lattices that can be covered by cells of this topology. Said more precisely, we require that every link of the lattice belongs to a cell that has the topology of $\mathcal{C}$.[2] The linear independence of NNVB states defined on the entire lattice can then be seen as follows [51]. If the sum in Eq. (3.2) is direct, then linear projection operators P_D acting on the cell $\mathcal{C}$ are well defined, which project onto the subspaces $\mathcal{H}(D)$. Said differently, the defining properties of these operators are

$$\begin{aligned} P_D \, |D'\rangle \otimes |\psi_f\rangle &= \delta_{D,D'} \, |D'\rangle \otimes |\psi_f\rangle \, , \\ \text{hence} \quad P_D P_{D'} &= \delta_{D,D'} P_D \, . \end{aligned} \tag{3.3}$$

We note that since the spaces $\mathcal{H}(D)$ are not orthogonal, the linear projection operators thus defined are not Hermitian. We also mention that to define these operators in within the full $2^{|\mathcal{C}|}$ dimensional Hilbert space of the cell $\mathcal{C}$, we need to specify their action on a suitably chosen complement of the local valence bond space $VB(\mathcal{C})$, which

[2] In general, one should exclude *by definition* any link between two boundary sites of C from the topology of C. This is not an issue for most cells considered here, except for the martini-B and the archimedean-B lattice, see Fig. (3.7) (a),(c), Fig. (3.8) (b),(d). It would also be relevant, e.g., to cells of the triangular lattice.

can be done in an arbitrary way. In the following, we will only need to know the action of these operators within the subspace $VB(\mathcal{C})$.

The operators P_D can now be defined for any cell $\mathcal{C}$ of some lattice $\mathcal{L}$, for which the nearest neighbor valence bond states are locally independent in the sense defined above. We may write $P_D^{\mathcal{C}}$ to explicitly refer to the cell $\mathcal{C}$ on which these operators act, but will continue to write P_D instead whenever no confusion is possible. Armed with these operators, we may consider a general linear relation of the form

$$\sum_{D'} \lambda_{D'} |D'\rangle = 0 \ . \tag{3.4}$$

Here, D' now represents a full dimerization of the entire lattice, and for simplicity, we assume that the lattice has no boundary, and can be covered by a single type of cell, as defined above. We will comment on the (simpler) case where the lattice has a boundary below. The states $|D'\rangle$ are thus NNVB states of the lattice $\mathcal{L}$. For definiteness, we may think of, e.g., a honeycomb lattice with periodic boundary conditions. The honeycomb lattice and its smallest cell for which the local independence property holds are shown in Fig. (3.4). We want to show that Eq. (3.4) implies that all coefficients $\lambda_{D'}$ are zero. For this we first focus on a single cell $\mathcal{C}$ of the lattice that has the topology shown in Fig. (3.4b), and a fixed dimer covering D of the entire lattice.

The dimer covering D determines a dimer covering $D_{\mathcal{C}}$ of the cell $\mathcal{C}$, consisting of those dimers of D that are fully contained in $\mathcal{C}$. Consider the action of the operator $P_{D_{\mathcal{C}}}$ defined for the cell $\mathcal{C}$ on any of the states $|D'\rangle$ in Eq. (3.4). Clearly, the dimer

covering D' determines a local dimer covering of $\mathcal{C}$, $D'_{\mathcal{C}}$, defined analogous to $D_{\mathcal{C}}$. From the definition of the projection operators, Eq. (3.3), we see that

$$P_{D_{\mathcal{C}}}|D'\rangle = \delta_{D_{\mathcal{C}},D'_{\mathcal{C}}}|D'\rangle\,. \tag{3.5}$$

This is so since the state $|D'\rangle$ is contained in the tensor product $\mathcal{H}(D'_{\mathcal{C}},\mathcal{C})\otimes\mathcal{H}(\mathcal{L}\setminus\mathcal{C})$, where the second factor denotes the Hilbert space associated with all lattice sites not contained in $\mathcal{C}$. $P_{D_{\mathcal{C}}}$ only acts on the first factor, and does so according to Eq. (3.3). Some further (but trivial) details are explicitly written in Ref. [51]. Hence, when $P_{D_{\mathcal{C}}}$ acts on Eq. (3.4), one obtains a similar linear combination on the left hand side, but with all dimer coverings D' omitted for which the cell $\mathcal{C}$ does not contain *exactly the same* dimers as for D. We can proceed by successively acting on this new linear relation with the operators $P_{D_{\mathcal{C}'}}$, where D is the same as before, but $\mathcal{C}'$ now runs over all cells of the lattice with the same topology as $\mathcal{C}$. Since by assumption, these cells cover the lattice in the sense defined above, only those states $|D'\rangle$ in Eq. (3.4) survive this procedure whose underlying dimer covering D' looks the same as D everywhere, i.e., only the term with $D' = D$ survives. The resulting equation is thus $\lambda_D|D\rangle = 0$, which implies $\lambda_D = 0$. Hence $\lambda_{D'} = 0$ for each dimer covering D', since D was arbitrary. This then proves the linear independence of the nearest neighbor valence bond states on the lattice $\mathcal{L}$.

So far we have considered lattices with periodic boundary conditions.

The above result, however, immediately carries over to lattices with a boundary. Let us consider any lattice $\mathcal{L}'$ with an edge that can be obtained from a lattice $\mathcal{L}$ with periodic boundary conditions, for which the linear independence of NNVB states has

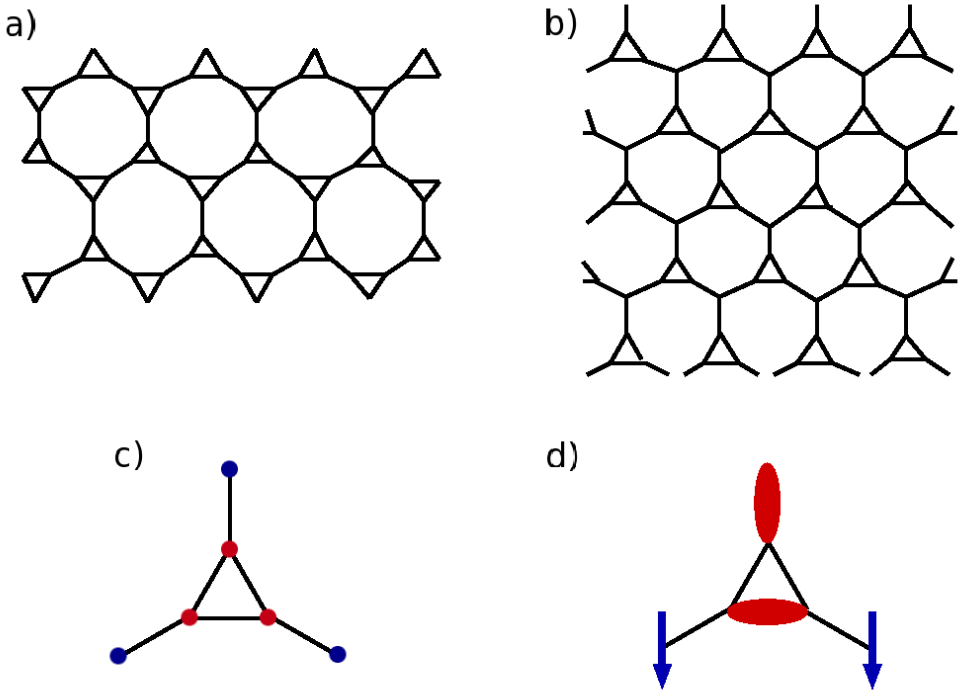

Figure 3.3. (Color online.) The star lattice (a), and its minimal cell (c) for which the local independence property could be established. (b) shows the martini-A lattice, with the same minimal cell (c). Different shades (colors) of dots identify internal and boundary sites. (d) shows a possible dimer covering: the internal sites must be touched by a dimer, boundary sites may or may not form a dimer (valence bond) with an internal site. In a local valence bond state, boundary sites not participating in valence bonds may be in an arbitrary spin configuration.

been proven, by means of the removal of certain boundary links. Then the set of full dimerizations D of $\mathcal{L}'$ is just a subset of those of $\mathcal{L}$, and likewise the corresponding set of NNVB states. Hence, if the linear independence of NNVB states holds for $\mathcal{L}$, it must also hold for $\mathcal{L}'$. More generally, it is easy to see that our result applies to any sublattice $\mathcal{L}'$ of $\mathcal{L}$, such that $\mathcal{L} = \mathcal{L}' \cup \mathcal{L}''$ is a disjoint union, and both $\mathcal{L}'$ and $\mathcal{L}''$ are fully dimerizable.

3.2.2 Twelve different 2D lattices

We now discuss the applicability of this method to various two-dimensional lattices. As discussed in Section 3.2.1, this merely requires the identification of a cell of the lattice, for which the local independence property holds, and which can cover the entire lattice in the sense defined there. Such cells have also been dubbed "bricks of linear independence" in Ref. [51]. For brevity, we will refer to the cells identified by us as "minimal cells", since there are presumably (in some case obviously) no smaller cells with this property on the respective lattices. We have, however, not carefully ruled out the existence of smaller cells in all cases, since this is of limited interest once sufficiently small "bricks of linear independence" have been identified. For the cell $\mathcal{C}$ in question, we pick an appropriate basis $|D\rangle \otimes |\psi_i\rangle$ for each space $\mathcal{H}(D)$, where $i = 1 \dots 2^{n_D}$, and n_D is the number of sites of the cell $\mathcal{C}$ that do not participate in the local dimer recovering D. The local independence property introduced in the preceding section is then equivalent to the statement that the overlap matrix

$$M_{D',j;D,i} = \left(\langle D'| \otimes \langle \psi_j|\right)\left(|D\rangle \otimes |\psi_i\rangle\right) \tag{3.6}$$

has full rank. It is clear that for a suitable choice of the factors $|\psi_i\rangle$, e.g. "Ising"-type basis states with well-defined local S_z, and suitable overall normalization factors, the matrix elements $M_{D',j;D,i}$ are integer. The question of the rank of this matrix can then be addressed using integer arithmetic free of numerical errors. We did this by using the LinBox package. [83] By choosing the ψ_i from an Ising-S_z basis, the matrix in

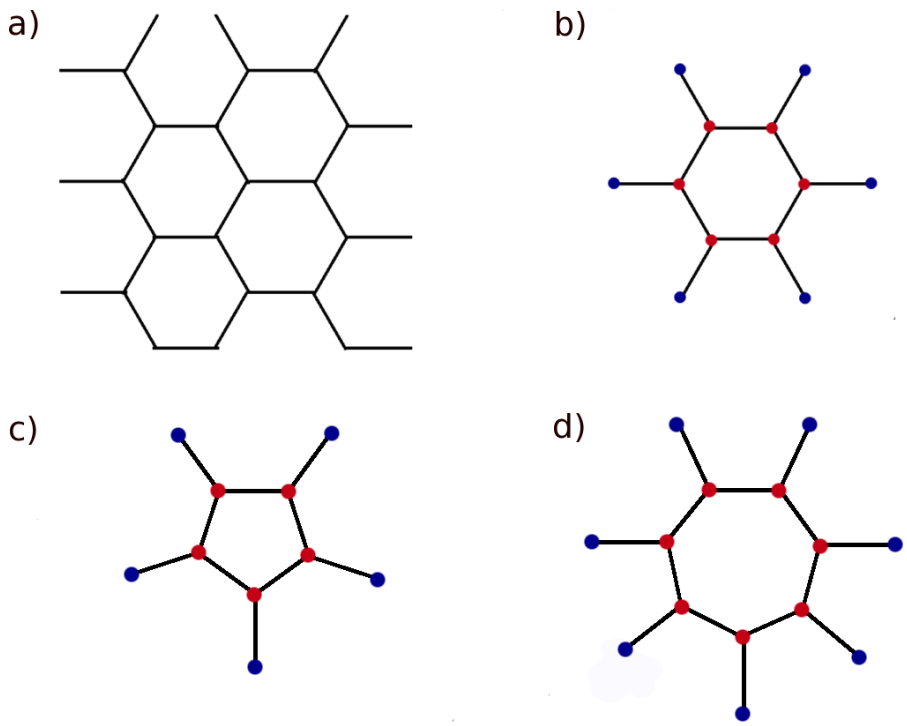

Figure 3.4. (Color online.) Honeycomb and related structures. (a) The honeycomb lattice. (b) its minimal cell with internal and boundary sites identified. (c) The minimal cell of the buckyball lattice (Fig. (3.9)). (d) A similar heptagonal cell that also satisfied the local independence property.

Eq. (3.6) is also block diagonal with blocks of definite total S_z. This let to manageable matrix sizes in all the cases discussed in this section.

We present twelve different 2D lattices which we successfully studied using the method described above, and their respective minimal cells $\mathcal{C}$, for which the local independence has been found to hold, Figs. 3.2-3.8.

These are, in order, the kagome lattice (treated in Ref. [51]), the star lattice, the martini-A lattice, the honeycomb lattice, the square-octagon lattice, the squagome lattice, the pentagonal and the "Cairo" pentagonal lattice, 2 more types of the"martini"

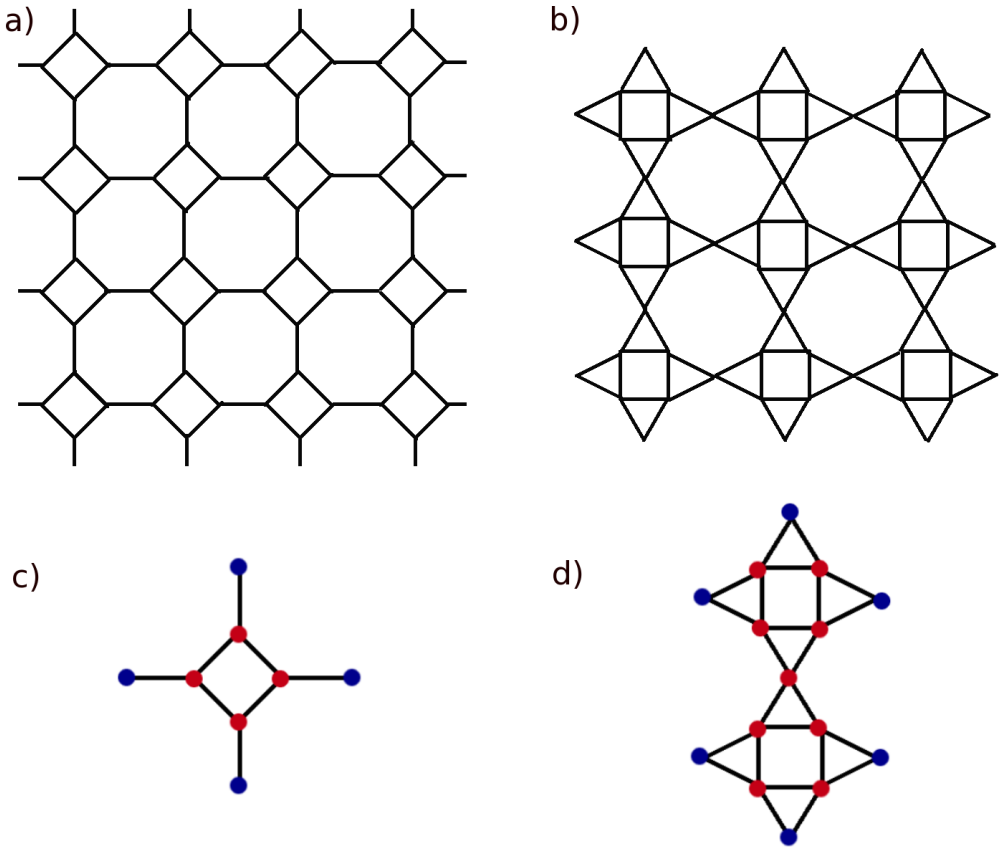

Figure 3.5. (Color online.) The square-octagon lattice (a) and the squagome lattice (b). (c) and (d) show the respective minimal cells.

lattice (martini-B and martini-C), and two types of so called archimedean lattices, denoted archimedean-A and archimedean-B. As proven above, for all these lattices, the identification proper "bricks of linear independence" implies the linear independence NNVB states for arbitrarily large lattices of this type (which must also be large enough to contain the minimal cell), for both open and periodic boundary conditions. For the square-octagon and the honeycomb lattices, the case of open boundary conditions had already been treated in Ref. [67] by a different method. It is interesting

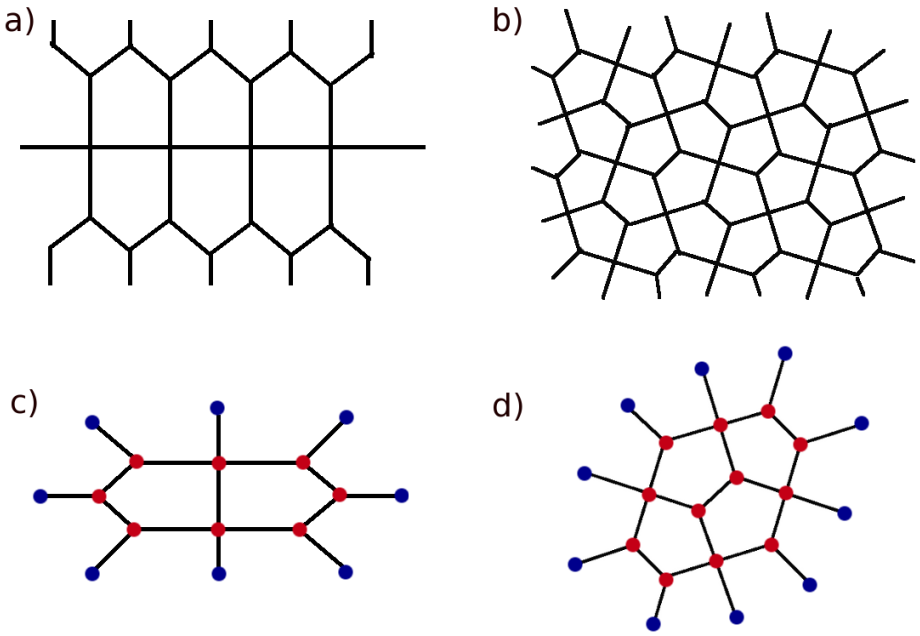

Figure 3.6. (Color online.) Two types of pentagonal lattices. (a) shows the pentagonal lattice and (b) shows the "Cairo" pentagonal lattice structure, (c) and (d) the respective minimal cells.

to note that the size of the matrix in Eq. (3.6) differs quite significantly for the 2D lattices discussed here: for the star and the martini-A lattice, which share the same minimal cell (Fig. (3.3)), the total matrix dimension (over all S_z-blocks) is only 13. For others, the matrix dimension is on the order of a few thousand, and for the square lattice cell treated separately in Section 3.2.4, the set of "local valence bond" states $|D\rangle \otimes |\psi_i\rangle$ defining the matrix has more than half a million elements.

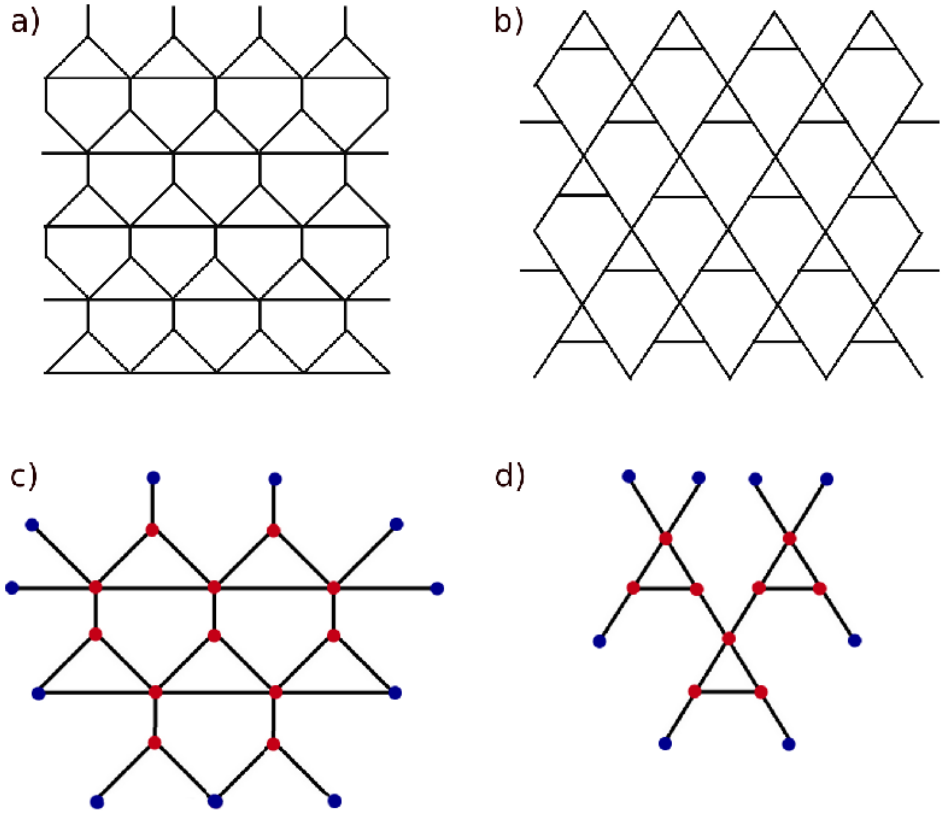

Figure 3.7. (Color online.) Two more types of martini lattices. (a) and (b) show the lattice structures of the martini-B lattice and the martini-C lattice, respectively, (c) and (d) the respective minimal cells.

3.2.3 Fullerene-type lattices

We now consider fullerene-type lattices, where each site has three nearest neighbors, and belongs to at least one hexagonal plaquette, where no two members of the same hexagonal plaquette share a nearest neighbor outside that plaquette. Such lattices can be covered, in the sense defined in Section 3.2.1, by the minimal cell of the honeycomb lattice, Fig. (3.4b). A famous example is the "Buckyball" lattice,

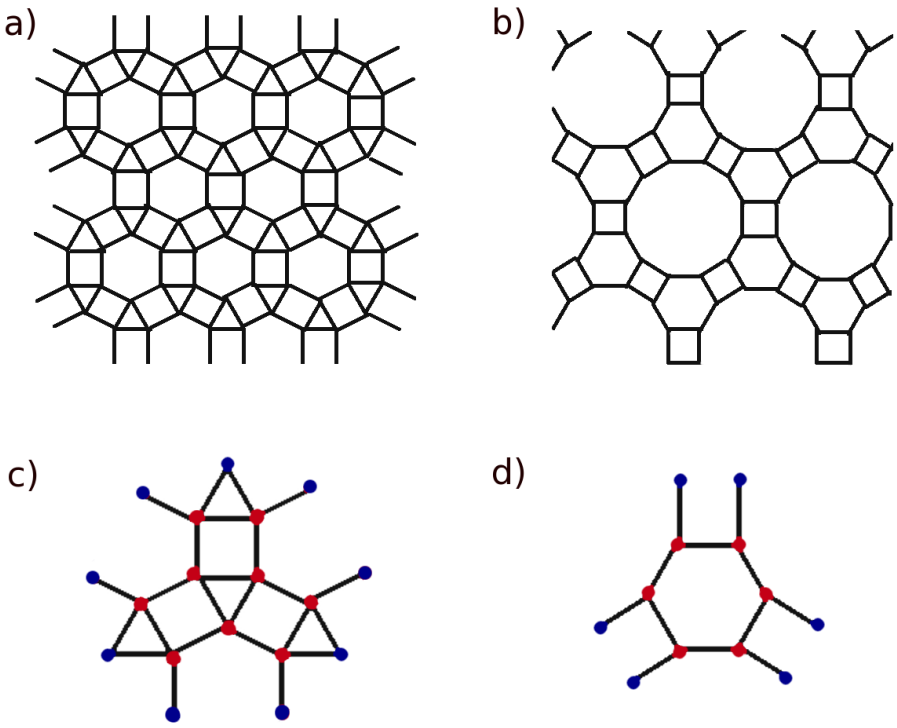

Figure 3.8. (Color online.) Two types of archimedean lattices. (a) shows the archimedean-A lattice and (b) shows the archimedean-B lattice structures, (c) and (d) the respective minimal cells. Note that the minimal cell in (d) is the same as that of the honeycomb lattice, Fig. (3.4b).

Fig. (3.9). By the results of the preceding sections, the NNVB states on these types of lattices are are linearly independent. This also demonstrates that our method, being essentially local, can be applied to general lattice topologies. [3] The Heisenberg model on fulleren-type lattices has been extensively studied within the NNVB subspace in Ref. [76] (there called Kekulé subspace). Good agreement with exact diagonalization results within the full Hilbert space was found. The authors also point out the central

[3]Strictly speaking, since we define a lattice only through its vertices and edges, while faces play no role, we can equally well regard the C_{60} lattice as having the topology of a sphere, or, through its Schlegel diagram, of a planar graph. This does not affect the general validity of this statement.

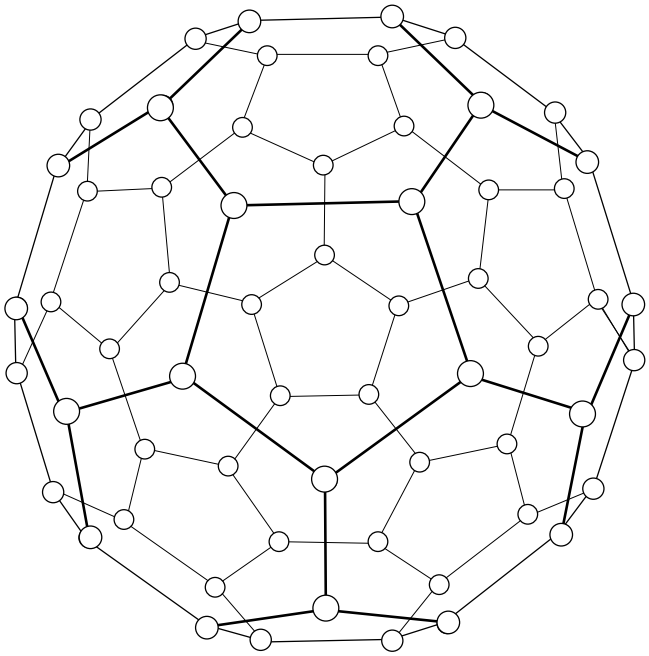

Figure 3.9. The lattice of the C_{60} molecule, or "buckyball". The lattice can be covered by the minimal cell of the honeycomb lattice, Fig. (3.4b). The actual minimal cell of this lattice is the pentagonal cell shown in Fig. (3.4c).

importance of the linear independence of the NNVB states to their approach. Since the fullerene lattices are finite in size, conventional brute-force numerics may in principle be used to establish this, although the feasibility of this depends, of course, on the actual lattice size. In contrast, the result derived here holds for arbitrarily large systems, and, given the small size of the minimal cells involved, could be obtained purely analytically. In this regard, it is worth noting that the actual *minimal* cell of the C_{60} molecule is not that of the honeycomb lattice, Fig. (3.4b), but the smaller pentagonal cell of Fig. (3.4c). We have verified that it likewise satisfies the local independence property, and each link of the Buckyball lattice belongs to such a cell.

For this rather small cell, an analytic proof of the local independence property seems feasible using the Rumer-Pauling method [84–87] referred to in the next section.

Based on the observations made thus far, we conjecture that all cells where the n inner sites form a single polygon, and each inner site is linked to exactly one of n boundary sites, have the local independence property. Examples of such cells, for which we have verified this, are given in Figs. (3.3c), (3.5c), and (3.4b-d), corresponding to $n = 3, 4, 5, 6, 7$. For all lattices that can be covered by any combination of such cells, we thus have the linear independence of NNVB states.

3.2.4 The square lattice

We find that the method presented in Sec. 3.2.1 cannot immediately be applied to the square lattice. The problem can be traced back to the fact that any local cell on this lattice necessarily that 90 degree corners. It turns out that by using the degrees of freedom near these corners, one can always form non-trivial relations between the states in different subspaces $\mathcal{H}(D)$. The projection operators in Eq. (3.3) are then ill-defined. We thus have to modify our method in order to deal with this case. Luckily, the local independence property introduced in Sec. 3.2.1, while it is found to hold for many lattice types, is overly restrictive. In fact, whenever this property holds, it can be literally extended to arbitrarily large lattices with an edge [51]. That is, for an arbitrarily large lattice $\mathcal{L}$, not only states $|D\rangle$ corresponding to full dimerizations of $\mathcal{L}$ are then linearly independent, but in fact all states of the form $|D\rangle \otimes |\psi_i\rangle$, where D does not necessarily cover all boundary sites of $\mathcal{L}$, and the factors $|\psi_i\rangle$ form a basis of

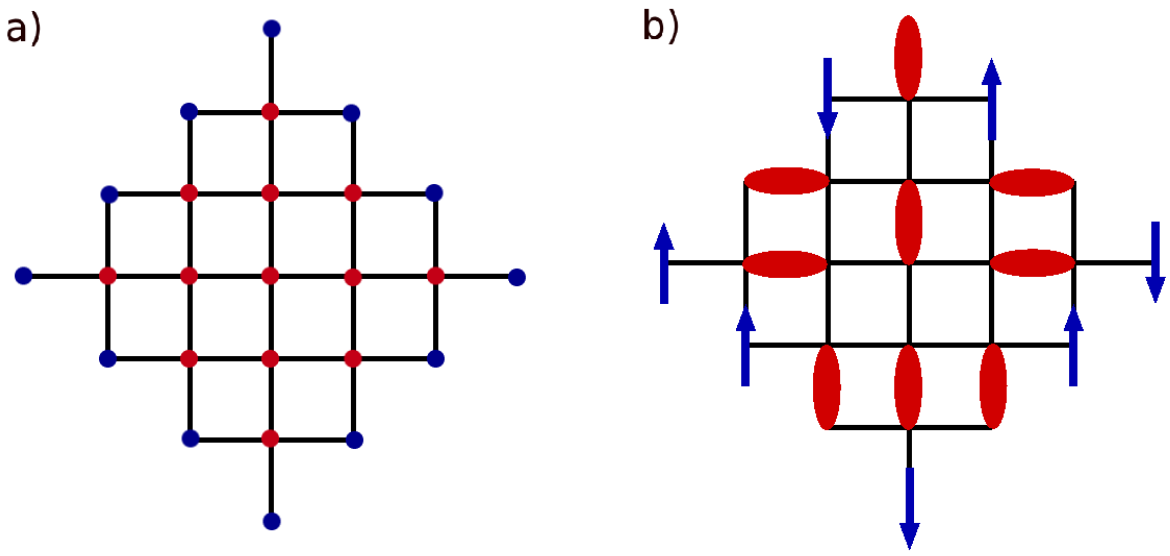

Figure 3.10. (Color online.) The square lattice. The general lattice structure is shown in Fig. (3.1). (a) The minimal cell for which the refined local independence property of Section 3.2.4 holds. (b) A local valence bond state with the central site forming a bond with its upper neighbor, corresponding to $\sigma =\uparrow$ as defined in the text.

the space associated with "free" boundary sites. Clearly, this is a stronger statement than just the linear independence of NNVB states corresponding to full dimerizations of the lattice. However, for the square lattice this stronger property simply does not hold. On the other hand, this "strong" linear independence property is not of primary interest. We are still interested in the linear independence of NNVB states associated with full dimerizations of the lattice, for which the stronger property is not necessary.

It turns out that a weaker version of the local independence property is sufficient to construct suitable projection operators for our purpose. To see this, note that the operators P_D defined in Eq. (3.3) are sensitive to the entire configuration of

valence bonds fully contained within the cell on which they act. To prove the linear independence of NNVB states, it is sufficient to work with operators that are sensitive, say, to the bonding state of any given site, as determined by which nearest neighbor this central site is bonding with. To accomplish this, we consider a square lattice $\mathcal{L}$ satisfying periodic boundary conditions, which is large enough to contain the cell $\mathcal{C}$ depicted in Fig. (3.10b). For this cell, we consider four subspaces of $VB(\mathcal{C})$, according to the bonding state of the central site. We define local dimer coverings D of $\mathcal{C}$ as before, where boundary sites of $\mathcal{C}$ need not be covered. By $\sigma(D)$ we denote the bonding state of the central site, i.e., $\sigma(D) = \uparrow, \downarrow, \leftarrow, \rightarrow$, depending on whether this site is paired with its upper, lower, left, or right neighbor in the covering D, respectively. As mentioned initially, the sum Eq. (3.2) defining the space of local valence bond states, $VB(\mathcal{C})$, is not direct for the present cell. However, we may also write the space $VB(\mathcal{C})$ as a "courser" sum of fewer spaces, each of which is formed by all valence bond states that have the central site in a certain bonding state:

$$VB(\mathcal{C}) = \sum_{\sigma'} VB_{\sigma'}(\mathcal{C}) \ , \tag{3.7}$$

where

$$VB_{\sigma'}(\mathcal{C}) = \sum_{\substack{D \\ \sigma(D)=\sigma'}} \mathcal{H}(D, \mathcal{C}) \ , \tag{3.8}$$

and σ' runs over all possible values $\uparrow, \downarrow, \leftarrow, \rightarrow$.

The key observation that renders the square lattice amenable to our method is that the sum in Eq. (3.7) is still direct. To show this, one must show that the dimensions of the spaces on the right hand side add up to the dimension of the space $VB(\mathcal{C})$. For

this it is sufficient to consider the matrix M defined in Eq. (3.6), together with the matrices $M_{\sigma'}$ that are the submatrices of M corresponding to the subspaces $VB_{\sigma'}(\mathcal{C})$, and show that the ranks of the $M_{\sigma'}$'s add up to that of M. Intuitively speaking, this means that while the states $|D\rangle \otimes |\psi_i\rangle$, as defined below Eq. (3.6), satisfy non-trivial linear relations, all these linear relations can be restricted to involve members of the same subspace $VB_{\sigma'}(\mathcal{C})$; there are then no further linear relation between members of different subspaces. If the sum in Eq. (3.7) is indeed direct, we may introduce projection operators $P_{\sigma'}$ onto the components on the right hand side. The defining property of these operators is

$$P_{\sigma'} \, |D\rangle \otimes |\psi_i\rangle = \delta_{\sigma',\sigma(D)} \, |D\rangle \otimes |\psi_i\rangle \, . \tag{3.9}$$

When acting on local valence bond states $|D\rangle \otimes |\psi_i\rangle$ living on the cell $\mathcal{C}$, the operator P_σ will thus annihilate the state if the bonding state of the central site in the dimer covering D is different from σ, and otherwise leave the state invariant. It is clear that any site i of the periodic (and sufficiently large) lattice $\mathcal{L}$ can be made the central site of a cell that has the topology of $\mathcal{C}$, Fig. (3.10b). The operators P_σ defined above can then be extended to the full Hilbert space of the large lattice, and there is an operator P^i_σ for any cell of the type $\mathcal{C}$ with central site i. The defining property (3.9) then extends to valence bond states $|D\rangle$ corresponding to full dimerizations D of the lattice: $|D\rangle$ survives the action of P^i_σ unchanged if the bonding state of site i in the dimer covering D is σ, otherwise it is annihilated. Detailed arguments for this are identical to those referred to in Sec. 3.2.1. It is then clear that by successive action with the operators P^i_σ, one can single out any dimer covering D in the linear

combination Eq. (3.4), just as carried out in Section 3.2.1, and thus prove that the states $|D\rangle$ are linearly independent.

We have verified that for the cell in Fig. (3.10b), the sum in Eq. (3.7) is indeed direct. The numerics were somewhat more challenging, due to size of the 25-site cell under consideration. To wit, this cell admits a total of 5376 different dimer coverings. Each of the dimer coverings has seven "free" outer sites not touched by a dimer, thus the total dimension of the M-matrix is a staggering 5376 x $2^7 = 688128$. To reduce the problem to blocks of manageable size, we use the full rotational invariance of the spaces appearing in Eq. (3.7). That is, we chose the basis $|\psi_i\rangle$ for the seven free sites to have a well-defined total spin S, in addition to a well-defined S_z. A suitable choice for a basis is obtained by choosing states corresponding to Rumer-Pauling diagrams [84–87]. The advantage of this is that for appropriate normalization, the matrix elements of the M-matrix then remain integer, and we may again make use of exact integer arithmetic [83]. We further used the mirror symmetry of the cell $\mathcal{C}$ along one of its diagonals. The largest blocks occurring then had dimensions on the order of 30,000.

The above then establishes that for *any* sufficiently large square lattice with periodic boundary conditions, the set of all NNVB states is linearly independent. The same statement then follows for lattices with an edge as discussed at the end of Section 3.2.1. The case of general open boundaries conditions has also been treated previously with different methods in Ref. [67].

3.3 Summary and discussion

In the preceding sections, we have described a method for proving linear independence of nearest neighbor valence bond states on certain 2D lattices with and without periodic boundary conditions. This method, originally designed for the kagome lattice, [51] was successfully extended here to the following lattice types: honeycomb, squagome, pentagonal and Cairo pentagonal, square-octagon, martini-A, -B, and -C, archimedean-A and archimedean-B, and to the star lattice, and furthermore to fullerene-type lattices. Subsequently, a refined method has been developed, which is applicable even in some cases where the original method is inadequate. Specifically, this was found to be the case for the square lattice.

Our method is based on the identification of a certain local independence property for finite clusters, which, when established, implies the linear independence of NNVB states for arbitrarily large lattices. Though here we prefer to validate the local independence property using exact numerical schemes, in those cases where smaller clusters are sufficient, a fully analytic approach is certainly feasible. Further remarks on this for the kagome case, where the cluster size is fairly large, can be found in Ref. [51].

We note again that the linear independence of the NNVB states for the square, the honeycomb, and the square-octagon lattice was already established in a paper by Chayes, Chayes, and Kivelson [67] in 1989. Their result, however, applies only to the case of open boundary conditions. For these lattices, our result extends the

one by Chayes et al. to the case of periodic boundary conditions, using a different approach. We have also discussed various applications of these results in RVB inspired approaches to quantum spin-1/2 systems.

A case of much interest, which we have not studied here, is that of the triangular lattice. We remark that since the square lattice can be thought of as a triangular lattice endowed with a coarser topology, obtained by removing certain nearest neighbor links, a candidate cell for the triangular lattice would have to be at least as large as our square lattice cell, Fig. (3.10b), with many more links included. This renders the M-matrix so large that we did not find this problem tractable at present. We currently see, however, no fundamental reason why the refined method of the preceding section should not be applicable to this case as well. In all cases thus far studied, we have found that local cells large enough to have *more* internal sites than boundary sites generally have a sufficiently strong local independence property, which then implies the desired linear independence of globally defined NNVB states. The only exception to this rule seem to be lattices where this "global" linear independence does not hold, for obvious, "local" reasons: These include the checkerboard and the pyrochlore lattice, or any lattice featuring tetrahedral units. By looking at the three dimerizations of a single tetrahedron, it is easy to see that for such lattices, linear independence of NNVB states does not hold. (That is, as long as there is any dimer covering of the lattice with two dimers on the same tetrahedron.)

Thus far, we are not aware of rigorous results on the problem studied here for any three-dimensional lattices (except for finite clusters). We are optimistic, however,

that our method is at least applicable to the hyperkagome case, which has recently enjoyed much attention in the study of frustrated quantum magnets [39, 88–92].

3.4 Extensions of the proof: Linear independence of Resonating Valence Loops (RVL) on the honeycomb and star lattices

This section will provide a proof that the valence loop states on the star lattice and on the honeycomb lattice are linearly independent. We will start by recalling the definition of the resonant valence loop states given in Ref. [93]. In the following, we consider a spin-1 system on the *star* and on the *honeycomb* lattice. On each site i, $S_i^\alpha = \frac{1}{2} b_{i\mu}^\dagger \sigma_{\mu\nu}^\alpha b_{i\nu}$, where σ^α are Pauli matrices and $b_{i\mu}$ are Schwinger bosons with the constraint $b_{i\uparrow}^\dagger b_{i\uparrow} + b_{i\downarrow}^\dagger b_{i\downarrow} = 2$. As explained in Ref. [93], each of the two bosons on every site can form a singlet bond with another boson on its nearest neighbor site, thus, each spin-1 can participate in two singlet bonds. A spin singlet bond on the link $\langle ij \rangle$ is created by $B_{ij}^\dagger = \epsilon^{\mu\nu} b_{i\mu}^\dagger b_{j\nu}^\dagger$ ($\epsilon^{\mu\nu}$ is the Levi-Civita symbol). With this we can come up with the following states:

$$|\Psi\rangle_{\mathrm{RVL}} = \sum_c |c\rangle; \ |c\rangle = (-1)^{n_c} \prod_{\langle ij\rangle \in c} B_{ij}^\dagger |0\rangle,$$

where c is a loop-covering configuration which consists of non-intercepting loops and which touches every site by one and only one loop, and n_c counts the number of singlet bonds of the loop configuration c on those vertical links with upper site in sublattice A (see Ref. [93]).

$|\Psi\rangle_{\mathrm{RVL}}$ is an *equal weight* superposition of all loop-covering configurations, which are

called "resonating valence loop" (RVL) states (see Ref. [93]). For the honeycomb or any other trivalent lattice like the star lattice, there exists a one-to-one correspondence between loop-covering and dimer-covering configurations: for any loop-covering c, a corresponding dimer configuration is obtained by occupying a virtual dimer on any link not covered by the loop. Here we are interested in the linear independence of the associated valence loop (VL) states $|c\rangle$. We found that a method used earlier to show the linear independence of nearest neighbor valence bond (NNVB) states can be successfully applied to this problem. This method was first published in Ref. [51]. Subsequently, the method was successfully applied to numerous two dimensional lattices in Ref. [68]. The strategy presented there was that it has to be shown that certain local generalizations of NNVB states - so-called snapshot states- are indeed linearly independent for a small cluster which we will call "basic cell" in the following. If linear independence can be established for the snapshot states "living" on the basic cell, it directly follows that all NNVB states on a larger lattice, which can be covered by the basic cell, are also linearly independent. We can use this strategy again when dealing now with the VL states. We first identify the basic cells for the star and the honeycomb lattice, which turn out to be the same ones that they were in the RVB case (see Fig. (3.11)). We now define the snapshot states for the VL states. We require that all "inner" sites of the basic cell, which have their three nearest neighbor sites also present in the basic cell, must participate in a loop, whereas the outer sites may or may not participate in a loop within the basic cell. If not, we can imagine that they belong to a loop which only "touches" the basic cell at this point, and lives on

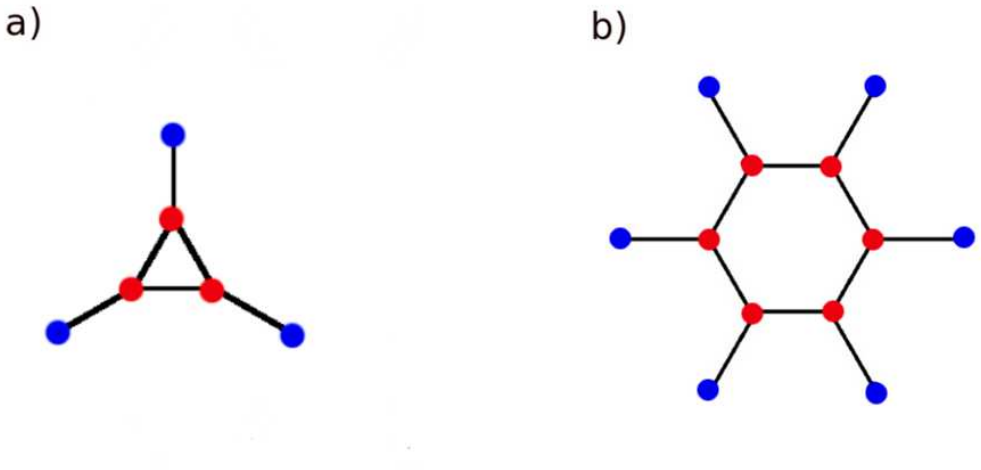

Figure 3.11. (a) shows the minimal cell of the star lattice for which the linear independence of both the RVB and the RVL states could be established. Red dots indicate inner sites that have all their 3 nearest neighbors also present in the cell, while blue dots label outer sites that do not all neighbor sites contained in the cell. (b) shows the minimal cell for the honeycomb lattice.

the larger lattice into which the basic cell is embedded. This leaves the spins at such boundary sites undetermined, and allows the site to be in an arbitrary spin state, that is, Sz = -1, 0, and +1. At the same time, loops may close within the basic cell, or they may be open, leading from one boundary site to another (Fig. (3.12) and Fig. (3.13)). In this case, a spin 1/2 degree of freedom can be chosen freely at each open end. The set of snapshot states is the set of all states associated with the loop coverings of the of the basic cell defined above, including all possible configurations of the free spin 1/2 or spin 1 degrees of freedom at boundary sites. The significance of these snapshot states is that in any VL state, the local density matrix on a basic

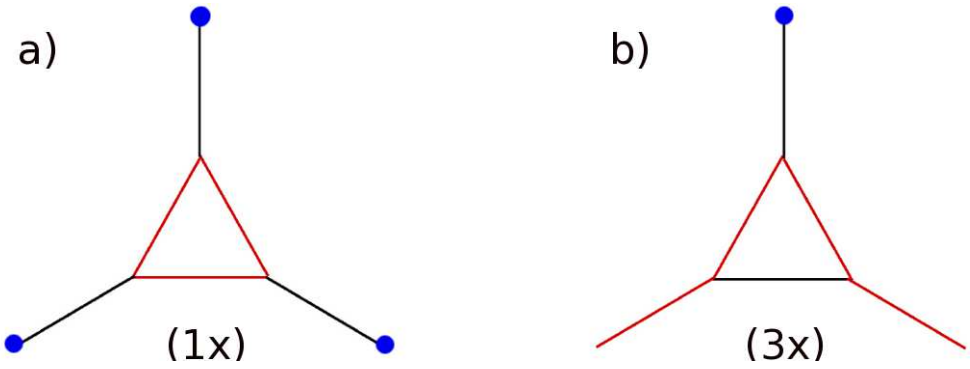

Figure 3.12. a) all inner sites participate in the loop while the three outer sites are in an arbitrary eigenstate of S^z = -1, 0, +1. b) all inner sites and two outer sites form the loop, apart from the configuration shown, there exists two rotated versions, thus, the total number for this kind of covering is three.

cell is given by a weighted sum over projections operators onto linear combinations of snapshot states. Said, differently, the range of such a density matrix (the linear span of its column vectors), is contained within the snapshot-subspace. A sufficient criterion for linear independence of VL states is that the overlap matrix between these snapshot states has maximum rank.

We thus have to generate all the snapshot states. To this end, we used the representation of the AKLT-states in terms of virtual spin 1/2-degrees of freedom, as developed in Ref. [94]. (This was, of course, the representation to which our old RVB code was most straightforwardly adapted.) General VL snapshot states naturally come as tensor products of open and closed AKLT-strings (the former carrying two free spin-1/2 degrees of freedom), and free sites (each carrying a spin 1). We have verified that the overlap matrix between all such snapshot states (which is of course block-diagonal within each sector of total S_z) does have maximum rank. This then

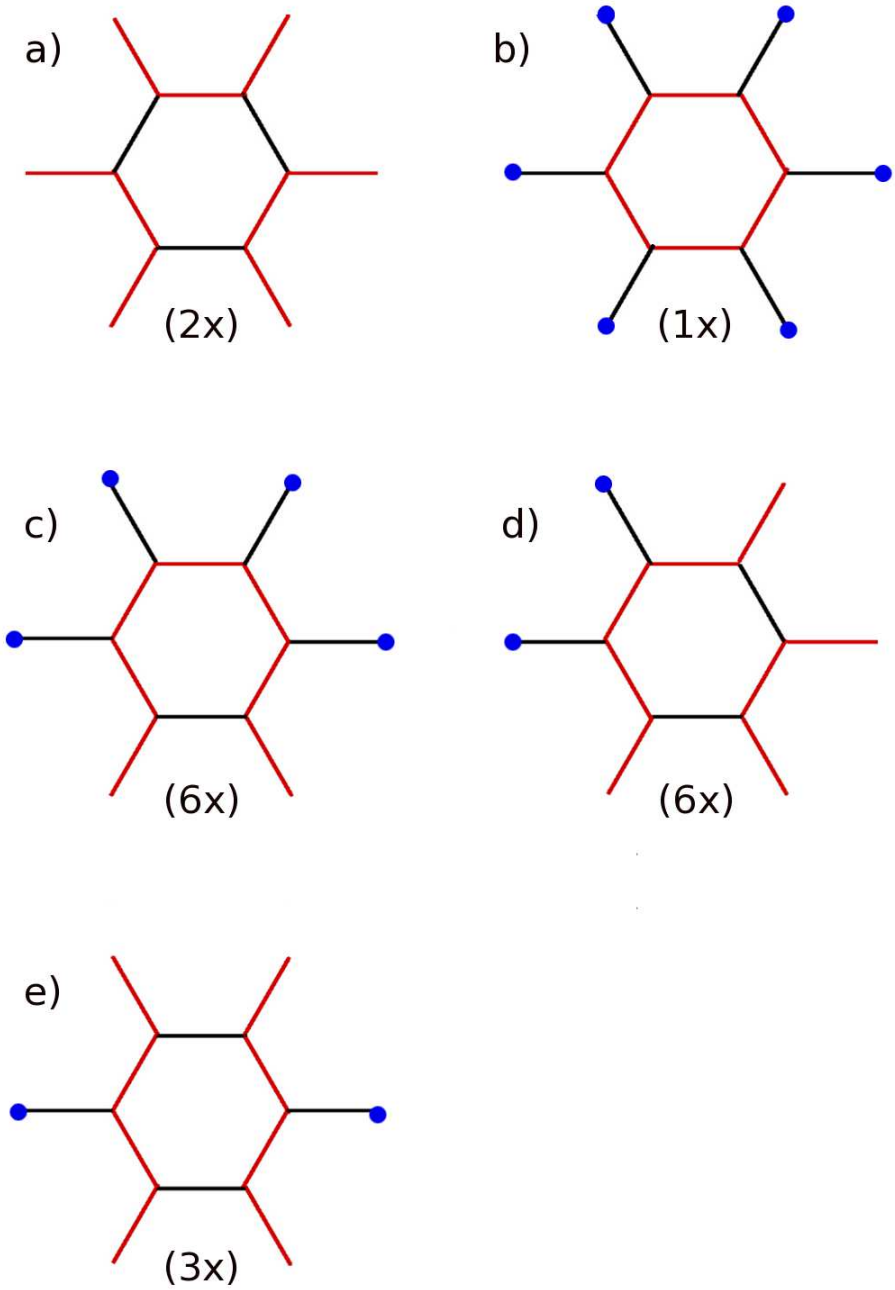

Figure 3.13. a) - e) show all possible loop coverings up to rotations for the honeycomb lattice.

allows one to define local projection operators, in complete analogy with Refs. [51,68].

The consecutive application of such operators allows one to single out any given VL

state in a generic linear combination of VL states. This then shows that VL states are linearly independent, on any lattice that can be covered (in the precise sense of Refs. [51, 68]) by the basic cells of Fig. (3.11).

4. Destruction of valence-bond order in a S=1/2 sawtooth chain with a Dzyaloshinskii-Moriya term

The final chapter is devoted to the investigation of the effect of a Dzyaloshinskii-Moriya (DM) interaction term on the valence bond order in a spin 1/2 Heisenberg sawtooth chain. This is an interesting and nontrivial question since, a small value of the spin gap in quantum antiferromagnets with strong frustration makes them susceptible to nominally small deviations from the ideal Heisenberg model. One of such perturbations worth an investigation is the anisotropic Dzyaloshinskii-Moriya interaction. The DM interaction is an important perturbation for the S = 1/2 kagome antiferromagnet, one of the current candidates for a quantum-disordered ground state. Here, we study the influence of the DM term in a related one-dimensional system, the sawtooth chain that has valence-bond order in its ground state. In the following, employing a combination of analytical and numerical methods, we show that a relatively weak DM coupling, 0.115J, is sufficient to destroy the valence-bond order, close the spin gap, and turn the system into a Luttinger liquid with algebraic spin

correlations. A similar mechanism may be at work in the kagome antiferromagnet. The results of this chapter have been published in

Zhihao Hao, Yuan Wan, I. Rousochatzakis, Julia Wildeboer, A. Seidel, F. Mila, and O. Tchernyshyov, Phys. Rev. B 84, 094452 (2011) .

4.1 Introduction

When it comes to finding or proposing a promising candidate system for an exotic ground state such as the quantum spin liquid state, one has to consider multiple circumstances that are considered supportive for such a quantum state. A promising system would be an $S = 1/2$ antiferromagnet on a nonbipartite lattice, since geometrical frustration and strong quantum fluctuations have a tendency to suppress long-range magnetic order. The resulting ground state does not break the symmetry of global spin rotations. However, there are still several scenarios possible concerning the behavior of the system, e.g. the system could be a valence-bond crystal that breaks some lattice symmetries [95–97] or it could indeed be a valence-bond liquid as mentioned above that fully preserves the symmetry of the Hamiltonian. [51, 98–100] In the very recent past, several antiferromagnetic materials without long-range magnetic order well below the characteristic Curie-Weiss temperature scale have been discovered. A prominent example here is the herbertsmithite $Cu_3Zn(OH)_6Cl_2$, [101]; no magnetic order has been detected down to 50 mK, [47, 48, 102–104] even though the exchange interaction is estimated to be $J = 180$ K. The compound is a "struc-

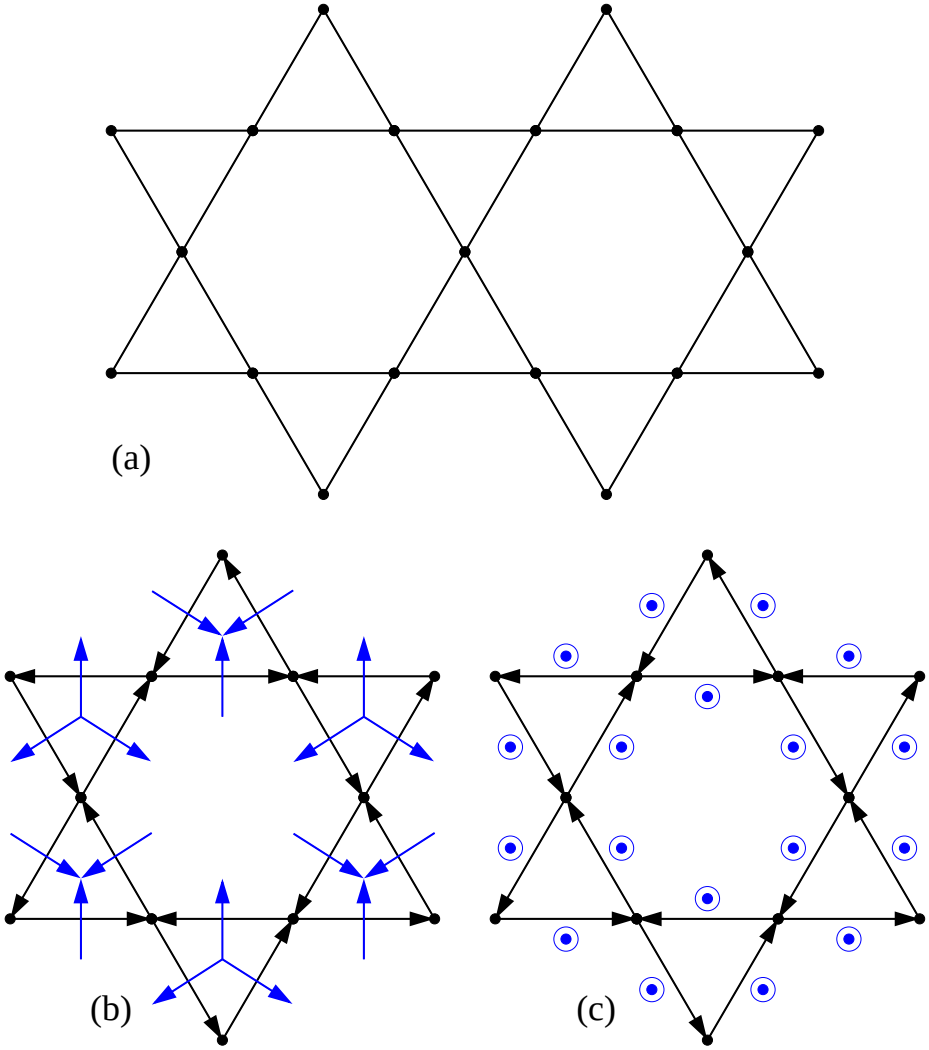

Figure 4.1. (a) The Kagome lattice. (b) and (c) In-plane and out-of-plane components of the DM vector $\mathbf{D}_{ij}$ shown for directed links $(i \to j)$ on the lattice.

turally perfect" [48, 105] realization of the $S = 1/2$ Heisenberg antiferromagnet on the kagome lattice (Fig. 4.1(a)). Although it remains a challenging question what the ground state of the nearest neighbor Heisenberg interaction on the kagome lattice is,[1] it is an equally interesting question to ask what happens upon turning on

[1]At this point, the tendency in the condensed matter community is to believe the ground state to be a quantum spin liquid [106, 107].

an additional interaction as real systems inevitably deviate from this idealization. Frustrated magnets tend to be sensitive to various nominally weak perturbations. This chapter deals with the additional term being the Dzyaloshinskii-Moryia (DM) interaction, [108, 109] the antisymmetric version of the Heisenberg exchange induced by the spin-orbit coupling. In this case, the Hamiltonian is

$$H = \sum_{\langle ij \rangle} [J\, \mathbf{S}_i \cdot \mathbf{S}_j + \mathbf{D}_{ij} \cdot (\mathbf{S}_i \times \mathbf{S}_j)]. \tag{4.1}$$

In herbertsmithite, the DM term is allowed by the crystal symmetry. The in-plane and out-of-plane components of the DM vector $\mathbf{D}_{ij}$ on the kagome lattice are shown in Fig. 4.1(b) and (c). The DM vector has the magnitude $D = 0.08J$ [110] with its stronger component being the out-of-plane component, whereas the in-plane component is relatively small, $D_{\text{in}} = 0.01J \pm 0.02J$. The DM term can be gauged away by an appropriate rotation of the local spin axes, [111, 112] if its "line integral" vanishes for any closed loop $abc \ldots yza$:

$$\mathbf{D}_{ab} + \mathbf{D}_{bc} + \ldots + \mathbf{D}_{yz} + \mathbf{D}_{za} = 0. \tag{4.2}$$

It can be seen from Fig. 4.1(b) that the in-plane component satisfies Eq. (4.2) and subsequetly can be gauged away. The out-of-plane component cannot be removed in this way and thus represents the actual physical perturbation, which we will focus on in this chapter.

Recent numerical studies [106, 113–116] indicate that the pure Heisenberg model, $D = 0$, has a $S = 0$ ground state with a small but finite energy gap for $S = 1$ excitations, with estimates ranging from $\Delta = 0.05J$ to $0.15J$. Since these values are

of the same order of magnitude in strength as the DM term, it is plausible that the low-energy properties of herbertsmithite are influenced by the DM interaction.

At this point, we just mention that there exist numerous studies on the effects of the DM interaction on the kagome antiferromagnet. Important results were obtained for example in Refs. [117], [118], [119], [120], [121], [122], [123], [124], and in Ref. [124].

The results of this chapter follow the findings of Ref. [125]. Here, it was demonstrated that the $S = 1/2$ Heisenberg antiferromagnet on a kagome lattice can be viewed as a collection of fermionic spinons—topological defects with $S = 1/2$—moving in an otherwise inert vacuum of valence bonds. These spinons interact with an emerging compact U(1) gauge field whose quantized electric flux is related to the valence-bond configuration through Elser's arrow representation [126] and the spinons carry one unit of the U(1) charge against a negatively charged background. Furthermore it was explained that strong, exchange-mediated attraction binds spinons into small and heavy $S = 0$ pairs and that low-energy $S = 1$ excitations result from breaking up a pair into "free" spinons. Subsequently, the spin gap is determined mostly by the binding energy of a pair, which was estimated to be $0.06J$.

With this knowledge, it seems plausible that one potential route to closing of spin gap could be via the destruction of the two-spinon bound state in the presence of a sufficiently strong DM coupling term. However, this appears an unlikely scenario for two reasons. First, the factors setting the pair binding energy—the spinon hopping amplitude and the strength of exchange-mediated attraction–are both of order J, thus it is unrealistic to have a fairly weak coupling $D = 0.05J$ to $0.10J$ disrupt the pairing.

Second, a quantum phase transition to a state with long-range magnetic order can be viewed as Bose condensation of magnons, [128] quasiparticles with $S_z = 1$ and there are no low-energy excitations of this kind in the pure Heisenberg model. Here a way out, could be thinking of condensing pairs of spinons with $S_z = 1$. However, such an object would carry a double U(1) charge, whereas a magnon is expected to be neutral.

Another possible way out is to postulate that the condensing objects are pairs consisting of a spinon and its antiparticle. In this case, the composite object would have zero U(1) charge and be topologically trivial, like a magnon. In the pure Heisenberg model, the energy cost of creating a spinon and its antiparticle is approximately $0.25J$. [129] We will see shortly that the DM term lowers the kinetic energy of both spinons and their antiparticles. Thus, it is reasonable to expect that at a critical coupling strength D_c, the energy cost of adding a pair vanishes.

In order to subject this hypothese to a test, we have studied a toy version of the kagome antiferromagnet known as the sawtooth spin chain, [130, 131] a one-dimensional lattice of corner-sharing triangles, Fig. 4.2(a). To make a connection with kagome, exchange couplings are set equal for all bonds. Without the DM coupling ($D = 0$), the chain has two valence-bond ground states, Fig. 4.2(b) and (c), that spontaneously break the mirror reflection symmetry. Spin excitations are topological defects, namely domain walls with spin $S = 1/2$, Fig. 4.2(d). The domain walls come in two flavors: kinks have zero energy and are localized, antikinks, on the contrary, are mobile and have a minimum energy of $0.215J$. [130] These excitations can only be

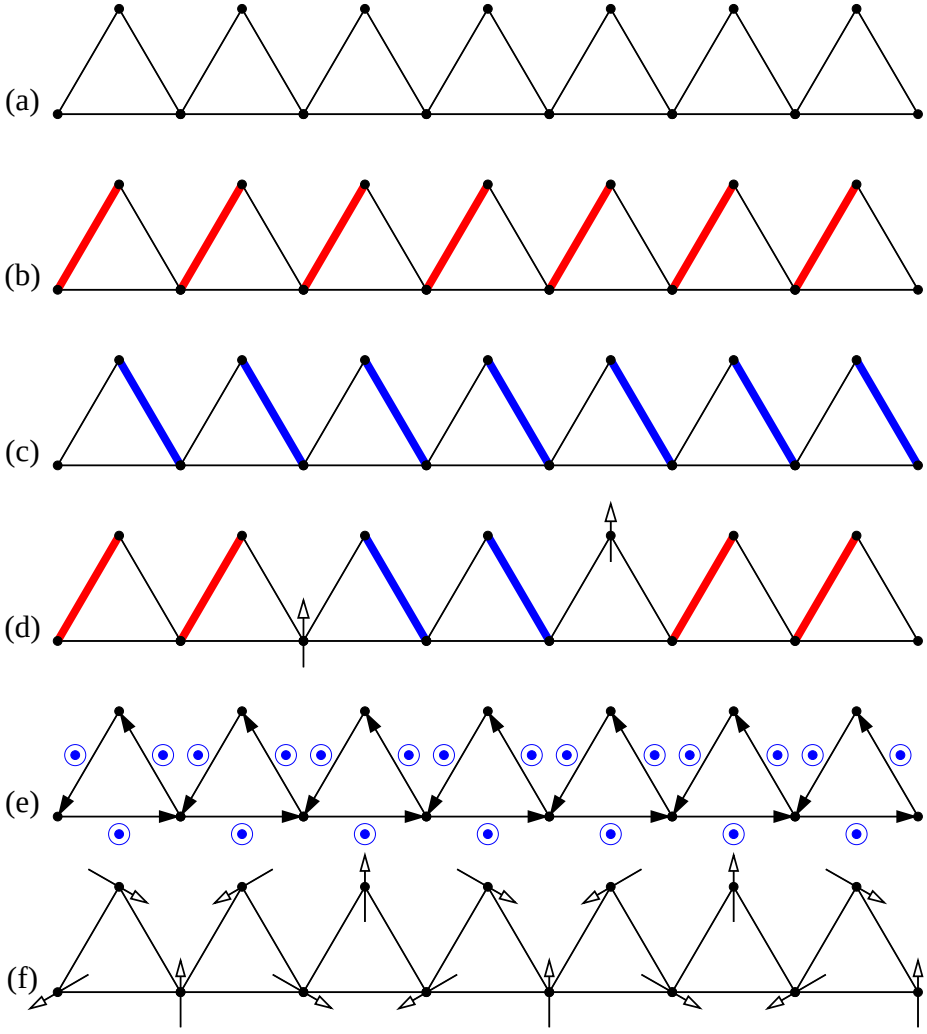

Figure 4.2. (a) The sawtooth chain. (b) and (c) Its valence-bond ground states. (d) Spin-1/2 excitations: kink (left) and antikink (right). (e) Orientation of the DM vectors $\mathbf{D}_{ij}$. (f) The ground state of the classical model has a commensurate magnetic order with the wave number $q/2\pi = -1/3$.

created in pairs by a local perturbation acting in the bulk. As discussed in Ref. [132], spinons of the kagome antiferromagnet have similar properties. However, the ground state of the sawtooth chain is free from the defects, whereas the kagome lattice has a finite concentration of antikinks (1/3 per site) bound into $S = 0$ pairs. This chapter

provides data on the sawtooth spin chain with exchange and Dzyaloshinskii-Moriya interactions, Eq. (4.1). The $\mathbf{D}_{ij}$ vectors have the same length and a uniform out-of-plane orientation preserving the translational symmetry of the chain (Fig. 4.2(e)). Upon turning on the DM term, the mirror symmetry of the Hamiltonian is preserved , so that the notion of a valence-bond order that spontaneously breaks this symmetry is still valid. The key result is that the valence-bond order survives to a finite value of the DM coupling.

Section 4.2 provides a calculation of the spinon spectrum in the presence of a nonzero D. From this data, an estimate for the critical DM coupling is $D_c = 0.087J$. For $D > D_c$, spontaneous creation of kink-antikink pairs leads to a finite concentration of topological defects, which obliterates the valence-bond order and restores the reflection symmetry of the lattice.

4.2 Spinon dispersions

4.2.1 $D = 0$

We start by briefly reviewing the physics of the sawtooth chain in the pure Heisenberg model without the DM term [130–132]. The Hamiltonian of the system is

$$H = J \sum_{\langle ij \rangle} \mathbf{S}_i \cdot \mathbf{S}_j = \frac{J}{2} \sum_{\Delta} \left(\mathbf{S}_{\Delta}^2 - 9/4 \right), \tag{4.3}$$

where the $\mathbf{S}_{\Delta}$ is the total spin of triangle Δ. The energy is minimized when $S_{\Delta} = 1/2$ for every triangle. This can be achieved by putting a singlet bond on every triangle.

The ground state degeneracy is two and both ground states (shown in Fig. 4.2(b) and (c)) violate the symmetry of reflection.

Two types of domain walls interpolate between the ground states: the kink and the antikink (see Fig.4.2(d)). A kink is an excitation with zero energy and it is also an exact eigenstate of the Hamiltonian (4.3). Thus, kinks are localized in the exchange-only model. The two degenerate states with Sz=1/2 have spin current going clockwise or counter clockwise around the triangle. The states also carry electric currents of opposite directions [135]. An alternative set of basis states would have distinct valence-bond averages $\langle \mathbf{S}_i \cdot \mathbf{S}_j \rangle$ on the three bonds, which translates to nonzero electric charge on the three sites [135].

An antikink is mobile and while moving it is accompanied by the emission and absorption of kink-antikink pairs. The existence of a finite spin gap guarantees that these excitations are virtual. Polarization effects can be taken into account by using a variational approach. At the crudest level, the Hamiltonian (4.3) is projected onto the Hilbert space with a single antikink to obtain an effective hopping Hamiltonian for an antikink:

$$H^{(1)}|x\rangle = \frac{5J}{4}|x\rangle - \frac{J}{2}|x+1\rangle - \frac{J}{2}|x-1\rangle. \tag{4.4}$$

where $|x\rangle$ is a state with an antikink on triangle x. The energy dispersion of the antikink is

$$E_a(k) = 5J/4 - J\cos k, \tag{4.5}$$

with the minimum energy $\Delta = 0.25J$. In view of the zero energy of a kink, this value is the spin gap.

From the previous discussion, it seems plausible that the variational approach provides a reliable description of the low-energy spin excitations in the pure Heisenberg model. Thus, we will use the lowest-order approximation for $D \neq 0$, without correcting for the vacuum polarization, to obtain a rough estimate for the critical coupling D_c.

4.2.2 $D \neq 0$

When the DM term becomes finite, kinks become mobile. For a single triangle, this means the splitting of the accidental degeneracy mentioned previously: the energy of a state with $S_z = +1/2$ now depends on the orbital momentum, reflecting the spin-orbit origin of the DM term.

We follow the variational method described above for a finite chain and work in the Hilbert space spanned by states $|x\rangle$ with a single kink located between triangles x and $x+1$. These states are not orthogonal to each other because they are not eigenstates of the same Hermitian operator; their overlap is

$$\langle x_1|x_2\rangle = 2^{-|x_1-x_2|}. \tag{4.6}$$

As with antikinks, [132] a simple rotation can be made to obtain an orthonormal basis $\{|\tilde{x}\rangle\}$:

$$|\tilde{x}\rangle = \frac{2}{\sqrt{3}}|x\rangle - \frac{2}{\sqrt{3}}|x-1\rangle. \tag{4.7}$$

The matrix elements of the effective Hamiltonian in this subspace are

$$\langle \tilde{x}_1|H|\tilde{x}_2\rangle = -\frac{3iD}{2}\, 2^{-|x_1-x_2|}\,\mathrm{sgn}(x_1-x_2), \tag{4.8}$$

where the sign function is defined in such a way that $\mathrm{sgn}(0) = 0$. A Fourier transform of the matrix element yields the energy dispersion of the kink:

$$E_{\mathrm{k}}(k) = \frac{6D \sin k}{5 - 4\cos k}. \tag{4.9}$$

The bottom of the band is at $E_{\mathrm{k}}^{\mathrm{min}} = -2|D|$. For $D > 0$, it is reached for an incommensurate wave number $k/2\pi = -\mathrm{acos}(4/5)/2\pi \approx -0.10$.

Turning our attention now to the antikink case, we note that the basis states $\{|x\rangle\}$, with an antikink located at triangle x, can be orthogonalized in the same way to yield an orthonormal basis $\{|\tilde{x}\rangle\}$. The DM term matrix element is

$$\langle \tilde{x}_1 | H_{DM} | \tilde{x}_2 \rangle = -iD\, 2^{-|x_1 - x_2|}\, \mathrm{sgn}(x_1 - x_2) \left[\frac{3}{2} - \frac{2}{3}(\delta_{x_1, x_2+1} + \delta_{x_1, x_2-1}) \right] \tag{4.10}$$

with an antikink dispersion of

$$E_{\mathrm{a}}(k) = 5J/4 - J\cos k + \frac{5D}{6}\sin k + \frac{3D(4\cos k - 1)\sin k}{10 - 8\cos k}. \tag{4.11}$$

For $D \ll J$, the lowest energy of an antkink is $E_{\mathrm{a}}^{\mathrm{min}} = J/4 - 14D^2/J + \mathcal{O}(D^4/J^3)$ and the bottom of the band is located at $k/2\pi = -8D/3\pi J + \mathcal{O}(D^3/J^2)$.

The above energy dispersions were computed for spinons with $S_z = +1/2$. For spinons $S_z = -1/2$, the dispersions can be obtained by changing $k \mapsto -k$.

The bottom edge of the two-particle continuum as a function of total momentum is shown as solid lines in Fig. 4.3 for $S_z = 0$ and in Fig. 4.4 for $S_z = +1$. The edge dispersion mostly tracks the dispersion of the heavier kink particle (4.9). The minimum energy of a kink-antikink pair

$$E^{\mathrm{min}} = J/4 - 2|D| - 14D^2/J + \mathcal{O}(D^4/J^3) \tag{4.12}$$

vanishes when the DM coupling reaches the critical strength $D_c = 0.09J$. The total momentum of a $S_z = +1$ spinon pair with the lowest energy is $k/2\pi \approx -0.15$. The gapless state arising at this critical point is expected to have transverse spin fluctuations with this wave number. The wavenumber of longitudinal spin fluctuations is determined by the bottom of the two-spinon continuum with $S_z = 0$, which occurs at $k/2\pi \approx \pm 0.06$.

4.3 Exact diagonalization

This section shows data obtained via an exact diagonalization study of the saw-tooth chain with exchange and DM interactions. Finite chains containing $2L$ sites in a system with L triangles with periodic boundary conditions were under investigation. The length varied from $L = 5$ to 15, the DM interaction was chosen to be uniform. The Lanczos algorithm was used which provides convergent results for the ground state energy and a limited number of low-lying excitations. The symmetry of translations along the chain and the O(2) symmetry of spin rotations around the z-axis allow an reduction of the Hilbert space.

Figure 4.3 shows the low-energy portions of the spectra in the $S_z = 0$ sector for a chain with length $L = 15$ (30 sites), several values of DM coupling D are presented. Time reversal of the Hamiltonian (4.1) ($S_z \mapsto -S_z$, $k \to -k$) guarantees that the $S_z = 0$ spectra are symmetric under mirror reflection ($k \to -k$). The lowest-energy excitations in the $S_z = 0$ sector are expected to be spinon pairs in two channels: a kink with $S_z = -1/2$ and an antikink with $S_z = +1/2$ or vice versa. The calculated edges

of the two-particle continua reproduce the shape of the dispersing bottom reasonably well. However, the calculated edge shifts downward with D faster than the numerical data do.

In the $S_z = +1$ sector, the spectra are not symmetric under the mirror symmetry (the $S_z = 1$ spectrum maps onto that of the $S_z = -1$ sector), Fig. 4.4. The lowest-energy excitations are expected to be spinon pairs consisting of a kink and an antikink, both with $S_z = +1/2$. Again, the calculated bottom edge of the excitation continuum has the right shape but advances downward with D somewhat too fast. In the two-spinon approximation, both the $S_z = 0$ and $S_z = 1$ continua touch zero energy at $D_c = 0.09J$. However, the numerical energy spectra appear to still have a gap at that point, see Fig. 4.3.

To locate the critical point, we turned to a scaling analysis of the ground state splitting. In the phase with valence-bond order, the ground state is doubly degenerate in the limit $L \to \infty$. In finite systems, the ground-state doublet is split thanks to quantum tunneling. Both members of the doublet have momentum $k = 0$ because the valence-bond order preserves translational symmetry. The tunneling amplitude decays exponentially with the system length L and so does the splitting.

Fig. 4.5(a) shows the splitting of the ground state for $D \leq 0.11J$. All of the data sets, with the exception of the largest coupling, are well fit by the scaling expression

$$\Delta E = AL^{-5/4} e^{-L/\xi} \cos(kL) \tag{4.13}$$

with the same prefactor A. The dependence of the tunneling length ξ and the wavenumber k is shown in Fig. 4.5(c). The tunneling length greatly exceeds the

maximum attainable system length $L = 15$, for $D > D_c = 0.115J$, it might even diverge. For $0.11J \leq D \leq 0.15J$, the finite-size dependence of the splitting was best fit by Eq. (4.13) with $\xi = \infty$ and a D-dependent amplitude A, Fig. 4.5(b). Apart from the oscillating factor, Eq. (4.13) suggests a scale-invariant ground state for $D \geq D_c$.

For $D > D_c$, a gapless phase with quasi-long-range incommensurate spin correlations decaying as a power of the distance is expected. Making D larger and larger, we move more and more into the classical model. Here, in the classical limit, the sawtooth chain has a spiral order for any nonzero value of D, Fig. 4.2(f). Low-energy excitations are spin waves with a speed

$$v \approx 2.7S\sqrt{JD}. \tag{4.14}$$

Quantum fluctuations disrupt the long-range spin order, thus, translational invariance and O(2) symmetry are restored. Such a phase would be a Luttinger liquid, whose lowest-energy $S_z = +1$ excitations are spin waves with a sound-like spectrum at $k_0/2\pi = -1/3$. The numerically determined $S_z = +1$ spectra for $D \geq 0.15J$ are consistent with spin waves. At $D = 0.19J$, the soft spot is located at $k_0/2\pi \approx -0.25$, not far from the classical value. The speed of sound can be estimated from the slope of the dashed lines in Fig. 4.3 and 4.4: $v = 0.36J$ is reasonable close to the classical estimate (4.14) obtained below.

4.4 Spin correlations in the ground state

In order to verify the location of the quantum critical point D_c and to confirm the critical nature of the ground state for $D > D_c$, the long-distance behavior of spin correlations was investigated, ($G^{\alpha\beta}(r) = \langle S^{\alpha}(0)S^{\beta}(r)\rangle$) in the ground state. In the Luttinger-liquid regime, transverse spin correlations are expected to decay as a power of the distance, [136]

$$|G^{+-}(r)| \sim \frac{C}{r^{1/2K}}. \tag{4.15}$$

The stiffness constant K varies between 1 (gas of dilute magnons) and 1/4 (gas of dilute spinons) [134, 137].

In a finite system of length L with periodic boundary conditions, the Green's function depends in the same way on the chord distance [138]

$$d(r) = (L/\pi)\sin(\pi r/L). \tag{4.16}$$

In a system with $2L$ spins, this distance varies from $d \approx 1$ to L/π. Therefore, the range of distances in a system with $2L = 30$ spins is not sufficient to reliably observe the critical behavior of the spin correlation function.

In order to obtain data from larger system sizes and to finally observe the critical behavior, we used the density-matrix renormalization group (DMRG) method implemented through the Matrix Product Toolkit [139] to obtain the ground state wave function in a periodic chain with up to $2L = 100$ spins. The system has a U(1) symmetry which we took into account to reduce CPU time. The number m of states kept was of order 1000 states. Indeed, our results for the ground state energy *per site*

for all values of DM coupling D investigated are consistent with the energy per site obtained from the ED calculations.

The resulting transverse spin correlations $|G^{+-}(r)|$ in a system of length $L = 50$ are shown in Fig. 4.6 as a function of the chord distance (4.16). The data for $D = 0.12J$ follow a power law C/d^2 at large distances d. This is consistent with the value $K = 1/4$ at the spinon condensation point. For $D > 0.12J$, spin correlations follow power laws with smaller slopes, indicating $K > 1/4$. Finally, for $D < 0.12J$, the power-law scaling breaks down at large d and we observe an exponential decay. The estimated critical point, $D_c = 0.12J$, is in reasonable agreement with the value $D_c = 0.115J$ obtained from the splitting of the ground-state doublet.

4.5 Discussion

Without the Dzyaloshinskii-Moriya term, the sawtooth chain has a doubly degenerate ground state with valence-bond order spontaneously breaking the reflection symmetry of the lattice. Elementary excitations are spinons namely localized kinks and mobile antikinks. The gap to spin-1 excitations, $\Delta = 0.215J$ is determined by the edge of the two-spinon continuum. The introduction of a DM term with the **D** vector pointing along the same axis for all bonds, Fig. 4.2, lowers the spin-rotation symmetry down to an O(2). Several key observations can be obtained. First, at weak coupling D, the lattice reflection symmetry remains spontaneously broken. However, a finite D lowers the excitation energies of both kinks and antikinks and the spin gap (understood as the lowest energy of $S_z = 1$ excitations) begins to close. The

gap closes roughly when the minimum kink energy equals the initial gap in absolute terms, $|D| = D_c \approx \Delta/2 \approx 0.1J$. This is confirmed by numerical work involving exact diagonalization of finite chains, with the result $D_c = 0.115J$. Beyond the critical coupling, the valence-bond order is destroyed and the lattice symmetry is fully restored. The resulting state is likely a Luttinger liquid with incommensurate spin correlations and spin-wave excitations.

An open question is whether a similar transition may occur in the $S = 1/2$ Heisenberg model on kagome with a DM coupling. The bare existence of the transition is not in doubt, since it is understood that at a large enough D the system should develop magnetic order [121–124]. However, the nature of the transition still remains subject to speculations.

In the kagome antiferromagnet, spinon excitations are very similar to those of the sawtooth chain. [132] With $D = 0$, kinks are localized and have zero energy, whereas antikinks follow one-dimensional trajectories with the same energetics as on the sawtooth chain. Turning on the DM term has similar consequences; delocalization of kinks is the main factor lowering the edge of the kink-antikink continuum. If anything, the gap may close even faster than on the sawtooth chain because on kagome kinks move in two dimensions and thus can lower their energy through delocalization more effectively than on a one-dimensional chain. Therefore, the critical DM coupling for the kagome case can be conjectured to be even lower than for the sawtooth chain.

However an important difference between the kagome antiferromagnet and the sawtooth chain is that it has a finite concentration of antikinks in the ground state.

The antikinks form tightly bound $S = 0$ pairs, whose binding energy $\Delta_{\rm aa} \approx 0.06J$ is lower than the threshold energy of kink-antikink creation $\Delta_{\rm ka} \approx 0.25J$. Thus, the spin gap in the Heisenberg antiferromagnet on the kagome lattice is determined by the binding energy of an antikink pair. Although the binding energy $\Delta_{\rm aa}$ is no doubt influenced by the introduction of the DM term, it is unlikely that this energy is very sensitive to the presence of a small perturbation like D as $\Delta_{\rm aa}$ is determined by a competition of two high-energy processes: the antikink hopping amplitude and the antikink attraction in the singlet channel, both with a strength of order J. It seems more likely that the larger gap Δ_{ka} will be quickly driven to zero as it is on the sawtooth chain.

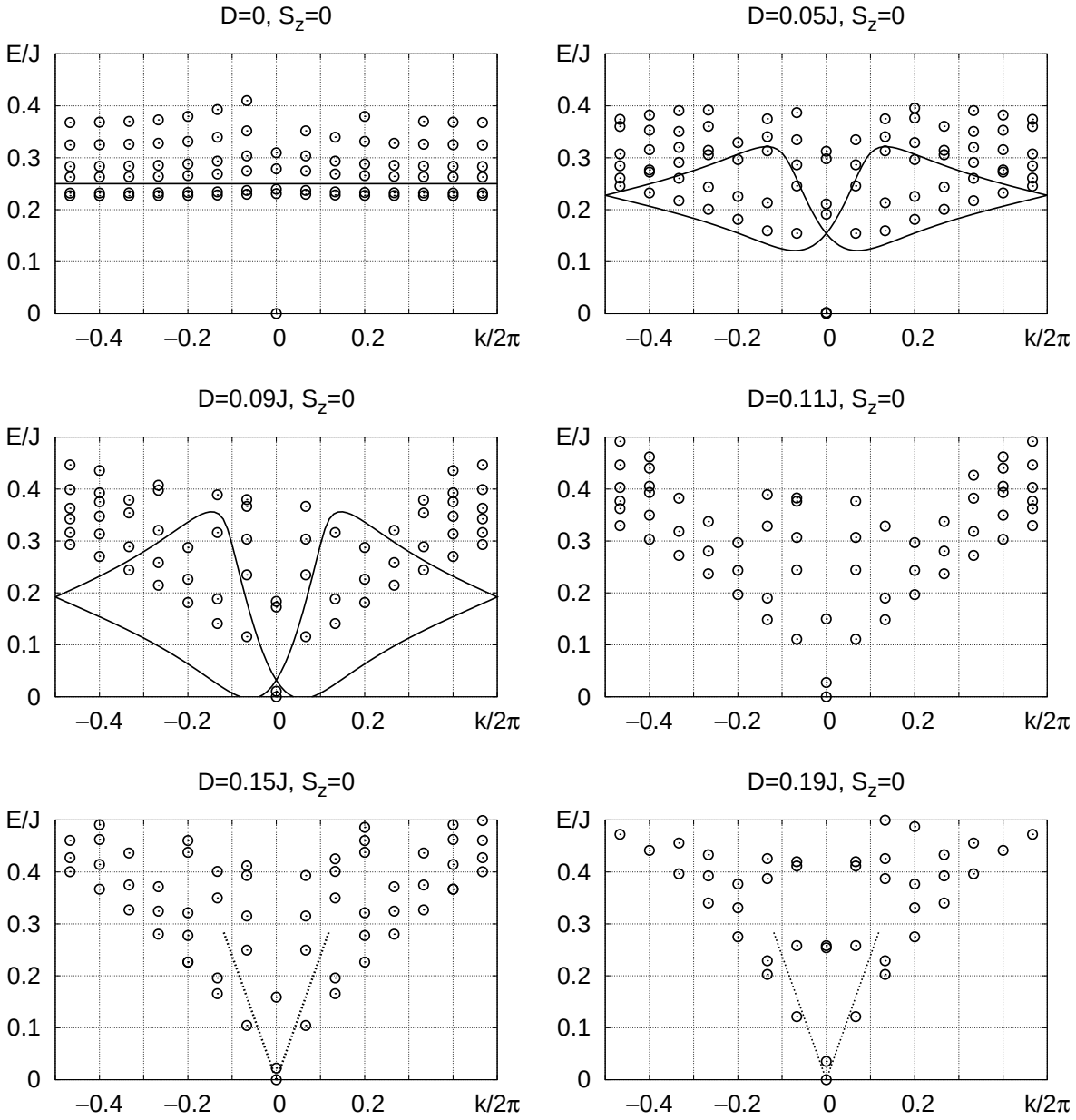

Figure 4.3. Low-energy spectra of the sawtooth chain with a uniform DM term in the $S_z = 0$ sector. Energy levels, measured relative to the ground state, are shown as a function of total momentum. Circles are the results of exact diagonalization for a periodic chain of length $L = 15$. Solid curves show the bottoms of the two-spinon continua computed analytically. Dashed straight lines show a linear dispersion with the speed $v = 0.36J$.

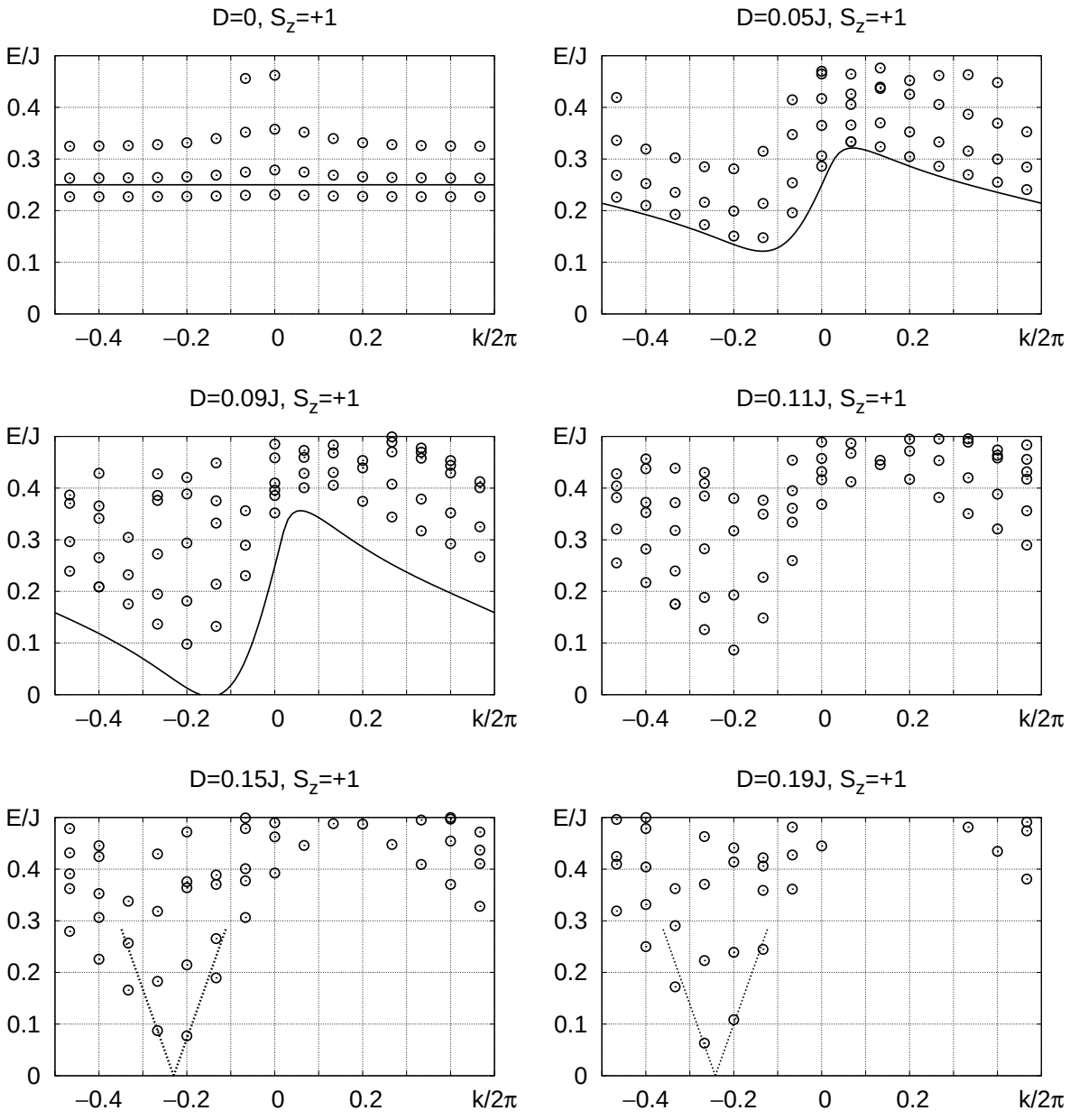

Figure 4.4. Low-energy spectra in the $S_z = +1$ sector. Notations are the same as in Fig. 4.3.

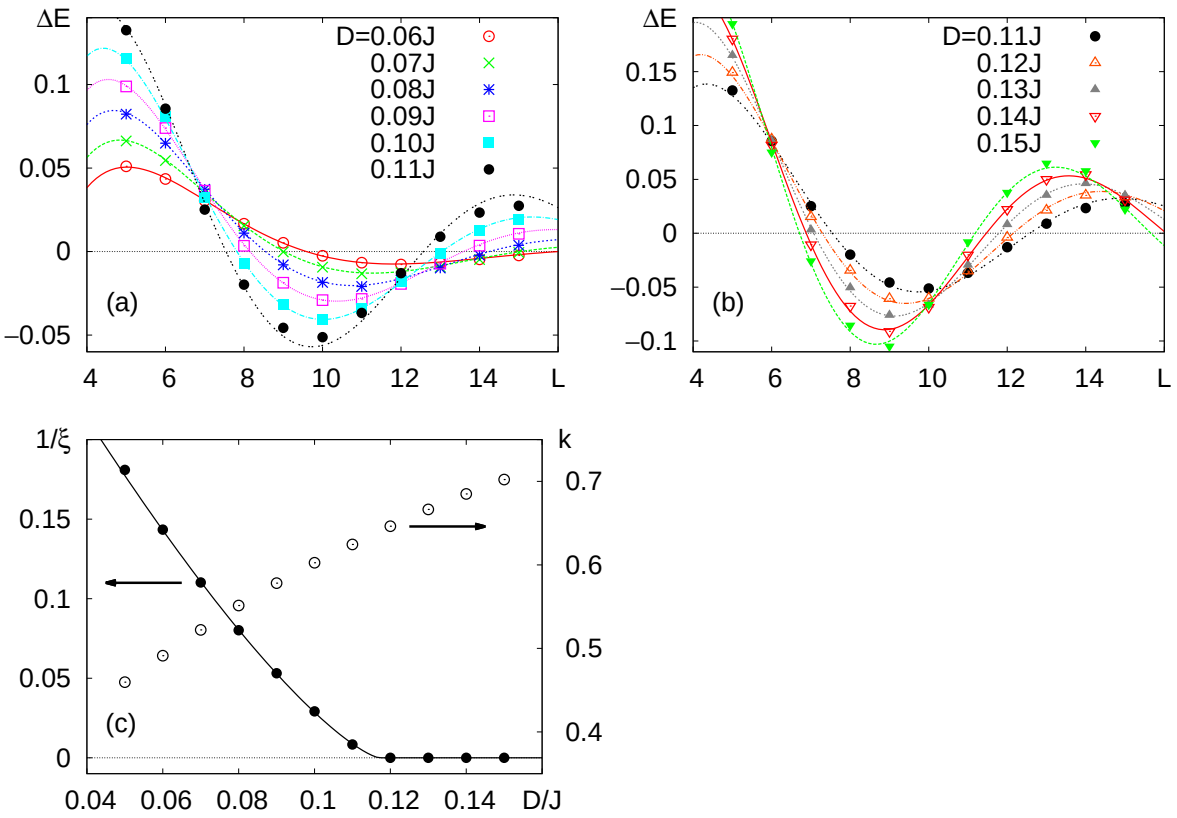

Figure 4.5. The splitting of the ground state doublet as a function of the system length L for (a) $D < D_c = 0.115J$ and (b) for $D > D_c$. (c) The dependence of the inverse tunneling length $1/\xi$ and the wavenumber k in the scaling form (4.13) on the DM coupling strength D.

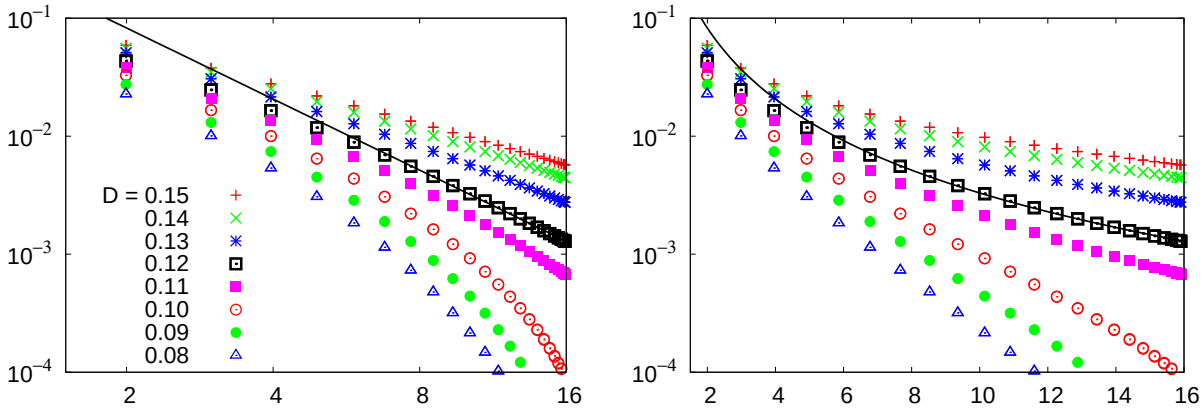

Figure 4.6. The amplitude of transverse spin correlations (4.15) as a function of the chord distance (4.16) on a log-log plot (left) and a simple log plot (right).

Bibliography

[1] P.W. Anderson, Mater. Res. Bull. **8**, 153 (1973).

[2] L.D. Landau, Phys. Z. Sowjetunion **11**, 26 (1937).

[3] V.L. Ginzburg and L.D. Landau, Zh. Ekaper. Teoret. Fiz **20**, 1064 (1950).

[4] J.G. Bednorz and K.A. Mueller, Z. Phys. B **64**, 189 (1986).

[5] P.W. Anderson, Science **235**, 1196 (1987).

[6] G. Baskaran, Z. Zou, and P.W. Anderson, Solid State Comm. **63**, 973 (1987).

[7] I. Affleck and J.B. Marston, Phys. Rev. B **37**, 3774 (1988).

[8] D.S. Rokhsar and S.A. Kivelson, Phys. Rev. Lett. **61**, 2376 (1988).

[9] I. Affleck, Z. Zou, T. Hsus, and P.W. Anderson, Phys. Rev. B **38**, 745 (1988).

[10] E. Dagotto, E. Fradkin, and A. Moreo, Phys. Rev. B **38** 2926 (1988).

[11] V. Kalmeyer and R.B. Laughlin, Phys. Rev. Lett **59**, 2096 (1987).

[12] X.-G. Wen, F. Wilczek, and A. Zee, Phys. Rev. B **39**, 11413 (1989).

[13] X.-G. Wen, Phys. Rev. B **40**, 7387 (1989).

[14] X.-G. Wen, Ind. J. Mod. Phys. B **4**, 239 (1990).

[15] X.-G. Wen, Phys. Rev. B **43**, 11025 (1991).

[16] A. Kitaev and J. Peskill, Phys. Rev. Lett **96**, 110404 (2006).

[17] M. Levin and X.-G. Wen, Phys. Rev. Lett **96**, 110405 (2006).

[18] X.-G. Wen and Q. Niu, Phys. Rev. B **41**, 9377 (1990).

[19] F.D.M. Haldane and E. Rezayi, Phys. Rev. B **31**, 2529 (1985).

[20] G. Kotliar and J. Liu, Phys. Rev. B **38**, 5142 (1988).

[21] N. Read and S. Sachdev, Phys. Rev. Lett **66**, 1773 (1991).

[22] X.-G. Wen, Phys. Rev. B **44**, 2664 (1991).

[23] P.A. Lee and N. Nagaosa, Phys. Rev. B **45** 5621 (1996).

[24] K. S. Raman, E. Fradkin, R. Moessner, S. Papanikolaou, S. L. Sondhi, Quantum Magnetism, NATO Science for Peace and Security Series 2008, pp 139-150

[25] B. Sutherland, Phys. Rev. B **37**, 3786 (1988).

[26] M. B. Hastings and X.-G. Wen, Phys. Rev. B **72**, 045141 (2005).

[27] X.-G. Wen and A. Zee, Phys. Rev. B **58**, 15717 (1998).

[28] S. Sachdev, Phys. Rev. B **40**, 5204 (1989).

[29] P.W. Leung, K.C. Chiu, and K.J. Runge, Phys. Rev. B **54**, 12938 (1996).

[30] R. Moessner, S. L. Sondhi, and P. Chandra, Phys. Rev. B **64**, 144416 (2001).

[31] R. Moessner, S.L. Sondhi, and E. Fradkin, Phys. Rev. B **65**, 024504 (2001 b).

[32] R. Moessner and S.L. Sondhi, Phys. Rev. Lett. **86**, 1881 (2001).

[33] G. Misguich, D. Serban, and V. Pasquier, Phys. Rev. Lett. **89**, 137202 (2002).

[34] A. Ralko, M. Ferrero, F. Becca, D. Ivanov, and F. Mila, Phys. Rev. B **71**, 224109 (2005).

[35] T. Senthil and M.P.A. Fisher, Phys. Rev. B **62**, 7850 (2000).

[36] R. Moessner and K.S. Raman, Quantum dimer models, Lecture notes, Trieste 2007, arXiv:condmat/0809.3051.

[37] D. Ivanov, Phys. Rev. B **70**, 094430 (2004).

[38] S. Wessel and M. Troyer, Phys. Rev. Lett **95**, 127205 (2005).

[39] E.J. Bergholtz, A.M. Laeuchli, R. Moessner, Phys. Rev. Lett. **10**, 237202 (2010).

[40] O.F. Syljuasen, Phys. Rev. B **73**, 245105 (2006).

[41] K.S. Raman, R. Moessner, and S.L. Sondhi, Phys. Rev. B. **72**, 064413 (2005).

[42] S. Fujimoto, Phys. Rev. B **72**, 024429 (2005).

[43] J. Cano and P. Fendley, Phys. Rev. Lett. **105**, 067205 (2010).

[44] R.B. Laughlin, Rev. Mod. Phys. **71**, 863 (1999).

[45] R. Rajaraman, arXiv:cond-mat/0103366

[46] V.R. Shaginyan, A.Z. Msezane, K.G. Popov, G.S. Japaridze, V.A. Stephanovich, Europhy. Lett. **97**, 56001 (2012).

[47] Oren Ofer, Amit Keren, Emily A. Nytko, Matthew P. Shores, Bart M. Bartlett, Daniel G. Nocera, Chris Baines, Alex Amato, arxiv:cond-mat/0610540

[48] J.S. Helton, K. Matan, M.P. Shores, E.A. Nytko, B.M. Bartlett, Y. Yoshida, Y. Takano, A. Suslov, Y. Qiu, J.-H. Chung, D.G. Nocera, Y.S. Lee, Phys. Rev. Lett. **98**, 107204 (2007).

[49] T.H. Han, J.S. Helton, S. Chu, A. Prodi, D.K. Singh, C. Mazzoli, P. Mueller, D.G. Nocera, and Y.S. Lee, Phys. Rev. B **83**, 100402(R) (2011).

[50] L. Clark, J.C. Orain, F. Bert, M.A. De Vries, F.H. Aidoudi, R.E. Morris, P. Lightfoot, J.S. Lord, M.T.F. Telling, P. Bonville, J.P. Attfield, P. Mendels, and A. Harrison, Phys. Rev. Lett. **11**, 207208 (2013).

[51] A. Seidel, Phys. Rev. B **80**, 165131 (2009).

[52] C. Zeng and V. Elser, Phys. Rev. B **51**, 8318 (1995).

[53] S. Furukawa, G. Misguich, and M. Oshikawa, Phys. Rev. Lett. **96**, 047211 (2006).

[54] Y. Tang, A.W. Sandvik, and C.L. Henley, Phys. Rev. B. **84**, 174427 (2011).

[55] A.F. Albuquerque and F. Alet, Phys. Rev. B **82**, 180408 (2010).

[56] F. Wang and F.Y. Wu, Phys. Rev. E **75**, 040105 (2007).

[57] P.W. Kasteleyn, J. Math Phys. **4**, 287 (1963).

[58] N. Schuch, D. Poiblanc, J.I. Cirac, and D. Perez-Garcia, arXiv:cond-mat/1203.4816 (2012).

[59] Z. Zhu, J. Wildeboer, and A. Seidel, to be published.

[60] R. Moessner, K.S. Raman, and S.L. Sondhi, AIP Conf. Proc. **816**, pp. 30-40 (2005).

[61] S. Liang, B. Doucot, and P.W. Anderson, Phys. Rev. Lett. **61**, 365-368 (1988).

[62] H.C. Jiang, Z.Y. Weng, and D.N. Sheng, Phys. Rev. Lett. **101**, 117203 (2008).

[63] B.S. Shastry and B. Sutherland, Physica B & C **108**, 1069 (1981).

[64] A.W. Sandvik and R. Moessner, Phys. Rev. B **73**, 144504 (2006).

[65] M. Troyer, B. Ammon, and E. Heeb, Lecture Notes in Comput. Sci. **1505**, 191 (1998).

[66] A.F. Albuquerque *et al.*, J. Magn. Magn. Mater. **310**, 1187 (2007).

[67] J.T. Chayes, L. Chayes, and S.A. Kivelson, Commun. Math. Phys. **123**, 53 (1989).

[68] J. Wildeboer, A. Seidel, Phys. Rev. B **83**, 184430 (2011).

[69] D.S. Rokhsar and S.A. Kivelson, Phys. Rev. Lett. **61**, 2376 (1988).

[70] R. Moessner and S.L. Sondhi, Phys. Rev. Lett. **86**, 1881 (2001).

[71] D. Poilblanc, M. Mambrini, D. Schwandt, Phys. Rev. B **81**, 180402(R) (2010).

[72] D. Schwandt, M. Mambrini, D. Poilblanc, Phys. Rev. B **81**, 214413 (2010).

[73] V. Elser, Phys. Rev. Lett. **62**, 2405 (1989).

[74] Z. Nussinov, C.D. Batista, B. Normand, and S.A. Trugman, Phys. Rev. B **75**, 094411 (2007).

[75] H. Yao and D.-H. Lee, arXiv:1010.3724 (2010).

[76] N. Flocke, T.G. Schmalz, and D.J. Klein, J. Chem. Phys. **109**, 873 (1998).

[77] Z. Noorbakhsh, F. Shahbazi, S.A. Jafari, and G. Baskaran, Journal of the Physical Society of Japan **78**, 054701 (2009).

[78] M. Mambrini and F. Mila, Eur. Phys. J. B **17**, 651 (2000).

[79] G. Misguich, C. Lhuillier, M. Mambrini, and P. Sindzingre, Eur. Phys. J. B **26**, 167 (2002).

[80] G. Misguich and C. Lhuillier, *Frustrated Spin Systems,* edited by H.T. Diep (World Scientific, Singapore, 2005), http://arxiv.org/abs/cond-mat/0310405.

[81] R. Moessner and S.L. Sondhi, Phys. Rev. B **63**, 224401 (2001).

[82] R.M. Ziff and C.R. Scullard, J. Phys. A: Math. Gen. **39**, 15083 (2006).

[83] *LinBox – Exact Linear Algebra over the Integers and Finite Rings, Version 1.1.6*, The LinBox Group (2008), http://linalg.org.

[84] G. Rumer, Göttinger. Nachr. p. 377 (1932).

[85] L. Pauling, J. Chem. Phys. **1**, 280 (1933).

[86] S. Mazumdar and Z.G. Soos, Synthetic Metals **1**, 77 (1979).

[87] S. Ramasesha and Z.G. Soos, Int. J. Quantum Chem. **25**, 1003 (1984).

[88] Y. Okamoto, M. Nohara, H. Aruga-Katori, and H. Takagi, Phys. Rev. Lett **99**, 137207 (2007).

[89] G. Chen and L. Balents, Phys. Rev. B **78**, 094403 (2008).

[90] M.J. Lawler, H.-Y. Kee, Y.B. Kim, and A. Vishwanath, Phys. Rev. Lett **100**, 227201 (2008).

[91] Y. Zhou, P.A. Lee, T.-K. Ng, and F.-C. Zhang, Phys. Rev. Lett **101**, 197201 (2008).

[92] M.J. Lawler, A. Paramekanti, Y.B. Kim, and L. Balents, Phys. Rev. Lett **101**, 197202 (2008).

[93] H. Yao, L. Fu, X.-L. Qi, arXiv:1012.4470.

[94] I. Affleck, T. Kennedy, E. H. Lieb, H. Tasaki, Commun. Math. Phys. **115**, 477-528 (1988).

[95] J.B. Marston and C. Zeng, J. Appl. Phys. **69**, 5962 (1991).

[96] P. Nikolić and T. Senthil, Phys. Rev. B **71**, 024401 (2005).

[97] M.B. Hastings, Phys. Rev. B **63**, 014413 (2000).

[98] S. Ryu, O.I. Motrunich, J. Alicea, and M.P.A. Fisher, Phys. Rev. B **75**, 184406 (2007).

[99] Y. Ran, M. Hermele, P.A. Lee, and X.-G. Wen, Phys. Rev. Lett. **98**, 117205 (2007).

[100] M. Hermele, Y. Ran, P.A. Lee, and X.-G. Wen, Phys. Rev. B **77**, 224413 (2008).

[101] R.S.W. Braithwaite, K. Mereiter, W.H. Paar, and A.M. Clark, Mineral. Mag. **68**, 527 (2004).

[102] M.A. de Vries, K.V. Kamenev, W.A. Kockelmann, J. Sanchez-Benitez, and A. Harrison, Phys. Rev. Lett. **100**, 157205 (2008).

[103] T. Imai, E.A. Nytko, B.M. Bartlett, M.P. Shores, and D.G. Nocera, Phys. Rev. Lett. **100**, 077203 (2008).

[104] A. Olariu, P. Mendels, F. Bert, F. Duc, J.C. Trombe, M.A. de Vries, and A. Harrison, Phys. Rev. Lett. **100**, 087202 (2008).

[105] M.P. Shores, E.A. Nytko, B.M. Bartlett, and D.G. Nocera, J. Am. Chem. Soc. **127**,13462 (2005).

[106] S. Yan, D.A. Huse, and S.R. White, Science **332**, 1173 (2011).

[107] Stefan Depenbrock, Ian P. McCulloch, Ulrich Schollwoeck, Phys. Rev. Lett. **109**, 067201 (2012).

[108] I. Dzyaloshinsky, J. Phys. and Chem. Sol. **4**, 241 (1958).

[109] T. Moriya, Phys. Rev. **120**, 91 (1960).

[110] A. Zorko, S. Nellutla, J. van Tol, L.C. Brunel, F. Bert, F. Duc, J.-C. Trombe, M.A. de Vries, A. Harrison, and P. Mendels, Phys. Rev. Lett. **101**, 026405 (2008).

[111] J.H.H. Perk and H.W. Capel, Physics Letters A **58**, 115 (1976).

[112] L. Shekhtman, O. Entin-Wohlman, and A. Aharony, Phys. Rev. Lett. **69**, 836 (1992).

[113] Ch. Waldtmann, H.-U. Everts, B. Bernu, C. Lhuillier, P. Sindzingre, P. Lecheminant, and L. Pierre, Eur. Phys. J. **B 2**, 501 (1998).

[114] R.R.P. Singh and D.A. Huse, Phys. Rev. B **76**, 180407 (2007).

[115] G. Evenbly and G. Vidal, Phys. Rev. Lett. **104**, 187203 (2010).

[116] H.C. Jiang, Z.Y. Weng, and D.N. Sheng, Phys. Rev. Lett. **101**, 117203 (2008).

[117] M. Rigol and R.R.P. Singh, Phys. Rev. Lett. **98**, 207204 (2007).

[118] M. Rigol and R.R.P. Singh, Phys. Rev. B **76**, 184403 (2007).

[119] J.S. Helton, K. Matan, M.P. Shores, E.A. Nytko, B.M. Bartlett, Y. Qiu, D.G. Nocera, and Y.S. Lee, Phys. Rev. Lett. **104**, 147201 (2010).

[120] M. Tovar, K.S. Raman, and K. Shtengel, Phys. Rev. B **79**, 024405 (2009).

[121] O. Cépas, C.M. Fong, P.W. Leung, and C. Lhuillie, Phys. Rev. B **78**, 140405 (2008).

[122] L. Messio, O. Cépas, and C. Lhuillier, Phys. Rev. B **81**, 064428 (2010).

[123] Y. Huh, L. Fritz, and S. Sachdev, Phys. Rev. B **81**, 144432 (2010).

[124] I. Rousochatzakis, S.R. Manmana, A.M. Läuchli, B. Normand, and F. Mila, Phys. Rev. B **79**, 214415 (2009).

[125] Z. Hao and O. Tchernyshyov, Phys. Rev. Lett. **103**, 187203 (2009).

[126] V. Elser and C. Zeng, Phys. Rev. B **48**, 13647 (1993).

[127] O. Ma and J.B. Marston, Phys. Rev. Lett. **101**, 027204 (2008).

[128] T. Giamarchi, C. Rüegg, and O. Tchernyshyov, Nature Physics **4**, 198 (2008).

[129] R.R.P. Singh, Phys. Rev. Lett. **104**, 177203 (2010).

[130] T. Nakamura and K. Kubo, Phys. Rev. B **53**, 6393 (1996).

[131] D. Sen, B.S. Shastry, R.E. Walstedt, and R. Cava, Phys. Rev. B **53**, 6401 (1996).

[132] Z. Hao and O. Tchernyshyov, Phys. Rev. B **81**, 214445 (2010).

[133] M. Fowler and M.W. Puga, Phys. Rev. B **18**, 421 (1978).

[134] J.B. Fouet, F. Mila, D. Clarke, H. Youk, O. Tchernyshyov, P. Fendley, and R.M. Noack, Phys. Rev. B **73**, 214405 (2006).

[135] L.N. Bulaevskii, C.D. Batista, M.V. Mostovoy, and D.I. Khomskii, Phys. Rev. B **78**, 024402 (2008).

[136] T. Giamarchi, *Quantum physics in one dimension* (Oxford University Press, New York, (2004).

[137] F.D.M. Haldane, Phys. Rev. Lett. **45**, 1358 (1980).

[138] F.D.M. Haldane, J. Phys. C **14**, 2585 (1981).

[139] I. McCulloch, Tech. Rep., RWTH Aachen University (2007), http://web.physik.rwth-aachen.de/ ianmcc/pmwiki/

[140] Z. Hiroi, H. Yoshida, Y. Okamoto, and M. Takigawa, J. Phys.: Conf. Ser. **145**, 012002 (2009).

[141] F.D.M. Haldane, Phys. Rev. Lett.**50**, 1153 (1983).